GESP-541
NASA-CR-72817

DESIGN AND FABRICATION OF SNAP-8 AUXILIARY LOOP HEAT EXCHANGERS

FINAL REPORT

By

E. S. Hsia
J. W. Zmurk

prepared for

NATIONAL AERONAUTICS AND SPACE ADMINISTRATION

NASA Lewis Research Center
Contract NAS 3-13445
Edward R. Furman, Project Manager

NUCLEAR SYSTEMS PROGRAMS
SPACE DIVISION
GENERAL ELECTRIC
CINCINNATI, OHIO 45215

NOTICE

This report was prepared as an account of Government sponsored work. Neither the United States, nor the National Aeronautics and Space Administration (NASA), nor any person acting on behalf of NASA:

A.) Makes any warranty or representation, expressed or implied, with respect to the accuracy, completeness, or usefulness of the information contained in this report, or that the use of any information, apparatus, method, or process disclosed in this report may not infringe privately owned rights; or

B.) Assumes any liabilities with respect to the use of, or for damages resulting from the use of any information, apparatus, method or process disclosed in this report.

As used above, "person acting on behalf of NASA" includes any employee or contractor of NASA, or employee of such contractor, to the extent that such employee or contractor of NASA, or employee of such contractor prepares, disseminates, or provides access to, any information pursuant to his employment or contract with NASA, or his employment with such contractor.

Requests for copies of this report should be referred to:

National Aeronautics and Space Administration
Scientific and Technical Information Division
Attention: USS-A
Washington, D.C. 20546

GESP-541
NASA-CR-72817

FINAL REPORT

DESIGN AND FABRICATION OF SNAP-8 AUXILIARY LOOP HEAT EXCHANGERS

by

E. S. Hsia
J. W. Zmurk

NUCLEAR SYSTEMS PROGRAMS
SPACE DIVISION
GENERAL ELECTRIC COMPANY
Cincinnati, Ohio 45215

prepared for

NATIONAL AERONAUTICS AND SPACE ADMINISTRATION

CONTRACT NAS 3-13445

NASA Lewis Research Center
Cleveland, Ohio
Edward R. Furman, Project Manager

Page intentionally left blank

TABLE OF CONTENTS

LIST OF ILLUSTRATIONS

LIST OF ILLUSTRATIONS (Continued)

LIST OF TABLES

NOMENCLATURE

Symbols	Descriptions	Dimensions
A	Area	in^2
A_F	Shell-side flow area	in^2
C_p	Specific heat	Btu/lb-^oF
C_0	Correction factor for bend other than 90^o	- -
C_{90}	Loss coefficient for a 90^o bend	- -
D	Diameter	inch
D_e	Equivalent diameter	inch
f	Friction factor	- -
g	Gravitational acceleration	ft/sec^2
G	Mass velocity	$lb/hr\text{-}ft^2$
h	Heat transfer coefficient	Btu/hr-ft^2-^oF
Δh	Measured manometer height	inch
H_v	Velocity head	psi
k	Thermal conductivity	Btu/hr-ft-^oF
K	Loss coefficient	- -
L	Length	inch
N_{Nu}	Nusselt number hD/k	- -
N_{Pr}	Prandtl number, $c_p \mu/k$	- -
N_{Re}	Reynolds number, $\rho VD/\mu$	- -

Nomenclature (cont'd)

Symbols	Descriptions	Dimensions
ΔP	Pressure drop	psi
q''	Heat flux	$Btu/hr\text{-}ft^2$
Q	Heat load	Btu/hr
R	Thermal resistance	$hr\text{-}ft^2\text{-}^oF/Btu$
T	Temperature	^oF
$(\Delta T)_{\ell m}$	Log-mean temperature difference	^oF
U	Overall heat transfer coefficient	$Btu/hr\text{-}ft^2\text{-}^oF$
V	Average velocity	ft/sec
W	Flow rate	lb/hr
ρ	Density	lb/ft^3
μ	Viscosity	lb/hr-ft
ϵ_m	Eddy diffusivity for momentum transfer	ft^2/hr
ν	Kinematic viscosity	ft^2/hr
ϕ	Function defined in equation (14)	- -

Subscripts

A	Auxiliary flow
an	Annulus
i	Inside, inlet
NaK	NaK flow, static NaK layer
o	Outlet, outside
P	Primary flow
s	Shell-side,flow, shell
ss	Stainless tube
t	Tube-side flow, Tube
W	wall

ABSTRACT

Analysis and design was performed for the SNAP-8 auxiliary loop heat exchanger. The heat exchanger will transfer 100 KW_t and operate at a maximum temperature of 1300°F. A shell side pressure drop of 0.27 psi was achieved as a result of shell side flow model tests. The design incorporates a double containment feature such that no single containment wall failure will permit mixing of the flowing NaK streams.

Two prototype heat exchangers were fabricated and delivered.

I. SUMMARY

The General Electric Company has conducted the design and fabrication of Prototype Auxiliary Loop Heat Exchangers (ALHE) for the SNAP-8 Power Conversion System. During system startup the ALHE provides an initial heat load for the reactor and preheats the boiler to turbine vapor line. During system shutdown the ALHE removes heat from the primary NaK loop. The ALHE is capable of transferring 100 KW_t and operates at a maximum temperature of 1300°F. It consists of a primary NaK loop shell and two separate flow passages on the auxiliary loop side for connection to two different power conversion systems. The design incorporates a double containment feature such that no single containment wall failure will permit mixing of the flowing NaK streams. The unit is made entirely of Type 316 stainless steel.

The ALHE was designed as a prototype in accordance with AGC - Specification 10622. In addition to the heat transfer requirements, the allowable pressure drop on the primary loop side (shell) was only 0.15 psi. Considerable effort was expended to meet this goal, including several model flow tests, but the final design resulted in a compromise between good heat transfer characteristics and low pressure drop such that the latter was 80% higher than the target.

A thermal analysis was performed and served as input to the thermal stress analysis. An environmental stress analysis was performed to insure that the unit could survive both launch and lunar landing loads. Both stress analyses indicated adequate margins of safety.

Stringent quality control measures were incorporated in material procurement, manufacturing, and inspections. The final assembly was subjected to quality conformance verification including proof pressure testing, flow testing, and cleaning to Level 5 of AGC-STD-1191B.

Page intentionally left blank

II. INTRODUCTION

A system that will produce a continuous electrical power supply is required for long-term space mission applications. One such system, presently under development, is the SNAP-8 power system. The basic SNAP-8 system is designed to produce a minimum of 35 kilowatts of usable electrical energy. The eutectic mixture of sodium and potassium (NaK-78) is used in both the reactor primary loop and heat rejection loop. During system startup an auxiliary loop heat exchanger (ALHE) provides an initial heat load for the reactor and preheats the boiler to turbine vapor line. During system shutdown the ALHE removes heat from the primary loop. The effort described in this report is aimed at providing a prototype ALHE for the SNAP-8 ground system test in the NASA Plum Brook Space Power Facility.

The final effort includes thermal, hydraulic, and stress analysis of the heat exchanger and fabrication of two prototype units. General discussions of design approaches for a liquid metal shell-and-tube type heat exchanger are presented in Section IV. Prediction of liquid metal heat transfer coefficients and analysis of heat exchanger hydraulic and flow distribution problems are definitely not in "handbook" design category at the present time even for single phase flow in tubes. A variety of theoretical and empirical predictions are available in the literature, but these predictions do not agree for a specific application and are further restricted to specific thermal and geometric boundary conditions. Considerable experience and careful evaluation are thus required to select and modify the available relationships to establish a particular design.

Presented in Section IV are the analytical thermal and hydraulic considerations for liquid metal heat exchangers consisting primarily of an analytical evaluation of the shell and tube side heat transfer coefficients and pressure drop as well as the uncertainties associated with these predictions. Complex problems such as shell-side flow distribution, shell-side temperature and heat flux asymmetry, the thermal shock protection and the selection of low pressure drop flow mixing promoters are also discussed.

Shell-side flow frictional characteristics and flow distribution are potential problems in the present heat exchanger design. These potential problems are created by two aspects of the heat exchanger specifications: (1) the very low (0.15 psi) allowable shell-side pressure loss and (2) the fact that only one of the two auxiliary NaK loops will be operated at one time, which creates temperature and heat flux asymmetry. These problems are generally very difficult to treat analytically and recourse to experimental results obtained from model flow tests using water or other easy fluids is useful and necessary.

A geometrically similar (except the curvature) ALHE shell-side flow model was built by Nuclear Systems Programs and a series of shell-side flow hydraulic tests were carried out. Wire coils and half-moon shaped flow blockages were used to promote the shell-side flow mixing. Frictional losses were individually measured for the inlet, outlet, spacers and axial flow sections. Test results and correlations are discussed in Section IV.

Step-by-step design calculations for the 100 KW NaK-NaK ALHE are provided in Section V.

III. MECHANICAL DESIGN

The SNAP-8 ALHE assembly as shown in Figure 1 is comprised of a dual-set of nested stainless steel tubes housed within a thick-walled stainless steel shell. The nested tubes, called the heat rejection loop tubes, are supported by wire brackets within the outer shell which carries the primary loop flow. Suitable connectors are provided to allow fluid flow in the primary and auxiliary loops without fluid exchange between these loops. The assembly is designed such that thermal energy from the primary loop is conducted to the auxiliary loop, which functions as the heat rejection circuit.

The primary loop shell is 5 in. OD x .120 in. wall. The diameter was chosen to meet the low pressure drop requirements and the .120 in. wall thickness provides adequate corrosion allowance and strength. The primary shell end caps are bored through at two places to accept the inlet and outlet fittings of the auxiliary tubes. The fittings have been designed with respect to thermal stresses during the startup transient. The fittings create two regions of static NaK and move the fitting ends farther from the primary tube to decrease thermal gradient stresses. A 0.625 in. diameter thermal sleeve inside the inner auxiliary tubes also decreases thermal stresses by heating the inlet NaK slightly before it impinges on the inner tube walls. The primary tube consists of three main sections to facilitate fabrication and assembly. A 3/8 in. diameter wire coil insert is welded to the inner wall of the shell to provide proper flow distribution and to enhance heat transfer. Two wire supports are welded inside the primary shell to restrain the auxiliary tubes during periods of shock and vibration. The supports are located adjacent to shell welds so that they are accessible for attachment during fabrication. The supports minimize flow blockage and provide relatively large restraint which is nearly equal in all directions. The adequacy of the supports was demonstrated in laboratory tests during the course of the program.

The auxiliary tubes have double walls to prevent the failure of any single weld from allowing primary loop fluid to mix with secondary loop fluid. The double walls also decrease the startup and shutdown

thermal gradients and shock. The 1.25 in. OD tube dimensions were chosen to give acceptable pressure drop and heat transfer area. The 1.5 in. OD tube was chosen to contain the smaller tube with a minimum blockage of primary tube flow.

All the components are designed to allow reliable inspections of the seal welds. The only exception to this is at the shell end caps where the HRL tubes penetrate. In this case it was not possible to obtain good radiographs, therefore, trial welds were made and inspected before the final assembly was attempted. This was essential to meet the quality assurance provisions and to insure zero NaK leakage.

A. AXIAL TEMPERATURE DISTRIBUTION

Axial temperature distributions for the tube, annulus and shell can be calculated by heat balance equations using the known NaK flow temperatures at both end points of the heat exchanger. Referring to the sketch below, the heat transfer equation gives, for any local axial increment ΔL,

$$q'' = U \frac{(T_{NaKp} - T_{NaKA})_i - (T_{NaKp} - T_{NaKA})_{i+1}}{\ell n \left[\frac{(T_{NaKp} - T_{NaKA})_i}{(T_{NaKp} - T_{NaKA})_{i+1}}\right]} \quad (1)$$

and heat balance equations

$$q''_A = \frac{W_A C_{PA}}{(\pi D_i)\Delta L} \left[(T_{NaKA})_{i+1} - (T_{NaKA})_i\right] \quad (2)$$

$$q''_p = \frac{W_p (C_p)_p}{(\pi D_i)\Delta L} \left[(T_{NaKp})_{i+1} - (T_{NaKp})_i\right] \quad (3)$$

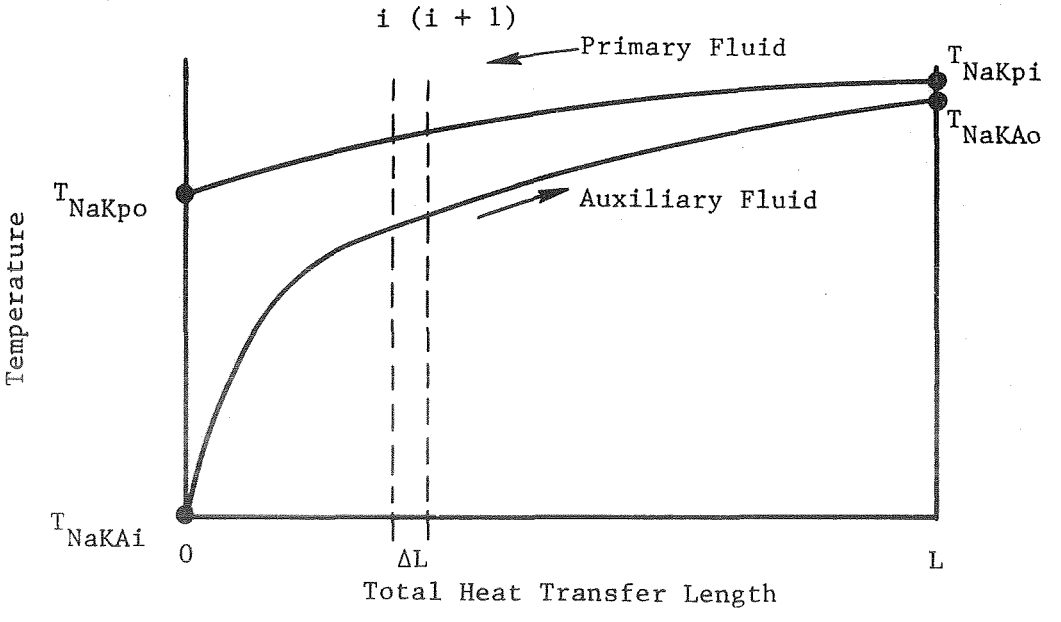

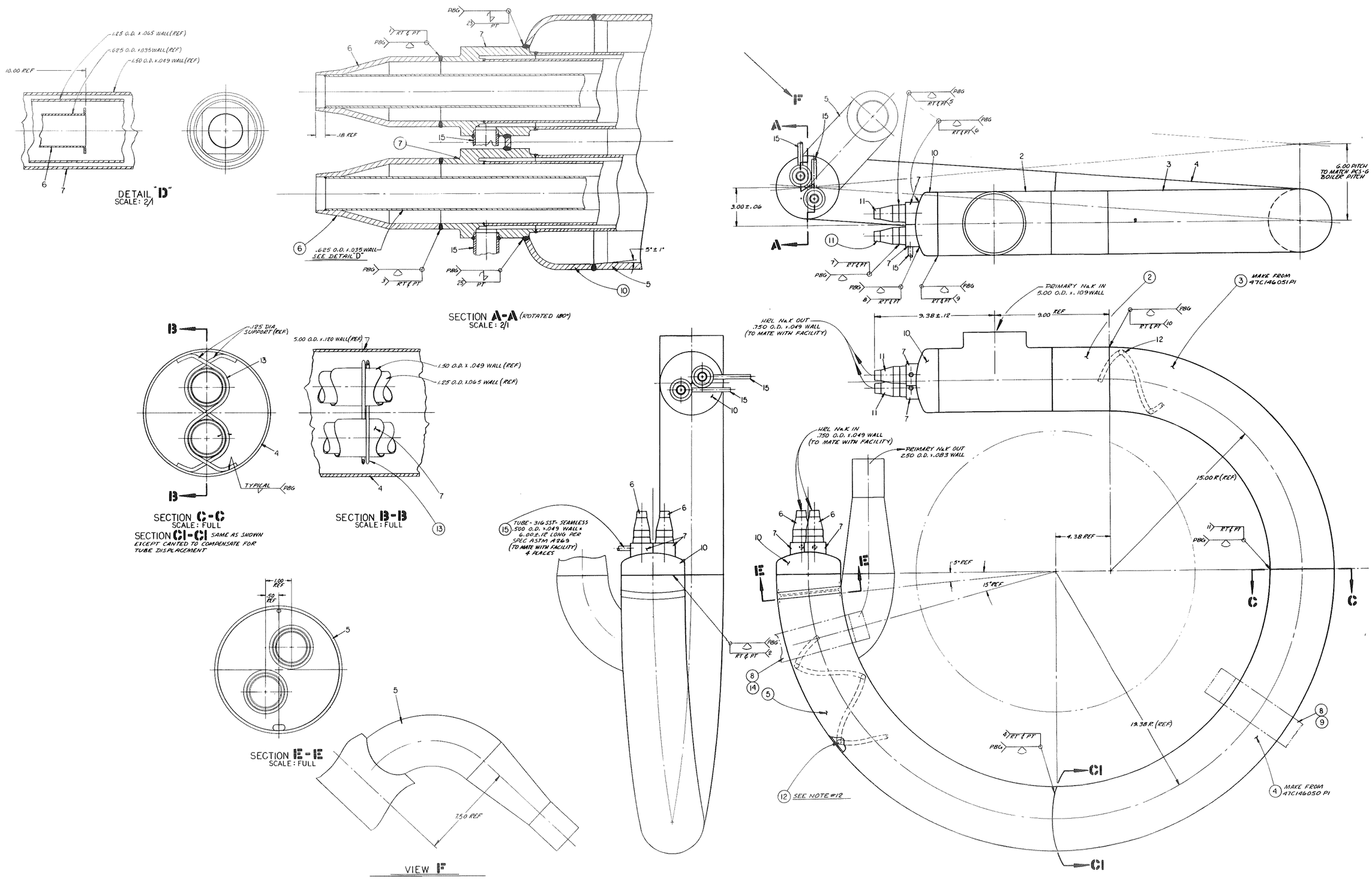

Figure 1. SNAP-8 Auxiliary Heat Exchanger. (Dwg. No. 47R199403)

Page intentionally left blank

The calculation proceeds from the auxiliary NaK flow inlet end where $T_{NaKpi} = 1240°F$ and $T_{NaKAi} = 110°F$. Then q" can be calculated by assuming values for $(T_{NaKp})_{i+1}$ and $(T_{NaKA})_{i+1}$ from equation (1). Using this calculated q", new values for $(T_{NaKp})_{i+1}$ and $(T_{NaKA})_{i+1}$ can be calculated from equations (2) and (3), respectively, by setting certain appropriate values for ΔL. The accuracy of this predicted temperature distribution depends solely upon the value of ΔL chosen. For the present calculation an increment of 0.05 of the total length was used. Finally, an iteration process was used to converge the calculated $(T_{NaKp})_{i+1}$ or $(T_{NaKA})_{i+1}$ to their assumed values. Calculations are repeated for the next axial position until the auxiliary NaK flow exit point is reached. Again the value for C_p for either primary or auxiliary NaK flow should be evaluated at the average temperature over that increment.

Furthermore, the temperature distribution along the tube wall, static NaK layer and annulus wall can be estimated by calculating the temperature drop across these thermal barriers. Once the axial temperature distribution for primary and auxiliary NaK flow are determined then the temperature of the inner tube wall can be calculated for any local axial position as follows,

$$(T)_{ti} = (T_{NaKp} - T_{NaKA}) \frac{U}{h_A} + 110 \qquad (4)$$

Similarily, calculation of tube outer wall temperature can be calculated as

$$(T)_{to} = (T_{NaKp} - T_{NaKA}) \frac{U}{h_{ss}} + T_{ti} \qquad (5)$$

where h_{ss} is the equivalent heat transfer coefficient for the tube wall and can be obtained from the equation listed in Part V.

Temperatures at the inner and outer surfaces of the annulus can be calculated in a similar way. Results are presented in Figure 2 for the following two cases.

(i) 1.25-inch OD tube with 0.030-inch wall
1.5-inch OD annulus with 0.050-inch wall
5-inch OD shell with 0.090-inch wall

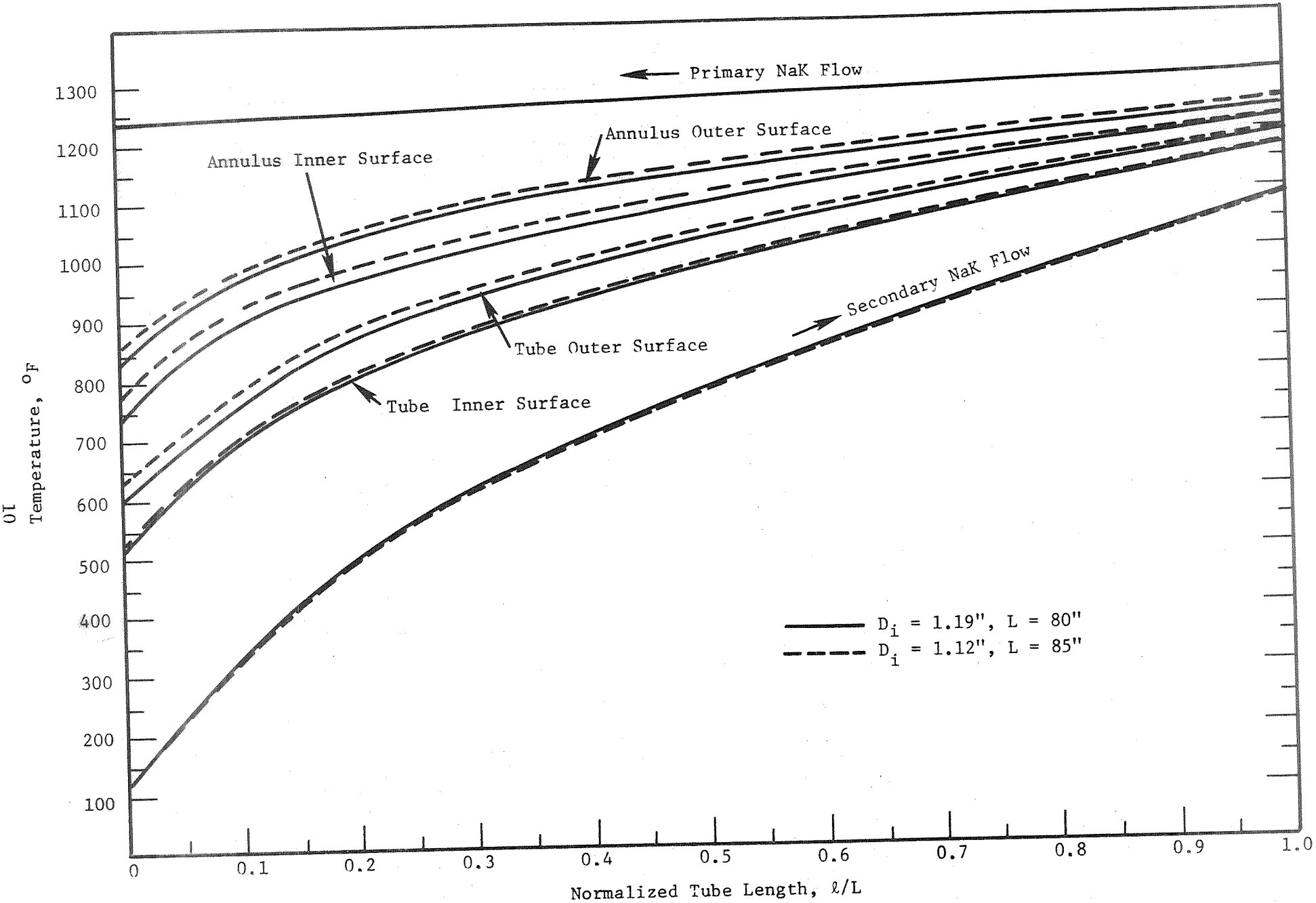

Figure 2. Axial Temperature Distribution of NaK-to-NaK ALHE.

80-inch total length ($\Delta L = 4.0$)

(ii) 1.25-inch OD tube with 0.065-inch wall
1.5-inch OD annulus with 0.050-inch wall
5-inch OD shell with 0.120-inch wall
85-inch total length ($\Delta L = 4.25$-inch)

As shown in Figure 2 , the severe point, as the thermal stress is concerned, is at the auxiliary NaK flow inlet where the temperature difference between tube NaK flow and tube inner wall is approximately 400°F by the present calculation. Hence, an additional tube with smaller diameter is necessary and is installed in this short region as a thermal protector. The second case shown above was selected for the thermostructural analysis, although, as shown in Figure 2, the temperature profiles are only slightly different for the two cases. It should be noted that the final design produced a total HRL active tube length of about 90 inches, but the thermostructural analysis was not corrected since the differences in stresses would be insignificant.

B. THERMOSTRUCTURAL ANALYSIS

The thermostructural analysis was conducted to determine the combined state of stress at various locations in the primary and auxiliary loop due to the operating pressure and temperature distributions.

Method of Analysis

The thermostructural analysis that was conducted by assuming that linear thermoelasticity theory was valid for the temperature ranges under consideration. Accordingly, plasticity and creep effects were not accounted for in the analysis. The MASS finite element program (Ref. 1) was used to determine the thermal stresses in the auxiliary loop heat exchanger. A suitable mathematical model was constructed (Fig. 3) which would suitably represent the design being analyzed. The analytic model shown in Figure 3 was divided into twelve finite meridional elements with the actual curvature of the designed assembly. In Table 1 are recorded the nodal or element interface locations at the center line in terms of Cartesian coordinates. This model includes the interaction of the tubes connected at the ends and the interaction between the 5 inch OD shell and the 1.5 inch OD tube at the three spring supports,

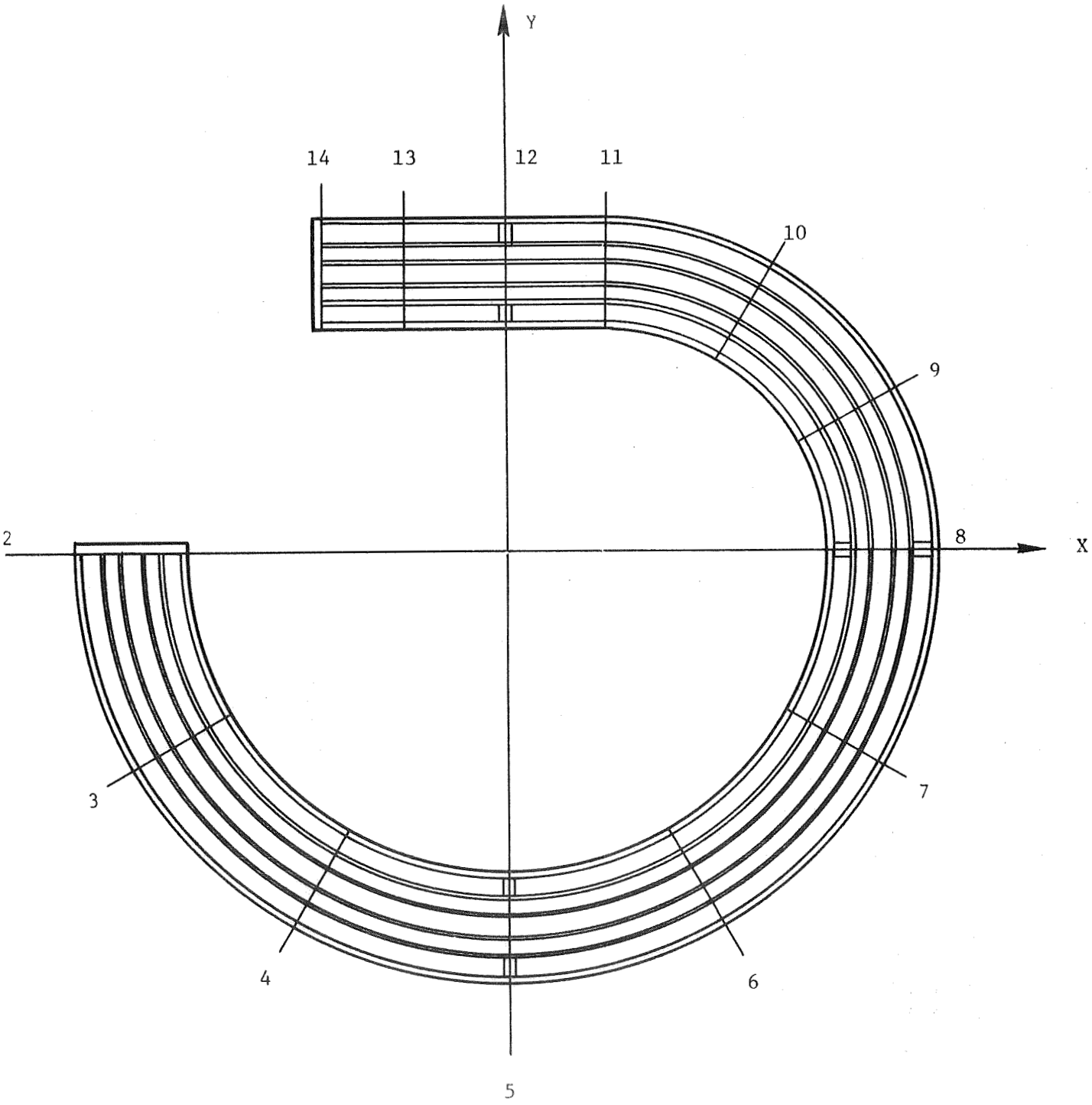

Figure 3. Analytic Model of SNAP-8 Auxiliary Heat Exchanger.

TABLE 1

CARTESIAN COORDINATE SYSTEM OF MODEL

JOINT NO.	X	Y
2	-19.38	0
3	-16.88	- 9.62
4	- 8.76	-17.26
5	0	-19.38
6	9.62	-16.88
7	16.88	- 9.62
8	19.38	0
9	17.37	7.50
10	11.76	13.0
11	4.38	15.0
12	0	15.0
13	- 4.5	15.0
14	- 9.12	15.0

which were assumed to be infinitely stiff, located at the nodal points 5, 8 and 12.

The analysis performed on the auxiliary loop heat exchanger included the temperature dependency of the mechanical material properties as shown in Table 2. The references from which these properties were obtained are contained in Table 3.

The thermostructural analysis was conducted by assuming a uniform temperature for each element with the temperature varying from element to element in the meridional direction to account for the temperature distribution in the direction of fluid flow. It was assumed that asymmetric temperature variations in the hoop direction were negligible and that the principal temperature gradients occurred through the tube thickness and in the meridional direction.

The hydrostatic pressure stresses were assumed to be uniform in the curved tubes, since the effect on the stresses due to pressure drop is negligible. The meridional and hoop pressure stresses, which vary in the hoop direction, due to tube curvature, were determined and superimposed on the thermal stresses.

The discontinuity stresses occurring during a transient thermal condition where the 1.25 OD and 1.5 OD tubes attach to the connector were evaluated by computing the thermal mismatch between two cylinders, as shown in the Appendix, which was based on the method of analysis presented in Reference 2.

Analytic Results

The results of the analysis conducted to determine the deflections of the tube assemblies at their center line are contained in Table 4. The important result obtained in this calculation is that thermal expansions could occur such that the 1.25 inch OD tube could press against the inside radius of the 1.5 inch OD tube in a region between the joint locations 7 to 8. This would mean that metal to metal contact is possible due to the small radial clearance between the OD of the 1.25 inch tube and the ID of the 1.5 inch tube. This is not a serious structural condition. It may be eliminated by off-setting the 1.25 OD tube outward of the curvature center line by 10 mils to compensate for this expansion behavior.

The results of the thermal stress analysis of the 1.5 OD tube, 1.25 OD tube and 5 inch OD shell are contained in Tables 5, 6, and 7, respectively. It is shown that both the primary and secondary stresses

TABLE 2

MATERIAL PROPERTIES - 316 STAINLESS STEEL SEAMLESS TUBING

TEMP.	A σ_{tu} x 10^{-3} PSI	B σ_{tu} x 10^{-3} PSI	C σ_{y} x 10^{-3} PSI	D S_M x 10^{-3} PSI	F $3S_M$ x 10^{-3} PSI	G E x 10^{-6} PSI	H σ x 10^{6} IN/IN/^{o}F
100	75	85.5	38.5	20	60	28.3	9.2
200	75			20	60		
300	71.6	76.0	31.0	20	60	27.2	
400	70.0			19.4	58.2		
500	69.0	73.5	27.0	18.2	54.5	26.4	
600	68.5			17.1	51.4		10.0
700	68.0	72.5	24.0	16.2	48.6	25.6	
800	67.0			15.6	46.9		
900	64.0	71.0	22.0			23.8	10.1
1000	56.0						
1100	41.6	66.5	20.5			22.5	
1200	27.2						
1300	12.0	46.0	19.5			21.0	10.3

TABLE 3

MATERIAL PROPERTY SOURCES

I ASME SECTION I, POWER BOILERS, A-24 - TABLE PG-23.1

COLUMN A - σ_{tu}: ULTIMATE TENSILE STRESS

II ASME SECTION III, NUCLEAR VESSEL, CLASS A, TABLE N-421

COLUMN D - S_M: DESIGN STRESS INTENSITY VALUE

F - $3S_M$

III USS CORP., NATIONAL TUBE DIVISION, PIPE & TUBES FOR ELEVATED TEMPERATURE SERVICE, BULLETIN #26

COLUMN B σ_{tu}: ULTIMATE TENSILE STRESS

C σ_y: .2% OFF-SET YIELD STRESS

G E: YOUNG'S MODULUS IN TENSION

H α: COEFFICIENT OF EXPANSION

TABLE 4

TUBING RADIAL CLEARANCE ANALYSIS

JOINT	TRANSVERSE DEFLECTION 5" OD TUBE δ_1	1.5" OD TUBE δ_2	1.25" OD TUBE δ_3	RELATIVE TRANSVERSE BETWEEN 1.5" OD & 1.25" OD TUBES $\Delta = \delta_2 - \delta_3$	INTERFERENCE
2	-.144	-.144	-.144	0	None
3	-.249	-.216	-.237	-.021	None
4	-.354	-.323	-.308	+.015	None
5	-.406	-.407	-.332	+.075	Just Touching
6	-.417	-.395	-.322	+.073	Just Touching
7	-.373	-.355	-.277	+.078	+.003
8	-.293	-.293	-.211	+.082	+.007
9	-.187	-.142	-.128	+.014	None
10	-.079	-.016	-.047	-.031	None
11	0	-.021	-.006	+.015	None
12	0	0	-.003	-.003	None
13	0	-.003	-.008	-.005	None
14	0	0	0	0	None

TABLE 5

THERMOSTRUCTURAL ANALYSIS -

1.5 OD TUBING

JOINT	SEGMENT TEMP. °F	DEFLECTION IN δ_x	DEFLECTION IN δ_y	SUPPORT FORCES LBS. F_x	SUPPORT FORCES LBS. F_r	STRESS PSI X 10^{-3} PRIMARY MEMBRANE σ_θ	PRIMARY MEMBRANE σ_ϕ	SECONDARY THERMAL σ_θ	SECONDARY DISCONTINUITY σ_θ	SECONDARY DISCONTINUITY σ_ϕ	FACTOR OF SAFETY FS ASME	FACTOR OF SAFETY FS AGC-10622
2		-.144	-.196	-289	286	.6	1.224	20.3	18.0	16.0	1.15	.725
3	900	-.096	-.268					8.3				
4	1000	-.024	-.350					7.2				
5	1070	.055	-.407	0	-560			19.5			2.04	1.3
6	1100	.150	-.368					7.0				
7	1200	.238	-.299					5.6				
8	1140	.293	-.205	662	0			23.8			1.68	1.08
9	1150	.241	-.133					7.8				
10	1160	.170	-.078					14.4				
11	1170	.096	-.021					4.7				
12	1190	.046	0	500				19.7			1.97	1.26
13	1200	0	0					6.9				
14	1210	-.058	0			.6	1.22	9.47	4.0	3.0	2.84	1.82

TABLE 6

THERMOSTRUCTURAL ANALYSIS -

1.25 OD TUBING

JOINT	SEGMENT TEMP. °F	DEFLECTION IN		SUPPORT FORCES LBS.		STRESS PSI X 10^{-3}					FACTOR OF SAFETY	
						PRIMARY MEMBRANE		SECONDARY THERMAL	SECONDARY DISCONTINUITY		FS ASME	FS AGC-10622
		δ_x	δ_y	F_x	F_r	σ_θ	σ_ϕ	σ_θ	σ_θ	σ_ϕ		
2		-.144	-.196	-2	-.5	.625	1.27	.45	17.0	14.0	2.67	1.7
3	690	-.127	-.255					.103				
4	800	-.068	-.311					.62				
5	900	.004	-.332					.84				
6	950	.091	-.318					.82				
7	990	.169	-.262					.52				
8	1010	.211	-.176					.345				
9	1040	.205	-.100					.4				
10	1070	.158	-.035					.77				
11	1090	.086	-.007					.97				
12	1100	.041	-.003					.95				
13	1140	-.008	-.001					1.0				
14	1160	-.058	0	2.2	+.5	.625	1.28	1.06	4.5	4.0	6.6	4.23

TABLE 7

THERMOSTRUCTURAL ANALYSIS -

5.0 OD TUBING

JOINT	SEGMENT TEMP. °F	DEFLECTION IN δ_x	DEFLECTION IN δ_y	SUPPORT FORCES LBS. F_x	SUPPORT FORCES LBS. F_r	STRESS PSI X 10^{-3} PRIMARY MEMBRANE	SECONDARY THERMAL	SECONDARY DISCONTINUITY	FACTOR OF SAFETY FS ASME	FACTOR OF SAFETY FS AGC-10622
						σ_θ σ_ϕ	σ_θ	σ_θ σ_ϕ		
2		-.144	-.196			.35 .752				
3	1146	-.116	-.299							
4	1166	-.028	-.383							
5	1186	.070	-.407							
6	1206	.179	-.378							
7	1226	.263	-.294							
8	1246	.292	-.181							
9	1266	.269	-.091							
10	1282	.201	-.024							
11	1298	.11	0							
12	1310	.056	0							
13	1318	0	0							
14	1326	-.058	0			.35 .770			50.6	30.0

NEVER EXCEEDS 3 PSI

in the 1.25 OD tube and the 5 inch OD shell are small and, consequently, provide substantial factors of safety for all locations in the meridional direction. The states of stress in the 1.5 OD tube are at a higher level than those in the other two component tubes. These stresses are highest at the ends where the tube is attached to the inlet and outlet connectors, and where the tube is supported by the 3 spring wire supports. These constraints at these five locations increase the state of stress due to the bending stresses that are induced. When Reference 3 is used to determine the structural integrity criteria, it was found that the factors of safety exceed one and, accordingly, indicate a safe operating condition.

If the more conservative evaluation is performed using Reference 5, it was found that the factor of safety exceeded one for all cases except at joint 2 when the criterion is normalized in order to be compared to the ASME criterion. At joint 2, the meridional discontinuity stress $\sigma\theta$ of 18,000 psi was determined by assuming a 50°F temperature difference at the connection. This temperature difference is highly conservative for a transient heat conduction case and was used as an upper bound case. The use of the two criteria for determination of the factors of safety was for comparison purposes. The stresses determined by linear analysis provide a conservative analysis, and the introduction of inelastic effects in the determination of the stress will appreciably reduce the calculated stresses.

In Appendix A the criteria used in the analysis is presented in outline form. The correction factors and failure criteria used are based on References 3 and 5.

The results of the discontinuity stresses are shown in Figures 4 and 5 for the 1.5 OD and 1.25 OD tubes, respectively. The meridional and hoop stresses in the connector and the tube are shown as a linear function of the temperature difference between these two components. This analysis is determined by assuming a compatibility relationship of the displacement and slope at the jointure between the connector and the tube. The derivation of these relations are shown in Appendix A.

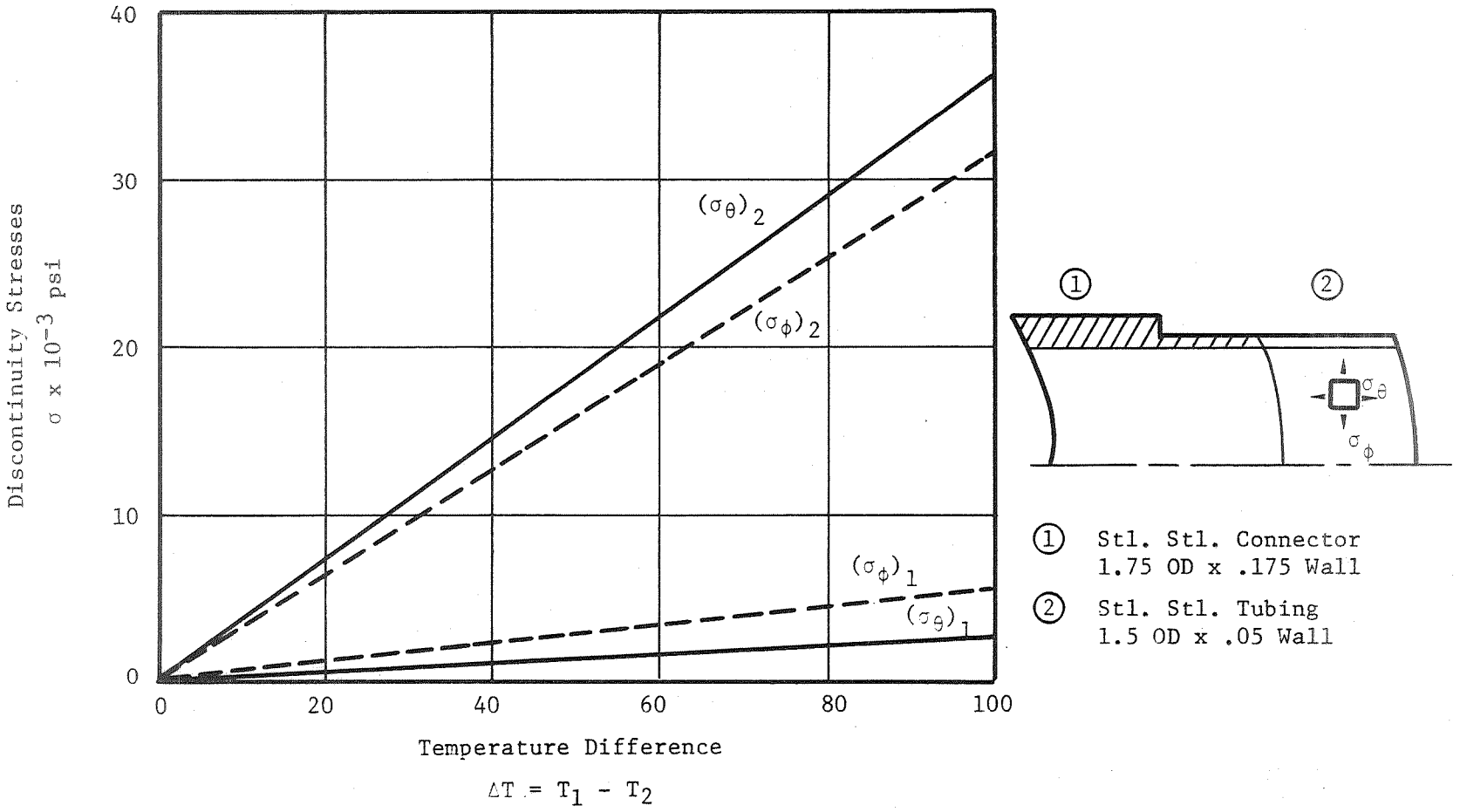

Figure 4. Discontinuity Stress - 1.5" OD Tubing.

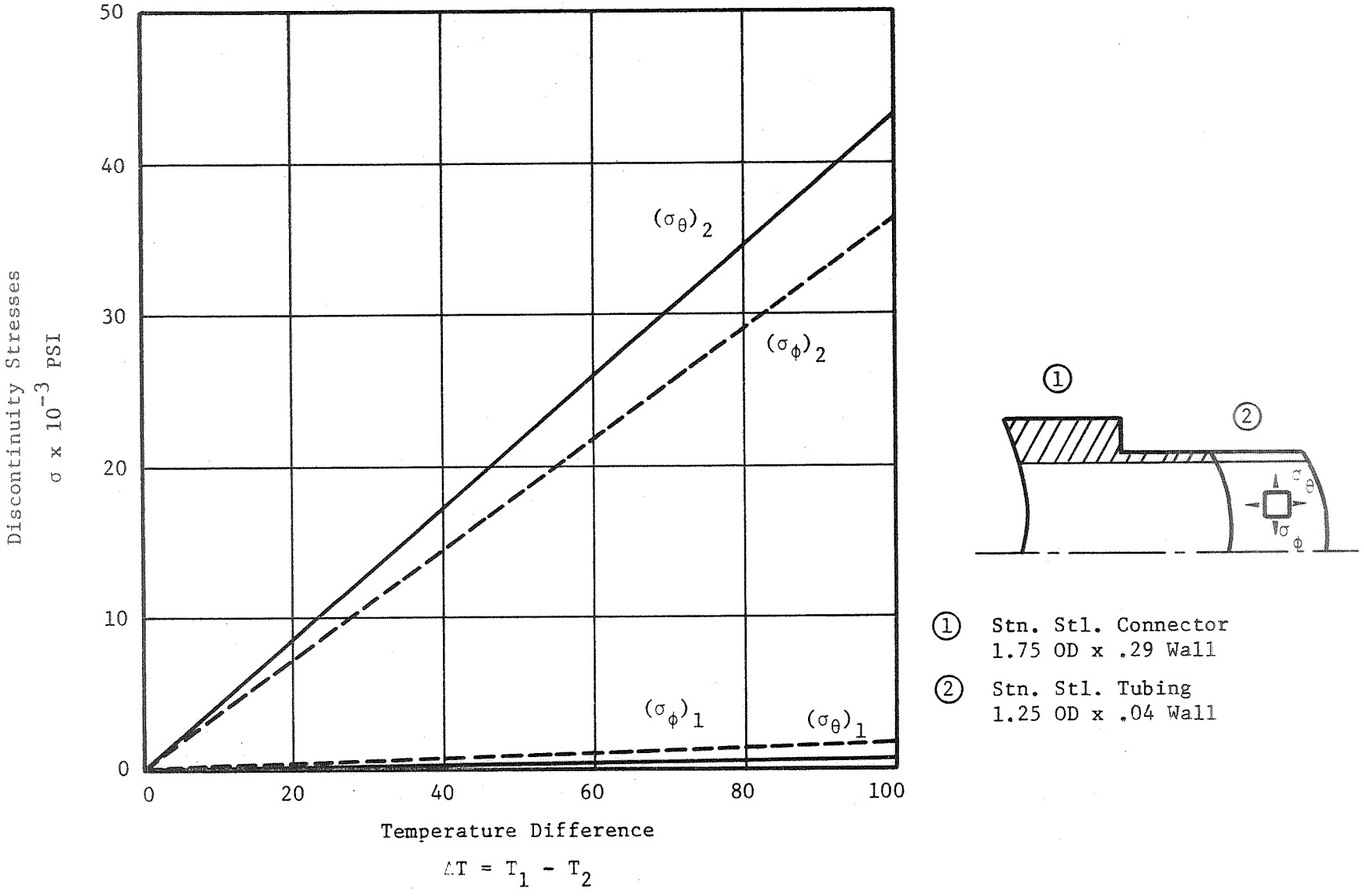

Figure 5. Discontinuity Stress - 1.25" OD Tubing.

C. DYNAMIC ANALYSIS

The dynamic environments specified for the design of the SNAP-8 ALHE are given in NASA Specification 417-2. The heat exchanger is required to withstand launch loads in the non-operating condition only. The random input spectra is shown in Figure 6. The shock pulse utilized is a half-sine-11 millisecond pulse with a peak acceleration level of 15 g's.

Due to limitations in program scope a detail dynamic model of the entire loop heat exchanger could not be developed. Since the secondary flow tube and the tube support appeared to be the most dynamic load critical component, and vertical excitation the most critical loading direction, a simplified model of a single secondary flow tube with intermediate supports was developed, as shown in Figure 7. This model was developed using finite element lumped mass approach (curve tube) with three degrees of freedom (coordinates) at each joint. Since this dynamic model was developed in a single plane the response to a vertical excitation (out of plane loading) will be uncoupled from any in plane response therefore allowing for the use of only three coordinates (vertical shear, in plane moment, and tube torsion) at each mass point. The intermediate wire supports were included by adding to the fixed and system stiffness matrices an additional linear support spring (K_X) at coordinates 2, 6 and 9 for the three (3) support model and 2, 6, 8 and 10 for the four (4) support configurations (Figure 7). For the three support configuration the response for support springs rates (K_X) of 360 lb/in and 1260 lb/in was determined. The four support spring configuration was analyzed for a support spring rate of 360 lb/in only. The support spring rate of 360 lb/in is more consistent with the present support spring design than the 1260 lb/in support spring.

Comparisons of the system natural frequencies for the three (3) support configuration with two support spring rates, the four (4) support configuration and an unsupported configuration are shown in Figure 8. It should be noted that variations in support configurations and spring rate show significant frequency variation only in the system first two natural frequencies. For the system higher frequency modes the natural frequency is relatively constant for all configuration variations.

Shown in Figure 9 is the system (single tube model) linear deflection (1 σ) due to a vertical random excitation and due to the half sine shock pulse. The maximum deflections occur in the area of mass point number 7 for all the configuration variations. The maximum deflection results from the random excitation for the minimum support spring rate configuration (3 σ deflection is .246 inches).

The end reactions and support loads due to vertical shock and random excitations are given in Figures 10 and 11 respectively. An estimate of the support loads considering the effects of the two secondary flow tubes due to the shock environment is given in 10 also. It was found that the major contributor to the support loads due to the shock pulse, was the system first mode whereas for the random input the major contributions occur in the higher frequency modes. In general, the maximum loads result from the random environment, with the maximum support loads of approximately 130 pounds occurring in support number 2 and 3 (Fig. 11) for the most rigid support spring rate. The maximum load occurring in support number 1 is relatively small (22.8 pounds) and this support was, therefore, removed with little or no consequence to the remaining support loads or end reactions.

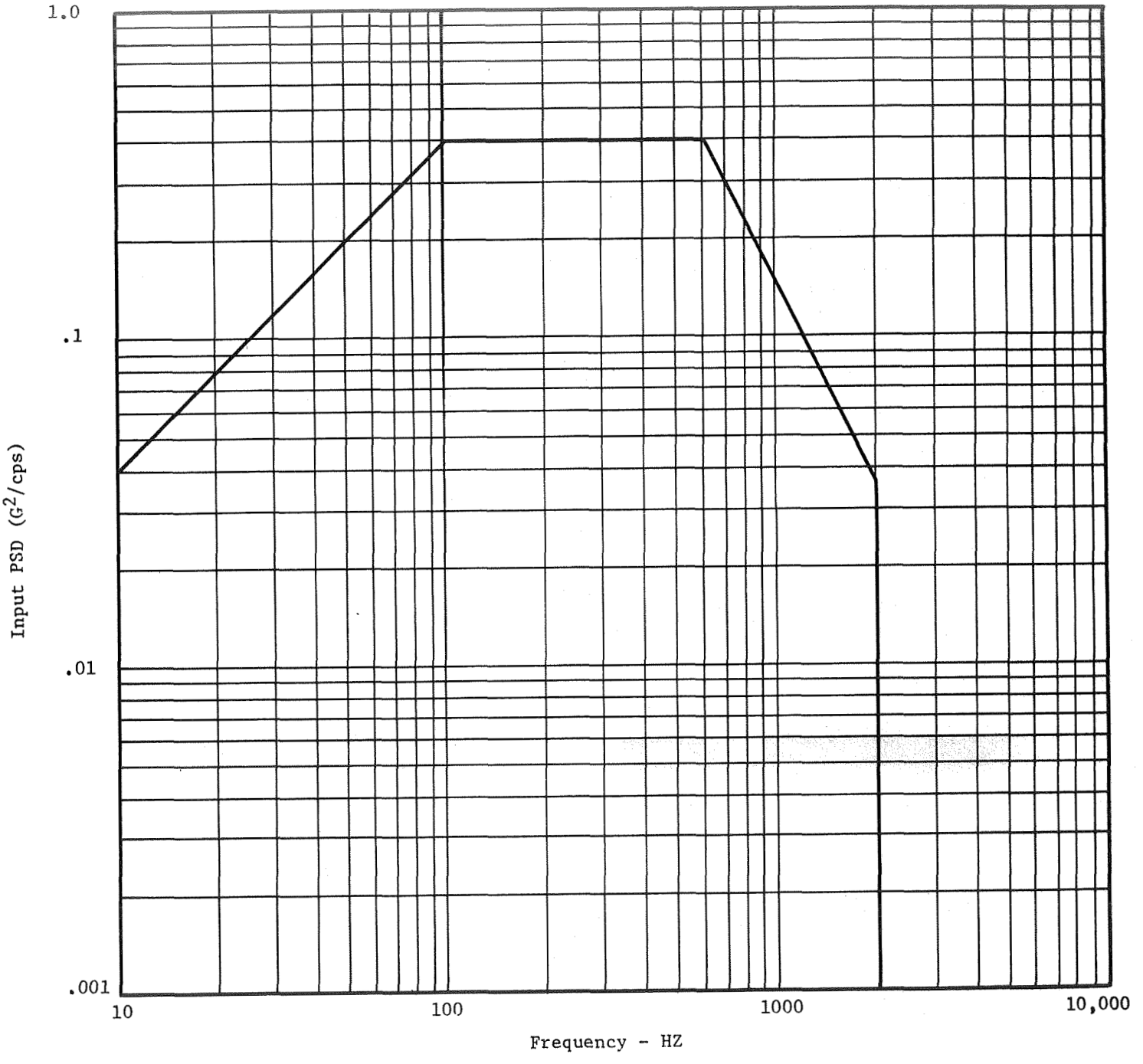

Figure 6. Random Vibration Specification.

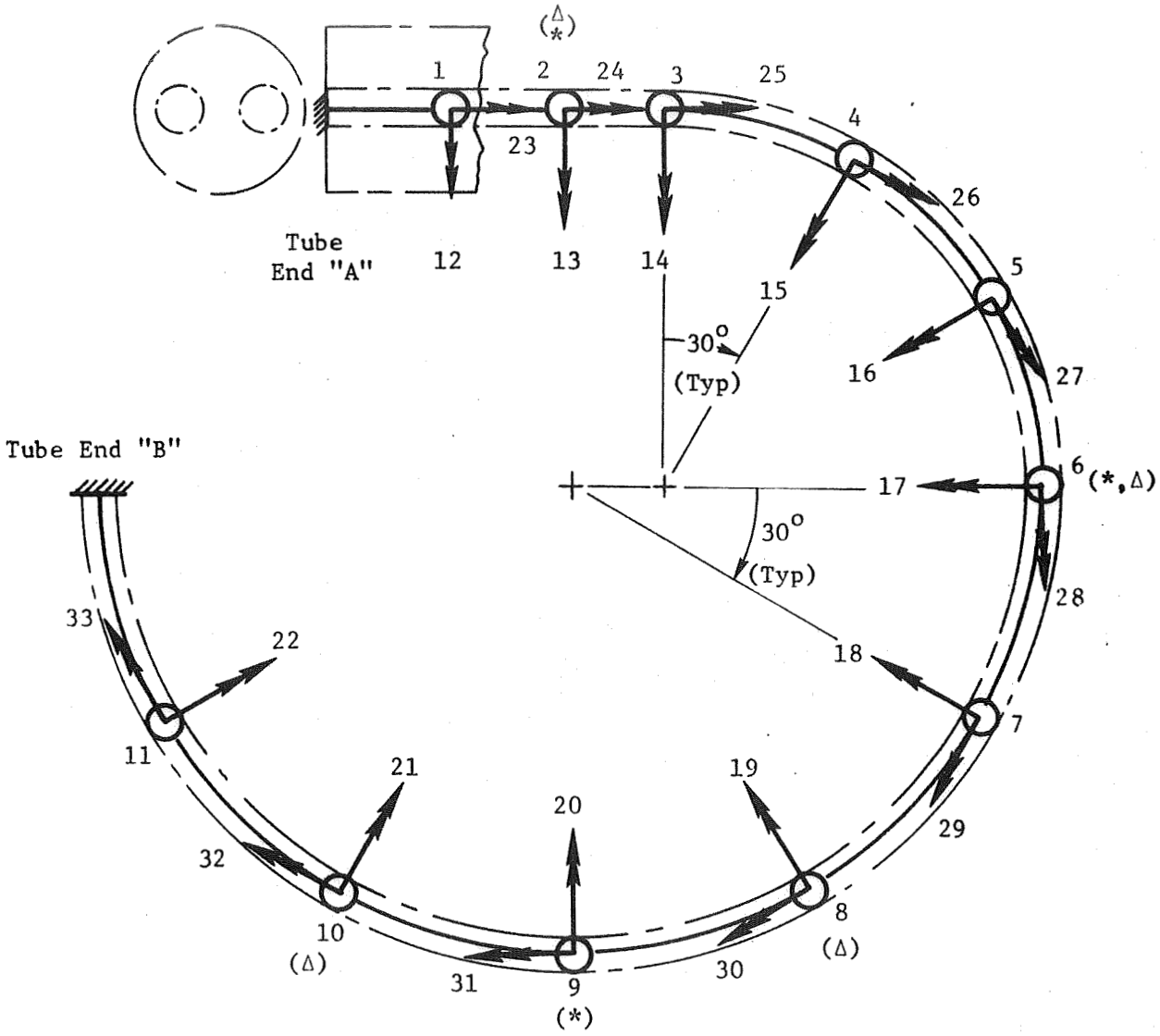

Vertical Deflection

Rotational Coordinate

Intermediate	(*)	3 Support Config.
Support Locations	(Δ)	4 Support Config.

Figure 7. Dynamic Model (Single Tube) System Coordinates.

CONDITION	3 INTERMEDIATE SUPPORTS		4 INTERMEDIATE SUPPORTS	NO INTERMEDIATE SUPPORTS
MODE NO.	K_x = 360 #/in	K_x = 1260 #/in	K_x = 360 #/in	
1	51.5	81.6	59.7	30.3
2	94.0	121.4	93.8	79.9
3	168.	173.4	172.0	165.9
4	284.5	293.2	286.6	280.9
5	416.0	423.6	415.2	413.1
6	575.0	578.4	575.5	573.7
7	741.4	743.9	741.7	740.4
8	919.2	920.6	919.5	918.7
9	1120.8	1121.3	1120.9	1120.6
10	1300.0	1300.4	1300.0	1299.5
11	1466.0	1466.6	1465.9	1465.7

Figure 8. System Natural Frequencies (CPS).

COORD. NO.	RANDOM INPUT 1σ DEFLECTIONS (IN) 3 SUPPORTS K_x = 1260	3 SUPPORTS K_x = 360	4 SUPPORTS K_x = 360	½ SINE PULSE MAX. DEFL. (IN) 3 SUPPORTS K_x = 1260	3 SUPPORTS K_x = 360
1	.001	.001	.001	.001	.001
2	.003	.004	.004	.002	.004
3	.006*	.007*	.008*	.004*	.008*
4	.012	.019	.019	.010	.024
5	.020	.038	.036	.020	.053
6	.034*	.060*	.055*	.033*	.034*
7	.052	.082	.072	.047	.113
8	.052	.081	.070*	.047	.112
9	.035*	.059*	.052	.032*	.082*
10	.019	.031	.028*	.016	.042
11	.007	.009	.008	.005	.011

*INTERMEDIATE SUPPORT LOCATIONS

Figure 9. A.L.H.E. Vertical Deflections - Single Tube.

LOAD LOCATION		K = 1260#/in	K = -360#/in
END		21. LBS	26.
SUPP 1	VERT V	5. LBS	2.8
SUPP 2	VERT V	41. LBS	30.
SUPP 3	VERT V	41. LBS	29.
END B	VERT V	126. LBS	313.
END A	MOM	162. IN/LB	243.
END B	MOM	562. IN/LB	1388.
END A	TORQUE	70. IN/LB	182.
END B	TORQUE	118. IN/LB	294.

SUPPORT LOADS FOR TWO TUBES

SUPP 1	8.5	4.8
SUPP 2	70.	50.
SUPP 3	70.	50.

Figure 10. Single Tube Response to 15 G - 11 M.S. ½ Sine Pulse.

LOAD LOCATION		K_x = 1260 ea.	K_x = 360 ea.	K_x = 360 ea.
END A	VERT V	88.2 LB	98.1	97.8
SUPP 1	VERT V	22.8 LB	8.1	8.1
SUPP 2	VERT V	127.8 LB	65.1	59.7
SUPP 3	VERT V	131.4 LB	63.6	
SUPP 4	VERT V	-	-	75.6
SUPP 5	VERT V	-	-	30.6
END B	VERT V	90.6 LB	87.3	79.6
END A	MOM	690.9 IN/LB	804.9	808.5
END B	MOM	977.1 IN/LB	1080.9	971.7
END A	TORQUE	266.4 IN/LB	416.4	364.8
END B	TORQUE	372.0 IN/LB	621.9	554.1

Figure 11. Response Loads Due to Random Environment.

Page intentionally left blank

IV. THERMAL AND HYDRAULIC DESIGN

A. HEAT TRANSFER ANALYSIS

The overall design approach for the NaK-NaK heat exchanger involves the determination of the tube length for any tentatively selected cross sectional geometry under the prescribed design conditions. For a given set of design parameters, i.e., flow rates, terminal temperatures and heat transfer load, a design analysis can be carried out to determine the effect on heat transfer and pressure losses of both shell and tube side flow by varying selected geometry parameters.

Considering the proposed tube and shell counterflow geometry, hot NaK flowing in the shell and cold NaK flowing in the tube, the heat transfer rate equation can be written as

$$dQ = U\,(T_s - T_t)\,dA \tag{6}$$

where the symbol dA denotes a differential element of the heat transfer surface area, and the subscripts s and t denote shell-side and tube-side respectively.

If the differential area dA refers to the surface area of the inner tube wall, then the overall heat transfer coefficient, U, can be written in terms of thermal resistance, R, between tube and shell as follows

$$U = \left[R_s + R_w + R_t\right]^{-1} \tag{7}$$

The term R_w indicates the combined wall thermal resistance. In the present design, the composite wall is formed by imposing a static NaK layer between shell and tube flows. A schematic drawing of such an arrangement is given in the following sketch:

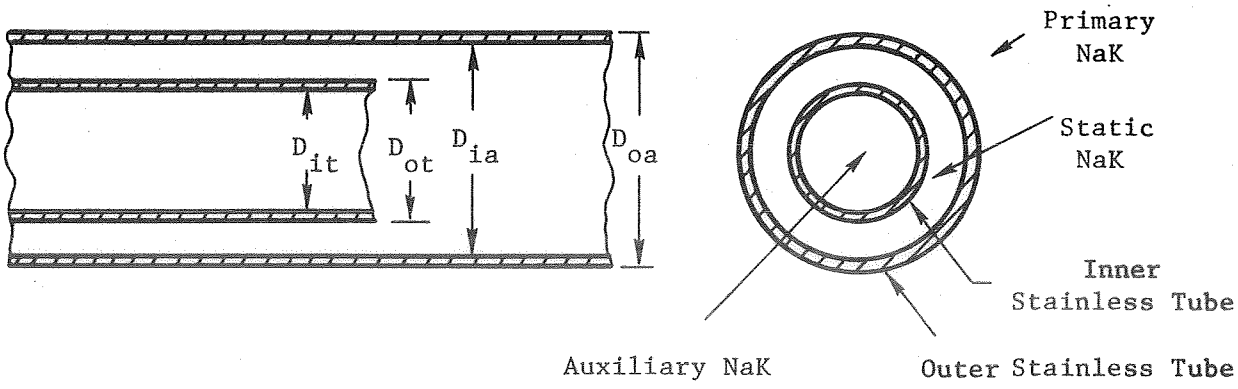

Sketch (a) Tube and Shell Double Pipe Heat Exchanger

Following the above sketch, the various contributions of thermal resistance referred to tube inside diameter can be evaluated as follows:

$$R_s = \frac{D_{it}}{h_s D_{oa}} \tag{8}$$

$$R_t = \frac{1}{h_t} \tag{9}$$

$$R_w = \frac{D_{it} \ln\left(\frac{D_{oa}}{D_{ia}}\right)}{2 k_{ss}} + \frac{D_{it} \ln\left(\frac{D_{ia}}{D_{ot}}\right)}{2 k_{NaK}} + \frac{D_{it} \ln\left(\frac{D_{ot}}{D_{it}}\right)}{2 k_{ss}} \tag{10}$$

where the thermal conductivities for the stainless steel tube and annulus, and the static NaK layer can be evaluated at appropriate mean temperatures.

As can be seen in Equation (7), the heat transfer coefficients of both side flows (h_s, h_t) must be known in order to calculate U. Once U is obtained, Equation (6) can be integrated to obtain the total surface area required for a given heat transfer load Q. By assuming the U and cross sectional dimensions independent of heat exchanger length, Equation (6) is integrated and the usual form

$$A = \frac{Q}{U(\Delta T)_{\ell m}} = \text{required heat transfer area} \tag{11}$$

The log mean temperature difference $(\Delta T)_{\ell m}$ can be written as

$$(\Delta T)_{\ell m} = \frac{(\Delta T)_o - (\Delta T)_i}{\ln\left[\frac{(\Delta T)_o}{(\Delta T)_i}\right]} \tag{12}$$

The subscripts i,o denote the terminal positions of the heat exchanger.

Prediction of h_t

During the past 20 years considerable work has been done to develop methods that would adequately predict forced convective heat transfer coefficients for liquid metal. Many useful and reliable predictions both analytical and experimental have appeared in the literature. However, for the design study, only liquid metal turbulent pipe flows were

reviewed. The early theoretical work of Martinelli on the liquid metal turbulent flow in a circular tube with uniform wall heat flux revealed that the Nusselt number of the flow is dependent upon flow Reynolds number and Prandtl number and a parameter ϕ, which is defined as the ratio of eddy transport diffusivities of heat transfer to momentum. Martinelli's final equation for h_t was very complicated for practical design use. However, later in 1951 Lyon[6] investigated Martinelli's result and found that for the case of Pr < 0.1, these results can be represented by the equation

$$Nu = 7.0 + 0.025\ (\bar{\phi}\ Re\ Pr)^{0.8} \tag{13}$$

$\bar{\phi}$ is a mean value of ϕ and can be taken as unity in most cases.

In 1955, Lubarksy and Kaufmann [7] summarized and reevaluated the experimental results of the various studies of liquid metal heat transfer in fully developed turbulent regions. They proposed an equation based on purely empirical grounds which correlates most of the heat transfer data and has the following form:

$$Nu = 0.625\ (Re\ Pr)^{0.4} \tag{14}$$

Equations (13) and (14) were used to predict h_t in the parametric design calculation. It is found that the two values of h_t calculated show reasonable agreement. However, Equation (14) gives a smaller value of h_t which serves as a conservative design approach.

Prediction of h_s

In the present design, the shell and tube arrangement is very far from the ordinary round tubes or annuli for which the predictions of h are generally available. For this reason one must accept the validity of the "equivalent concept" in predicting h for flow passages different from round tube or annuli. The equivalent concept generally implies that the heat transfer or pressure drop relations hold approximately the same as they do for the circular pipe or concentric annuli if the equivalent diameter of the passage other than circular pipe is employed in these relations.

In order for this approach to be valid, however, the velocity field must be reasonably uniform throughout the primary flow area.

Flow blockage baffles or some other mixing devices are necessary to assure this uniformity. Without such flow distribution baffles, the velocity field around the tubes would be quite nonuniform, leading to considerable uncertainty in heat transfer performance.

Based upon this argument, Equations (13) and (14) can still be used to predict h_s if the shell-side equivalent diameter is used to evaluate Nu and Re in these equations. The equivalent diameter, D_e, can be calculated by the following relation:

$$D_e = 4 \left(\frac{\text{Shell-side net flow area}}{\text{Shell-side wetted perimeter}} \right) \tag{15}$$

Besides Equations (13) and (14), several available semi-empirical correlations are quite useful to predict h for liquid metal flowing in an annuli as follows:

$$Nu = 5.8 + 0.02 \ (Re \ Pr)^{0.8}, \quad \frac{D_o}{D_i} \leq 1.4 \tag{16}$$

For annuli of diameter ratio greater than 1.4, the Liquid Metal Handbook recommends that

$$Nu = 0.75 \left(\frac{D_o}{D_i} \right)^{0.3} \left[7.0 + 0.025 \ (Re \ Pr)^{0.8} \right], \quad \frac{D_o}{D_i} > 1.4 \tag{17}$$

More recently, Dwyer[3] proposed the following equation for heat transfer through the inner wall of the annular passage:

$$Nu = (4.63 + 0.686y) + (0.02154 - 0.00043y) \ (\bar{\phi} \ Re \ Pr)^a \tag{18}$$

with $a = 0.752 + 0.0165y - 0.000\ 883y^2$

and $y = \dfrac{\text{outer radius}}{\text{inner radius}} = \dfrac{D_o}{D_i}$

The term $\bar{\phi}$ in Equation (18) is expressed as, due to Dwyer,[8]

$$\bar{\phi} = 1 - \frac{\frac{1.82}{Pr}}{\left(\frac{\varepsilon_\mu}{\nu} \right)_{max}^{1.4}} \tag{19}$$

The term $\left(\frac{\varepsilon_\mu}{\nu} \right)_{max}$ is furnished by Dwyer in Reference (8). One should

notice that the equivalent diameter concept still applies to these equations for annular passages, i.e., the outer diameter, D_o, must be replaced by D_e and D_e must be used in evaluating Nu and Re. One thing which should be kept in mind is that all the equations listed above for predicting heat transfer coefficients are based on the fully developed turbulent flow and uniform wall heat flux conditions. In other words, in the present design analysis effects due to flow development at the inlet, nonuniformity of heat flux and other thermal boundary conditions which deviate from the theoretical are not considered. Due to the lack of reliable information on these uncertainties, the equations listed above are still used to predict these coefficients. Maximum effort in flow passage design is required, however, to minimize deviations from the proper boundary conditions and a confirmatory NaK heat transfer test is the only certain way to obtain adequate data to demonstrate these results.

B. HYDRAULIC ANALYSIS

In most heat exchangers, turbulent flow outside of and parallel to the axis of a tube bundle is of frequent occurrence and pressure drop data specifically applicable to a particular geometry are not generally available in the literature. Furthermore, the calculation or prediction of the shell-side fluid-flow frictional characteristics when the fluid flows across the tube supporting spacers, turbulence promoters, and exit or inlet flow distribution devices is complicated by the fact that there is no analytical way to predict their loss coefficients. For this reason, model tests are also necessary in order to secure a dependable heat exchanger design.

In general, frictional losses are calculated as recommended by McAdams [9] by calculating a hydraulic equivalent diameter for the shell-side flow and subsequently using it as a round tube diameter in a conventional friction factor correlation equation. The pressure drop due to axial flow can be estimated by

$$(\Delta P)_{axial} = f_e \left(\frac{L}{D_e}\right) H_v \qquad (20)$$

where f_e ie the equivalent friction factor evaluated by employing D_e, and H_v is the shell-side flow velocity head.

The friction factor, f, can either be calculated by some appropriate correlation equations or by simply using the Moody curve as shown in Figure 12 .

Equation (20) is applicable for both shell and tube side flows for predicting axial frictional losses. In a recent SNAP-8 model multiple tube boiler shell-side hydraulic test, the results revealed that the shell-side friction factor is about 90% of the value calculated by using conventional correlating equations. The data are shown in Figure 13 .

For the shell-side flow passing obstacles, changes in passage directions and changes in passage cross sections, the conventional way for predicting these pressure losses is using an appropriate velocity head of shell-side flow multiplied by a loss coefficient, K. That is,

$$\Delta P = K H_v \tag{21}$$

There are no simple analytical means for prediction of the loss coefficient K for various complicated flow passages. Approximate predictions of these K's are generally obtained by summarizing rather complex combinations of contraction and expansion losses and turning losses. One can imagine that the uncertainty will increase as the flow passage becomes more complex. In the recent SNAP-8 model multiple-tube boiler shell-side hydraulic test, various shapes of spacers and flow baffles were tested and the results were generalized and presented in Figure 14 . For flow passages involving sudden expansion, sudden contraction and turning directions, Figure 15 to 17 cited from References (11) and (12) can be used to predict the loss coefficients.

One thing that appears very critical to the hydraulic design is the restriction of 0.15 psi shell-side allowable pressure drop. To keep under this limitation, very careful selection of tube and shell cross sectional geometries is required and very careful design is necessary regarding the tube supporting devices, inlet and outlet flow passages and shell-side turbulence promoters.

Shell-side flow maldistribution presents a serious problem in the design of liquid metal to liquid metal heat exchangers. Several sodium to sodium intermediate heat exchangers (IHX) designed for liquid metal

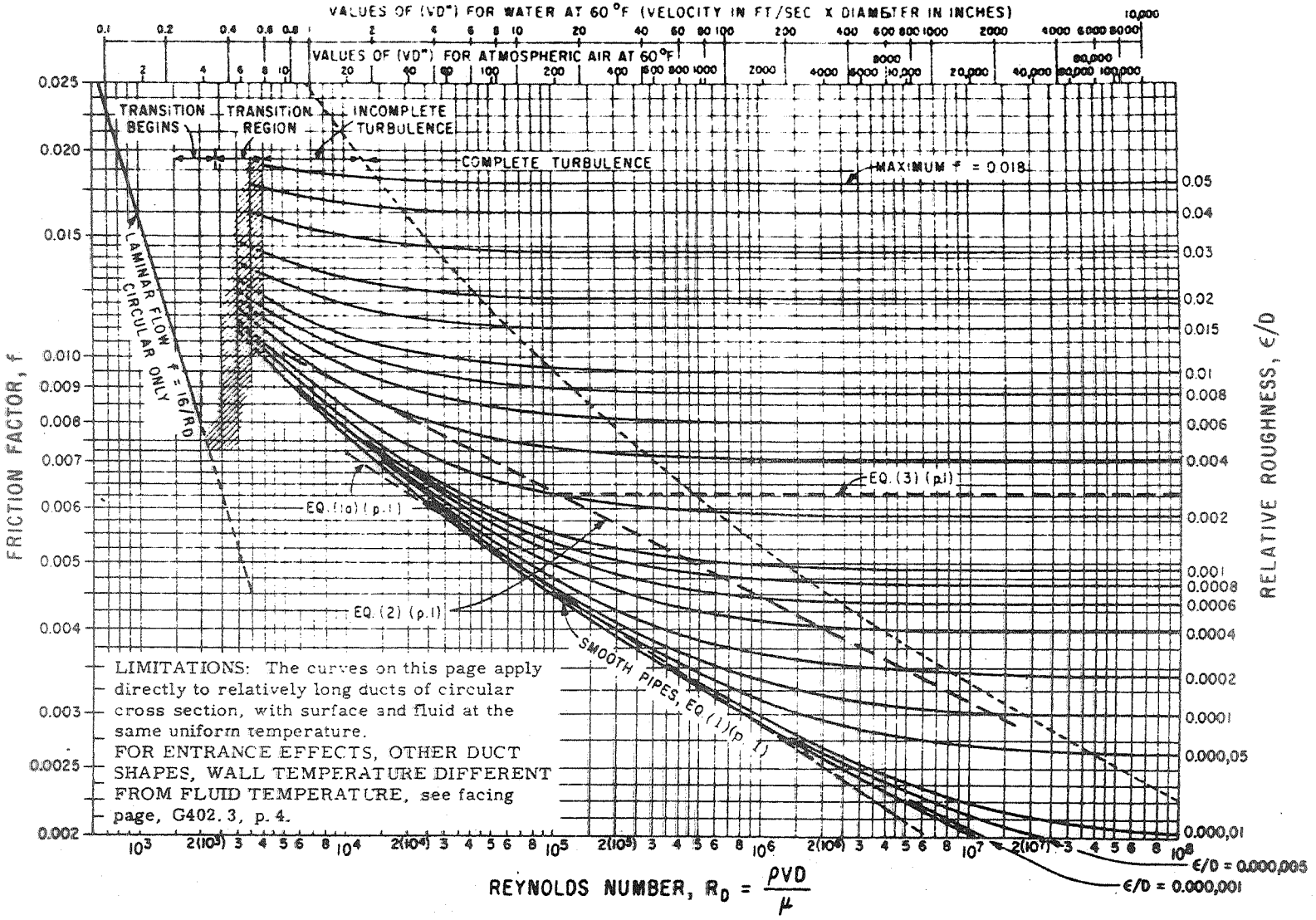

Figure 12. Moody Diagram for Friction Factor in Isothermal Pipe Flow.

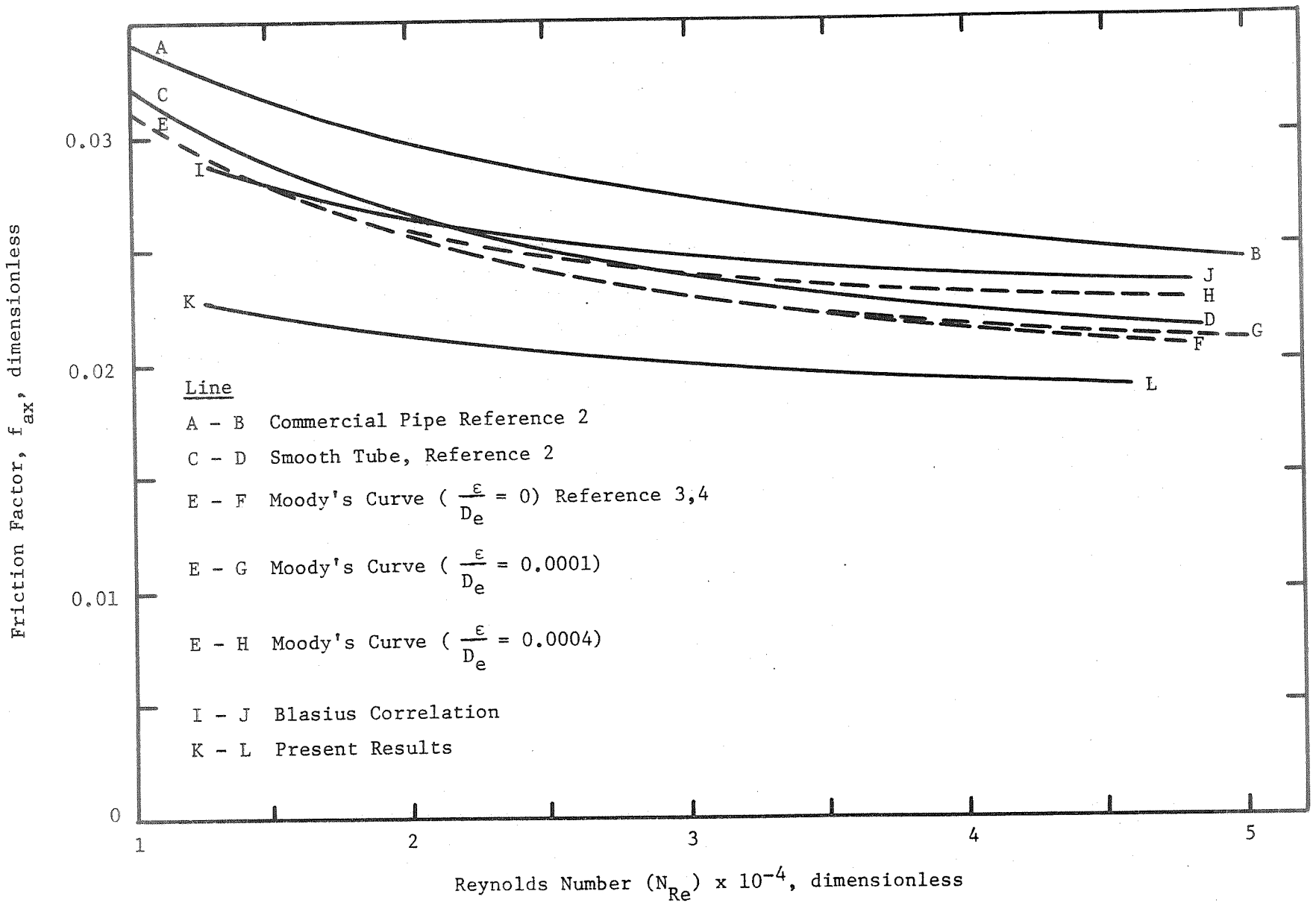

Figure 13. SNAP-8 Multiple-Tube Boiler Hydraulic Test Results.

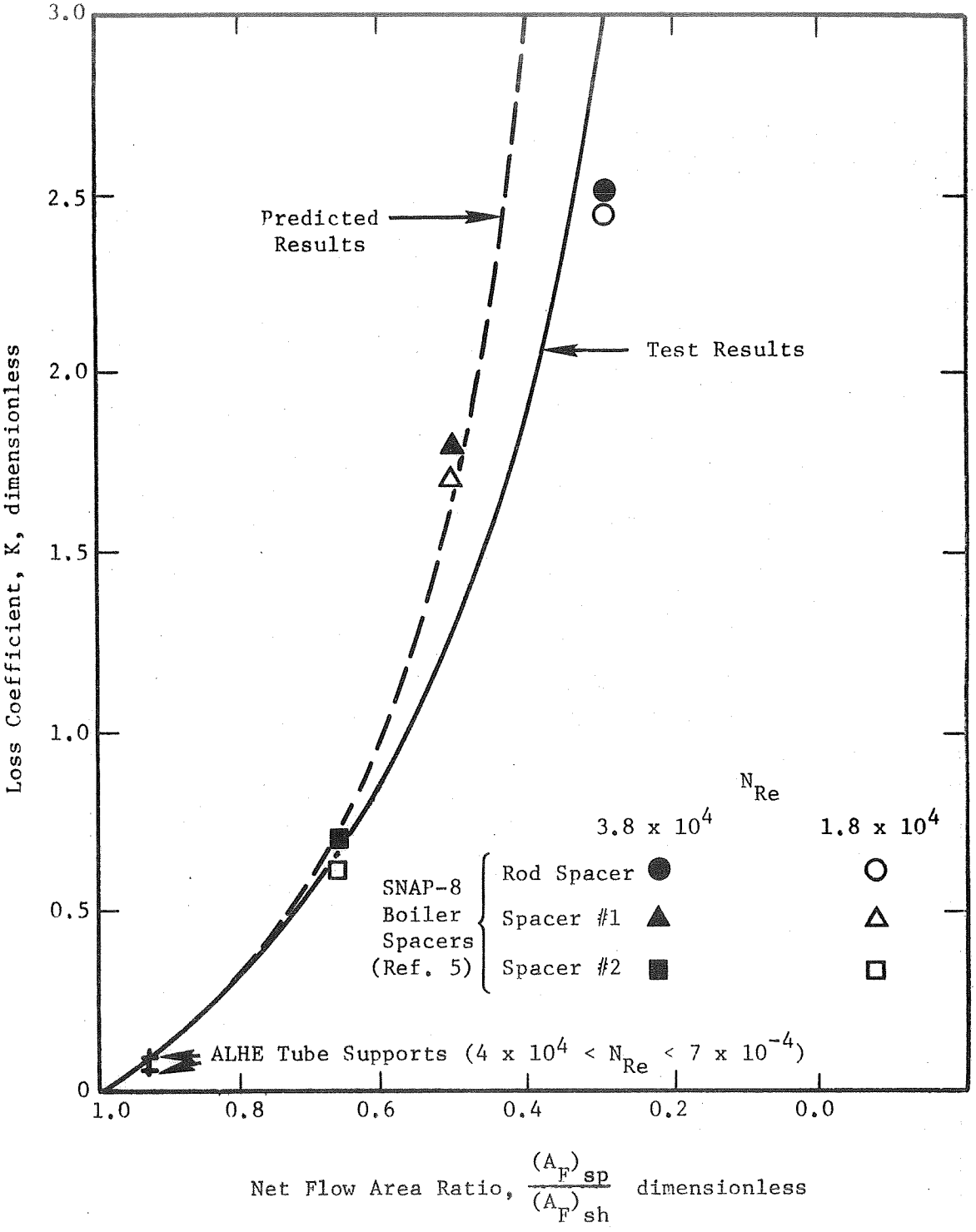

Figure 14. Spacer Loss Coefficient (Based Upon Upstream Shell-Side Velocity Head) as a Function of Net Flow Area Ratio.

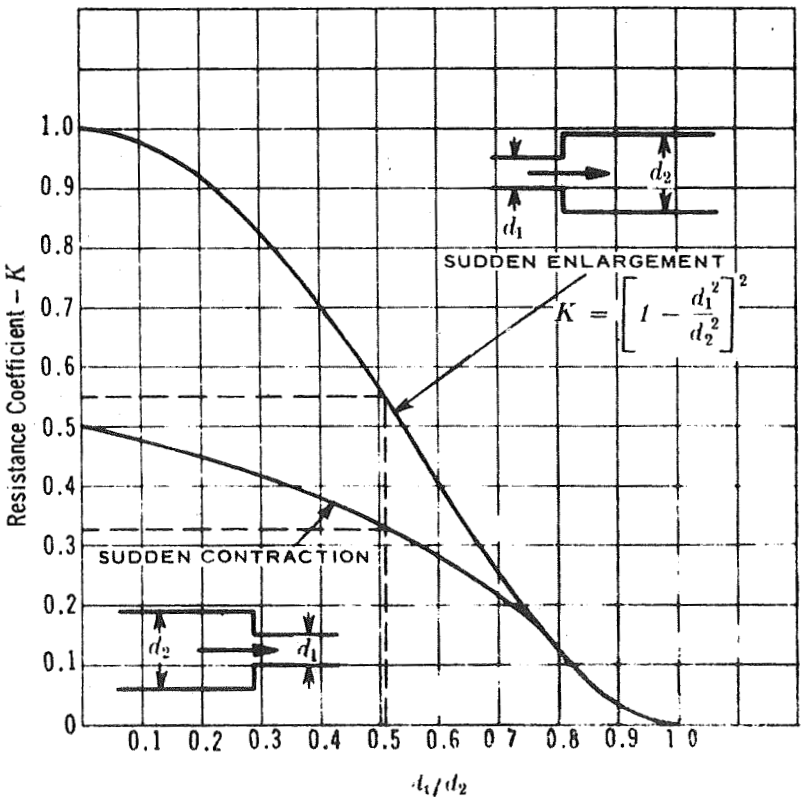

Figure 15. Resistance in Pipe Due to Sudden Enlargement and Contractions.

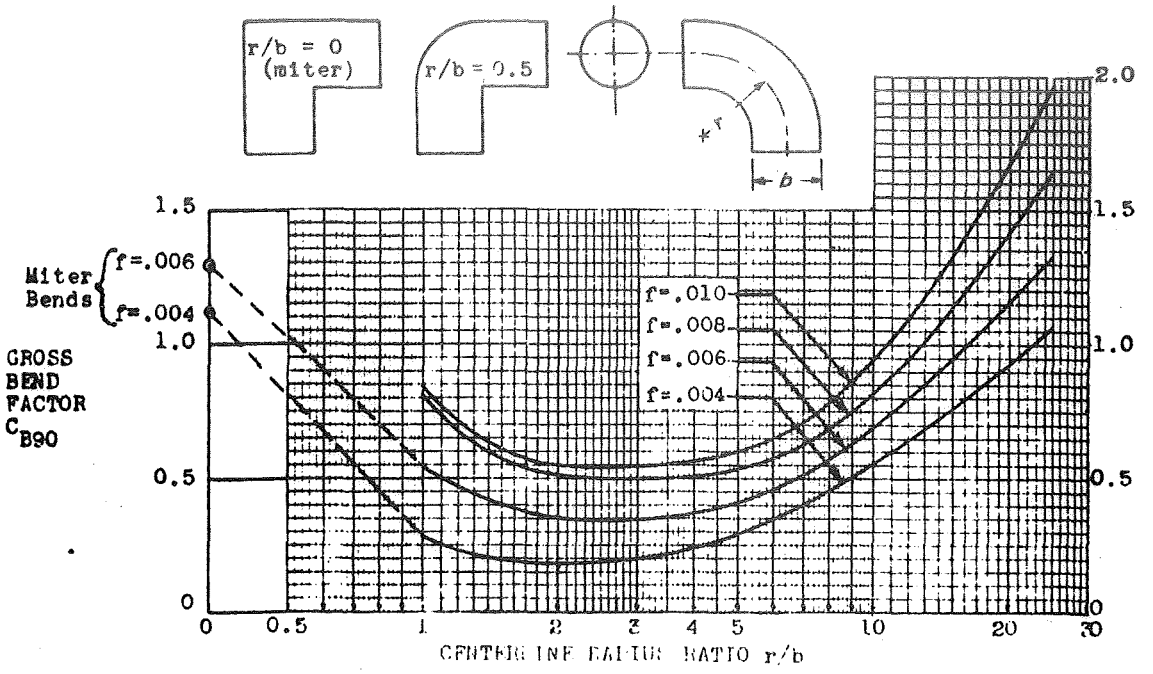

Figure 16. Bend Loss in a 90° Bend of Circular Cross-Section (Expressed in Number of Velocity Heads Lost)

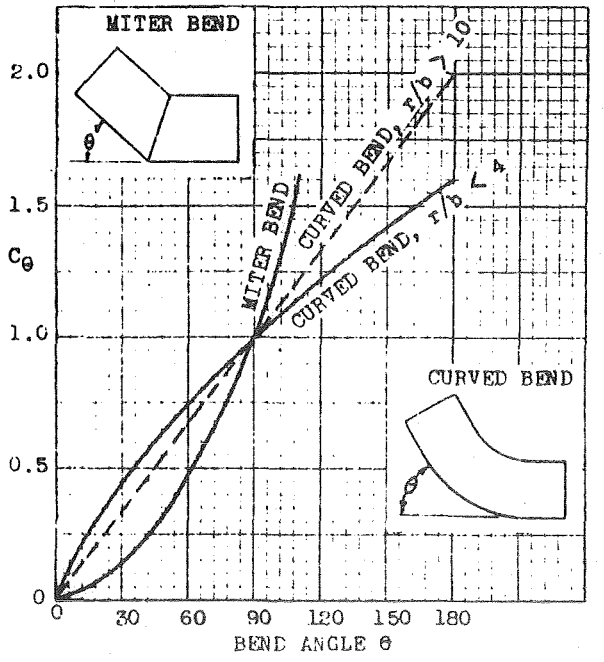

Figure 17. Ratio of Loss to Loss of a 90° Bend.

fast breeder reactor systems have suffered from this problem. The IHX designed for the Enrico Fermi Atomic Power Plant, for example, performed at only 30% of its rated capacity due to poor shell-side flow distribution. The Sodium Reactor Experiment IHX units suffered from performance degradation due to shell-side flow maldistribution and stratification. Certain early SNAP-8 boilers, in addition, suffered from poor flow distribution, evidenced by a large variation of temperature around the circumference of the shell.

The overall effects of poor shell-side flow distribution are low and unpredictable heat transfer effectiveness and unpredicted temperature variation which may lead to high stress or fatigue problems. Flow distribution problems are generally encountered when one or more of three situations occur: (1) the shell side pressure loss is low, (2) the inlet to exit temperature change of the shell-side fluid is large and (3) the minimum shell-side to tube-side temperature difference is small. Low shell-side pressure loss situations generally produce flow distribution problems, whereas large shell-side fluid temperature differences create large heat transfer effects for a given flow problem. Shell-side flow distribution problems can be grossly categorized in terms of flow channelization and poor mixing. These points are illustrated by Sketch (b) following, which shows cross sections of the proposed 2-tube auxiliary heat exchanger design.

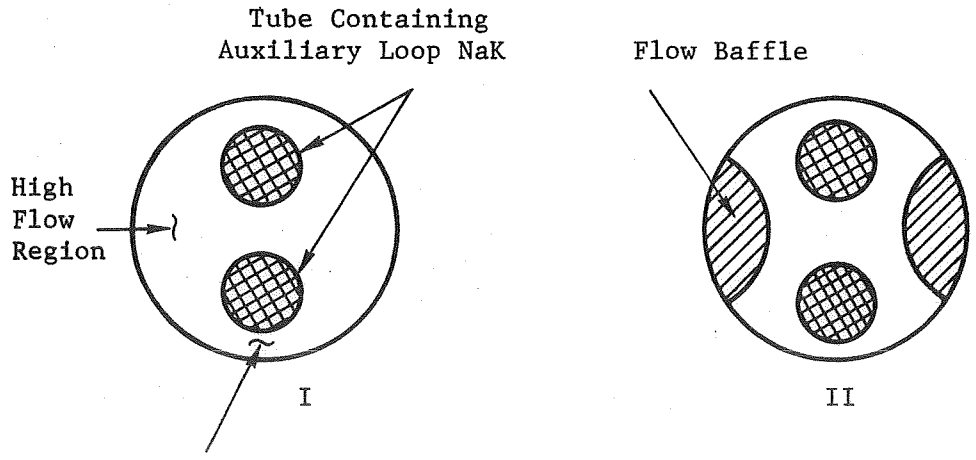

Sketch (b)

Channelization of the primary fluid in Section I of Sketch (b) would be expected, since the fluid sees less wetted perimeter and flow resistance in the region indicated "High Flow" than in the region indicated "Low Flow". The temperature change of the fluid in the high flow region as it passes through the heat exchanger would be less than the fluid in the low flow region, producing circumferential temperature variations in the downstream end of the heat exchanger. Such temperature variations always reduce heat transfer effectiveness. Section II of Sketch (b) shows flow blockage baffles which would reduce the flow maldistribution. Good mixing induced by a miximg promoter such as wire coil would also minimize the effects of flow maldistribution as the temperature variations would be reduced.

The primary NaK pressure loss specified for the SNAP-8 Auxiliary Loop Heat Exchanger is very small in relation to general practice, and flow distribution problems must be recognized and provided for in the design. The fact that only one of the two auxiliary NaK loops will be thermally active at one time creates heat transfer asymmetry and is an additional major problem in terms of flow and temperature stratification. In order to minimize the effects of such stratification, the operating auxiliary NaK tube will be uppermost. Since the tubes are heat sinks, this orientation will insure that any secondary circulation will have a mixing rather than a stratification effect. As described subsequently, a combination of hydraulic testing and theoretical calculations were employed to explore these flow distribution problems. The temperature change in the primary fluid is fortunately small (60°F) and less than the minimum tube to shell temperature difference (200°F). This means that a certain degree of shell-side maldistribution can be tolerated without encountering substantial heat transfer effects.

C. SHELL-SIDE FLOW MODEL TEST

Due to the potential seriousness of shell-side flow maldistribution and low shell-side pressure drop limitation (0.15 psi) a series of shell-side flow hydraulic tests of a full-scale ALHE plastic model were carried out, using water as the working fluid. The tests included mainly the following measurements:

(1) The pressure loss across the proposed tube spacer.

(2) The pressure loss for the inlet turn.

(3) The pressure loss for axial flow with half-moon shaped flow blockage.

(4) The pressure loss for axial flow with wire coil mixing device.

(5) The pressure loss for the exit turn.

(6) The velocity distribution in the shell and the extent of mixing were visually studied by dye injection.

Pressure loss test data were accumulated and correlated over the turbulent Reynolds number range of $2.8 \times 10^4 \leq N_{Re} \leq 7.7 \times 10^4$. For the purpose of design use, the conventional loss coefficients were evaluated from these measured data for various sections along the heat exchanger model.

A schematic of the test setup and the test section used to conduct the shell-side flow study is shown in Figure 18. Plant water at a maximum pressure of 50 psia was first passed through a standard 2.1-inch orifice where the water flow rates were measured with a mercury manometer. The water then flowed through a 2.5-inch fire hose and was introduced to the transparent model heat exchanger where all the pressure loss measurements and visual studies with dye-injection were taken.

The test section consisted of a 4.25-inch O.D. inlet pipe, a 92-inch long, 5.25-inch O.D. test section and a 3-inch O.D. exit pipe. Two 1.5-inch O.D. tubes were fitted into the test section shell as shown in Figure 18. The construction of the test section closely resembled the geometry of the actual ALHE as specified in the preliminary design, except for the curvature. The test section was made of transparent plexiglass for the purpose of flow visualization.

Two copper wire coils (3/8-inch x 6-inch, 3/8-inch x 12-inch wire diameter x coiling pitch) were tested as turbulence promoters for the shell-side flow by wrapping them around the inner diameter of the shell. Half-moon

TEST (I)

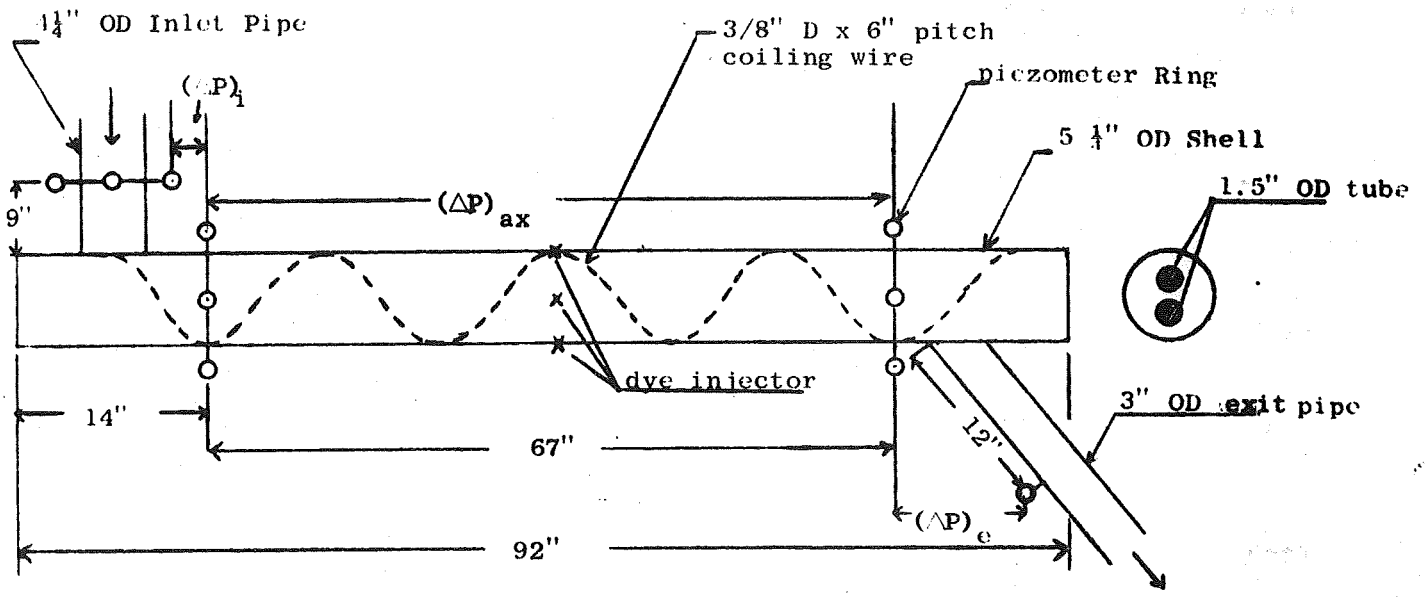

TEST (II)

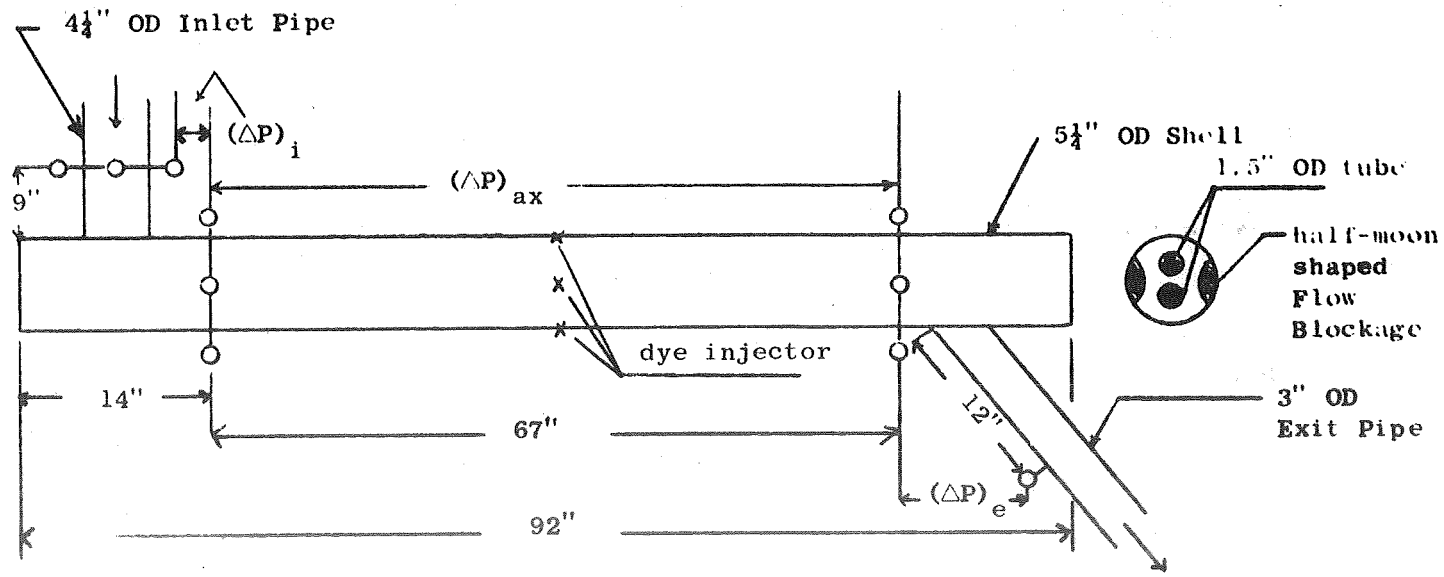

Figure 18. Schematic Drawing of ALHE Model Flow Test Section.

shaped flow blockage devices employed to enhance shell-side flow velocity distributions were mounted on the shell inner wall as shown in Figure 18.

Static pressure tap holes, suitably located for measuring individual pressure drop for shell-side flow across the entire heat exchanger assembly were provided in each of the measuring stations. For the purpose of obtaining accurate and reliable pressure data, an effort was made to use a piezometer ring on each measuring station, that is, an interconnected set of static pressure holes (three or four holes per station) around the perimeter of the shell in a plane normal to the direction of fluid flow.

Three standard 30-inch manometers made by the Meriam Instrument Company were used to measure the pressure differential across each test station. The indicating fluid employed is Meriam D2883 which has a specific gravity of 2.95 at normal temperature. The manometers are subdivided to 0.1-inch.

Three dye injectors located at the position shown in Figure 18 were employed for the photographic recording and visual observation of the flow mixing and distribution. A hypodermic needle and syringe was used to inject dye into the stream at a sufficient rate to insure adequate color. A tank of compressed argon gas was used to supply the back pressure for the hypodermic.

CRITERION OF MODELING

In general, two systems are said to be similar if the following conditions are met:

(1) geometrically similar

(2) Dynamically similar

The condition (1) states that the geometry of two systems should be the same, i.e., the same diameter, length and curvature or that the ratio of these quantities is proportional to some constants according to scaling laws. The condition (2) states that two systems are similar if the respective Reynolds numbers are equal.

For the present modeling test, condition (1) was approximately met except for the minor effect of the curvature. Condition (2) was not met because the Reynolds number of the actual system (at design flow rate, 7.5 lb/sec NaK flow at average temperature 1250^{o}F) is 1.66 x 10^{5} which requires a water flow

rate of 48 lb/sec for the modeling system. Such a high water flow rate was beyond the range of the water supply system of the present test. Fortunately, the main concern was to evaluate the loss coefficient for the shell-side flow and as the data showed, these loss coefficients are generally very weak functions of the Reynolds number. This is to say that the present results obtained over a Reynolds number range of 2.8×10^4 to 7.7×10^4 can be used for the real NaK shell-side flow without losing any appreciable accuracy.

HYDRAULIC TEST RESULTS

The loss coefficient, defined as the ratio of the measured pressure drop to the velocity head, can be written as,

$$K = \frac{(\Delta P)_{measured}}{H_v} \tag{22}$$

where $(\Delta P)_{measured}$ in psi is calculated from the manometer reading Δh in inches as follows,

$$(\Delta P)_{measured} = 62.4\ (2.95\text{-}1)\ \frac{\Delta h}{1728} \tag{23}$$

and the velocity head H_v is calculated as follows:

$$H_v = \frac{1}{2g\rho}\left(\frac{W_{H_2O}}{A_F}\right)^2 \tag{24}$$

with A_F denoting the shell-side net flow area.

The Reynolds number for water flow is calculated by

$$N_{Re} = \frac{\rho D_e V}{\mu} = \frac{D_e}{\mu}\left(\frac{W_{H_2O}}{A_F}\right) \tag{25}$$

where the equivalent diameter for shell-side passage can be calculated from its definition as

$$D_e = \frac{4\ (\text{Shell-side net flow area})}{\text{Shell-side flow wetted perimeter}} \tag{26}$$

(i) Loss Due to Inlet Turn

The measured pressure drops for the shell-side flow through the inlet turn are presented in Table 8. This pressure drop consists of static head loss due to a 90 degree turning and an expansion from flow area changes. Loss coefficients K_i and K_i^* based upon different velocity heads are also presented in Table 8 and graphically given in Figures 19 and 20.

(ii) Loss Due to Axial Flow

Axial flow pressure drop data are presented in Tables 8 and 9 and in Figure 21. Cases were tested with the shell-side equipped with copper coiling wire and half-moon shaped flow blockages. Two combinations of copper wire (3/8 -inch x 6-inch and 3/8-inch x 12-inch) were tested and the results are given in Figure 22 for comparison. As shown in this figure, tighter pitch coiling wire gives higher pressure drop. Loss coefficients based on shell-side velocity heads for various cases are also presented in Tables 8 and 9 and Figures 19 and 23. As shown by these data, the pressure drop by installing wire coil on the shell-side is about three times higher than the pressure drop obtained using half-moon shaped flow blockages.

(iii) Loss Due to Tube Supports

The tube support proposed for use in the actual heat exchanger is made of stainless steel wire of 1/8-inch diameter bent into the shape shown in Figure 24. The pressure drop data for shell-side flow across the spacer is shown in Figure 25 and correlated into loss coefficients in Figure 14.

(iv) Loss Due to Exit Turn

The exit turn losses measured for the configuration shown in Figure 18 are given in Table 8 and Figure 21. This loss consists of an approximately 45^o turning loss and a contraction loss due to a very abrupt change of the flow cross sectional area. The exit pressure loss is exceptionally high as shown by the data. Subsequently a modified exit section composed of a partial reducer, a 45 degree elbow and a 32-1/4-inch long extended pipe was built to replace the original exit section. The following sketch shows some essential dimensions for this modified exit section.

TABLE 8

WATER FLOW TEST RESULTS

Shell-Side Equipped with Copper Coiling Wire (3/8" D X 6" Pitch)

R_e	$(\Delta P)_i$	K_i	K_i^*	$(\Delta P)_{ax}$	K_{ax}	$(\Delta P)_e$	K_e	K_e^*
$\times 10^{-4}$	psi	--	--	psi	--	psi	--	--
2.95	0.03	2.19	1.53	0.069	5.00	0.275	20.1	2.25
3.35	0.041	2.26	1.58	0.084	4.65	0.341	18.8	2.10
3.7	0.048	2.2	1.54	0.096	4.36	0.41	18.8	2.10
4.15	0.057	2.06	1.44	0.117	4.26	0.502	18.3	2.04
4.30	0.065	2.19	1.53	0.127	4.28	0.544	18.3	2.04
4.70	0.073	2.03	1.42	0.146	4.06	0.643	17.8	2.0
5.0	0.083	2.06	1.44	0.162	4.01	0.739	18.3	2.04
5.40	0.092	1.95	1.36	0.178	3.79	0.891	19.0	2.10
5.55	0.096	1.96	1.37	0.185	3.78	0.849	17.3	1.93
5.70	0.101	1.93	1.35	0.199	3.81	0.903	17.3	1.93
5.90	0.111	1.98	1.39	0.210	3.74	0.967	17.3	1.93
6.25	0.113	1.78	1.25	0.265	3.62	1.065	16.8	1.88
6.50	0.125	1.83	1.28	0.263	3.58	1.13	16.5	1.86
6.70	0.130	1.78	1.25	0.265	3.62	1.218	16.7	1.87
7.15	0.142	1.73	1.22	0.287	3.51	1.334	16.3	1.83
7.50	0.157	1.72	1.21	0.315	3.46	1.47	16.2	1.81

Note: K_e^* based on exit pipe velocity head.

K_e, K_i and K_{ax} all based on shell-side velocity head.

K_i^* based on inlet pipe velocity head.

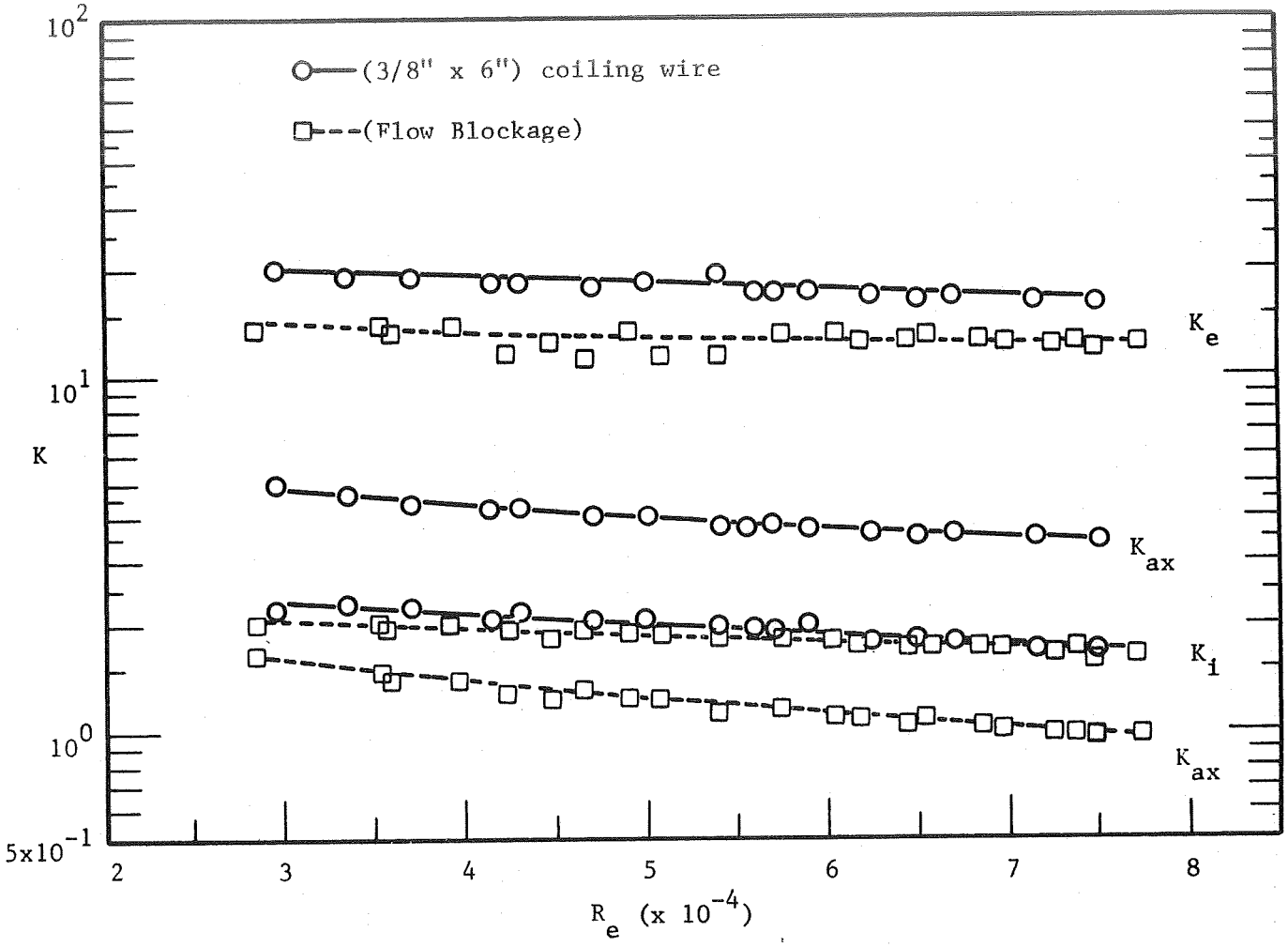

Figure 19. ALHE Model Hydraulic Test Results - Loss Coefficients.

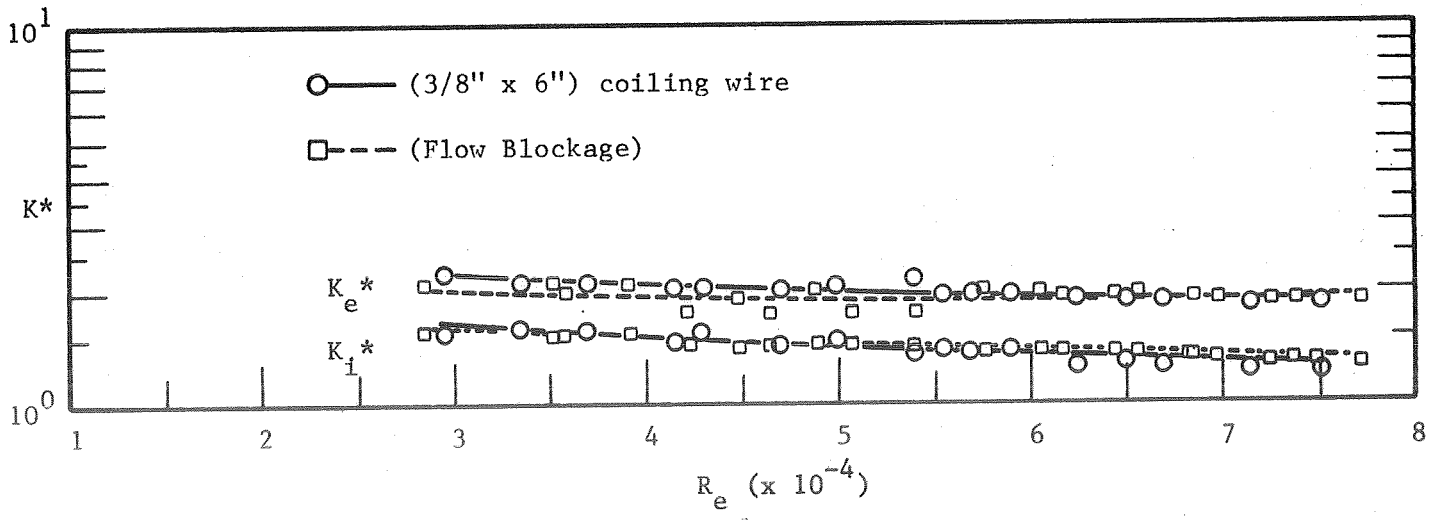

Figure 20. ALHE Loss Coefficient Based Upon Smaller Area Velocity Heads.

TABLE 9

WATER TEST RESULTS

Shell-Side Equipped with Semi-Circular Flow Blockages

R_e	$(\Delta P)_i$	K_i	K_i^*	$(\Delta P)_{ax}$	K_{ax}	$(\Delta P)_e$	K_e	K_e^*
x 10^{-4}	psi	--	--	psi	--	psi	--	--
2.84	0.037	2.01	1.53	0.030	1.66	0.25	13.7	2.07
3.52	0.056	2.0	1.52	0.041	1.46	0.391	13.9	2.10
3.58	0.058	2.0	1.52	0.042	1.44	0.380	13.1	1.97
3.92	0.070	2.01	1.53	0.048	1.39	0.479	13.8	2.08
4.23	0.080	1.94	1.47	0.051	1.25	0.567	11.5	1.74
4.48	0.090	1.84	1.40	0.060	1.23	0.608	12.5	1.89
4.65	0.094	1.90	1.44	0.065	1.31	0.665	11.3	1.71
4.90	0.104	1.89	1.43	0.068	1.23	0.733	13.3	2.02
5.08	0.111	1.88	1.42	0.074	1.25	0.792	11.6	1.76
5.40	0.124	1.82	1.38	0.077	1.13	0.88	11.4	1.73
5.75	0.136	1.81	1.37	0.088	1.16	0.989	13.1	1.98
6.05	0.152	1.82	1.38	0.092	1.095	1.09	13	1.97
6.18	0.155	1.77	1.34	0.094	1.075	1.11	12.6	1.91
6.45	0.169	1.78	1.35	0.099	1.05	1.206	12.7	1.92
6.55	0.171	1.77	1.34	0.104	1.07	1.250	12.9	1.95
6.85	0.185	1.74	1.32	0.111	1.04	1.348	12.6	1.91
6.98	0.192	1.74	1.32	0.115	1.035	1.392	12.5	1.89
7.25	0.203	1.69	1.28	0.118	0.99	1.570	12.2	1.84
7.37	0.211	1.71	1.30	0.122	0.985	1.585	12.4	1.88
7.47	0.215	1.68	1.27	0.125	0.98	1.595	12.2	1.84
7.72	0.227	1.66	1.26	0.132	0.975	1.682	12.3	1.86

Note: K_e^* based on velocity head in exit pipe.

K_e, K_i and K_{ax} all based on shell-side velocity head.

K_i^* based on inlet pipe velocity head.

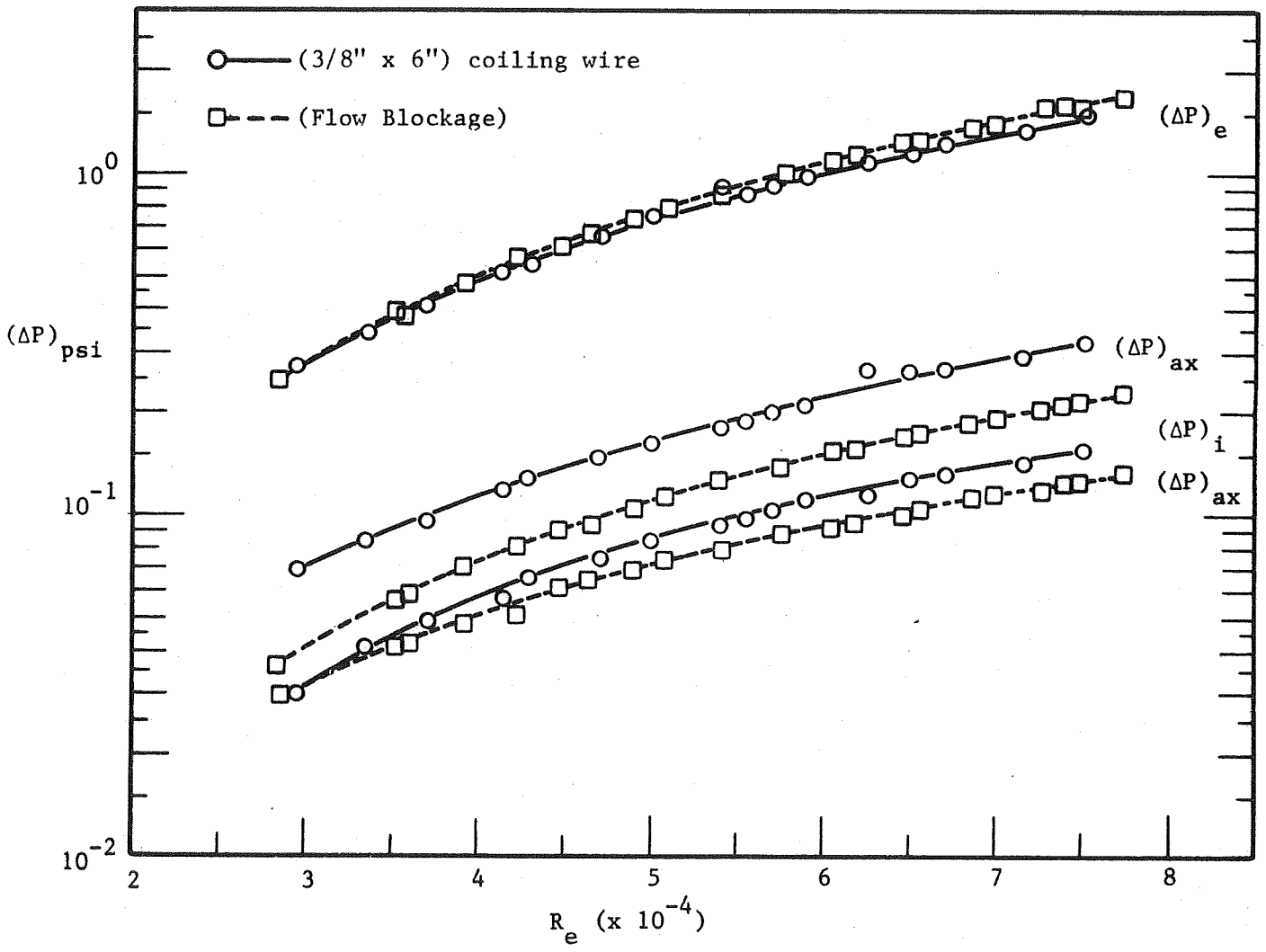

Figure 21. Water Hydraulic Test Results for ALHE Shell-Side Flow Model.

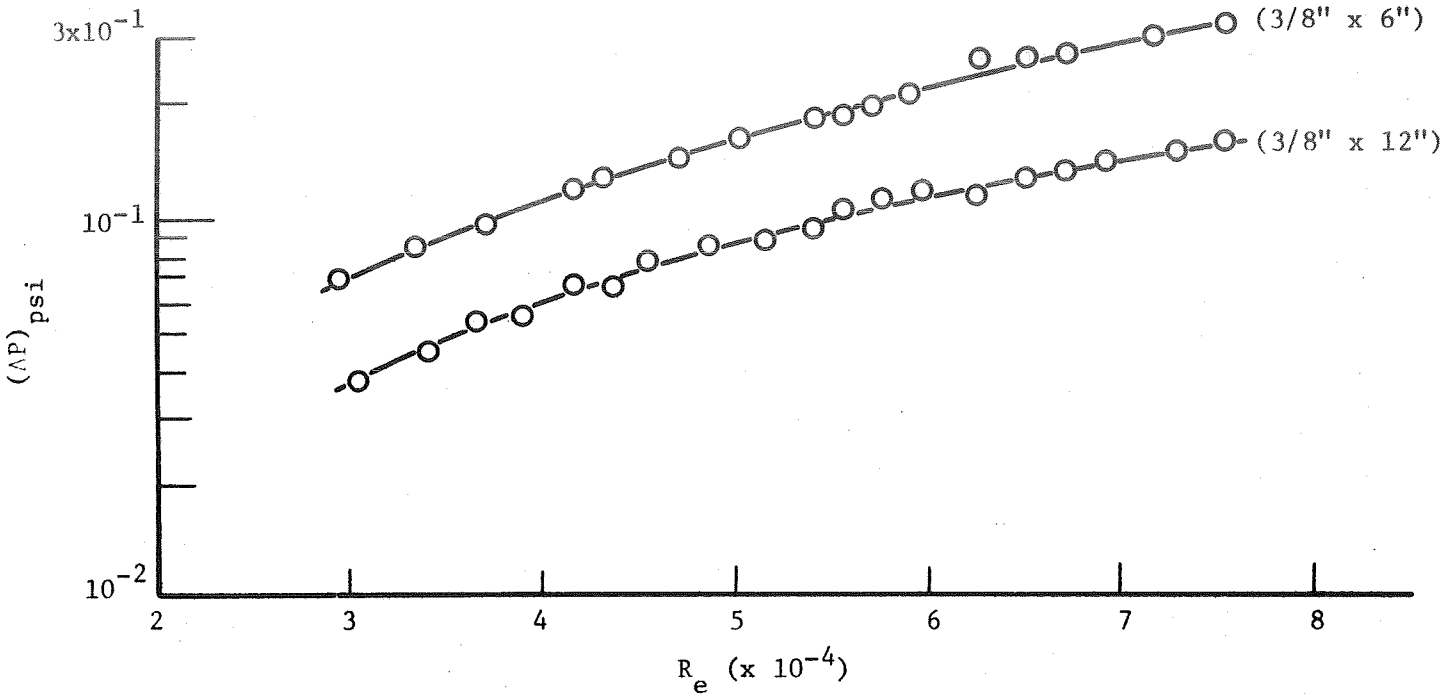

Figure 22. Comparison of Pressure Drop for 3/8" Diameter Wire With Different Coiling Pitches.

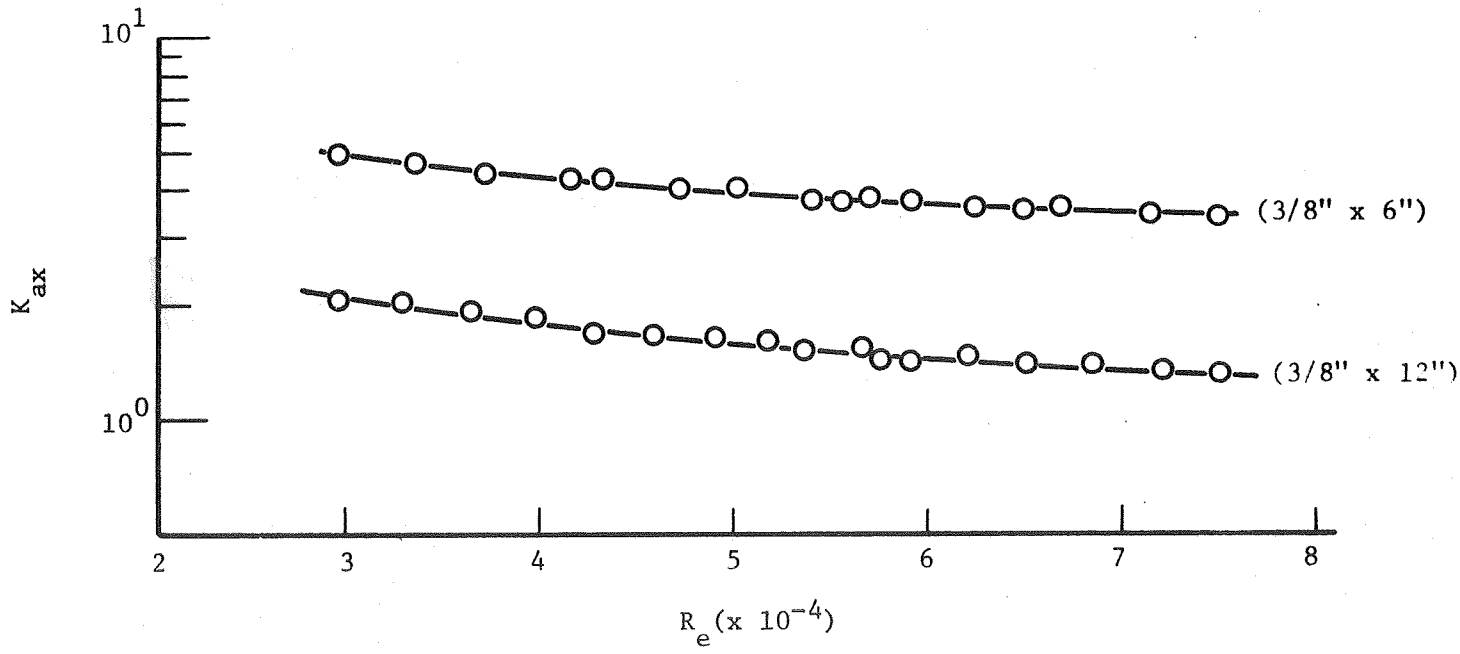

Figure 23. Comparison of Loss Coefficient for 3/8" Diameter Wire With Different Coiling Pitches.

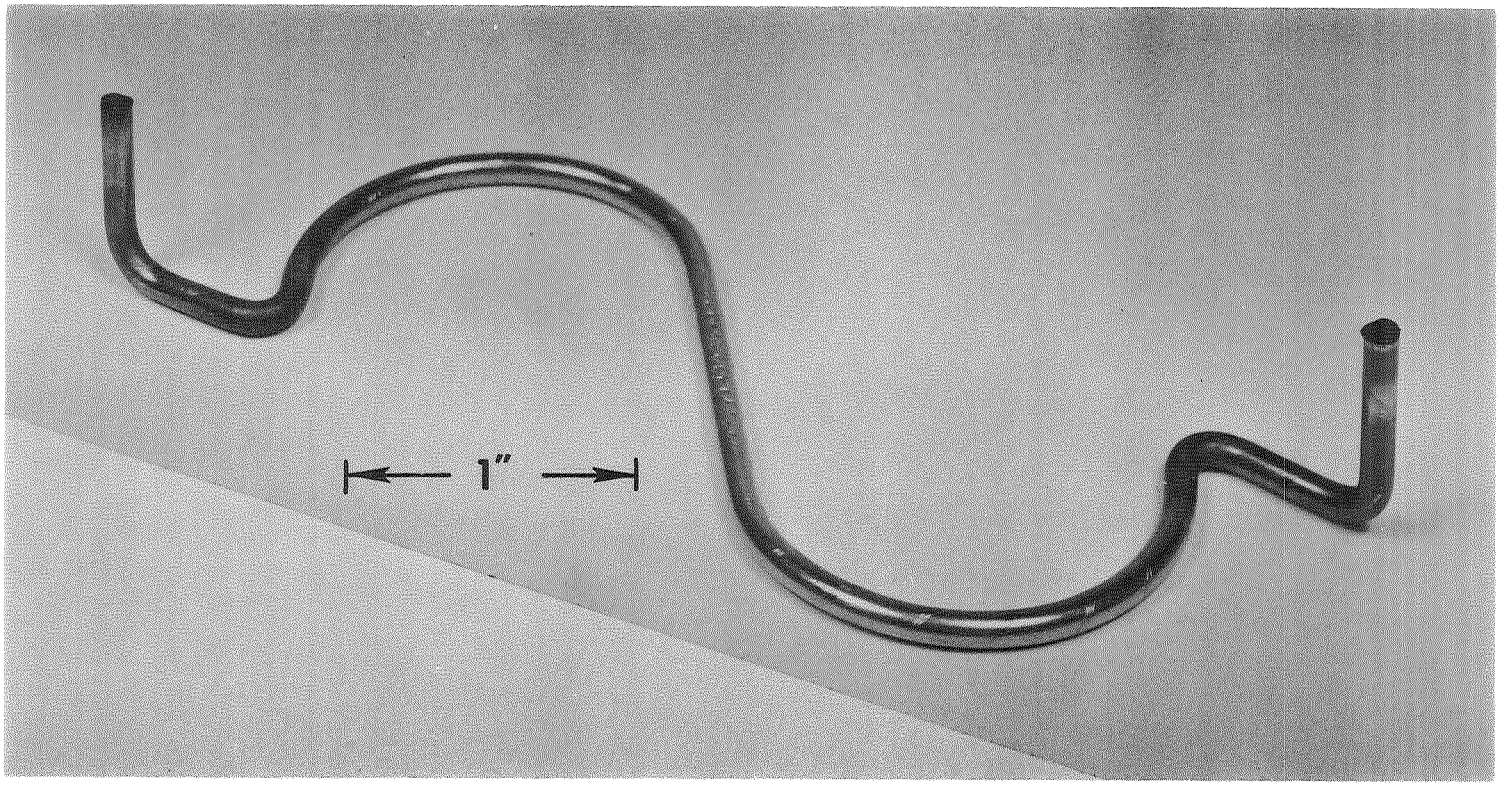

Figure 24. Tube Support Wire Shape for the SNAP-8 Auxiliary Loop Heat Exchanger. (P69-5-18F)

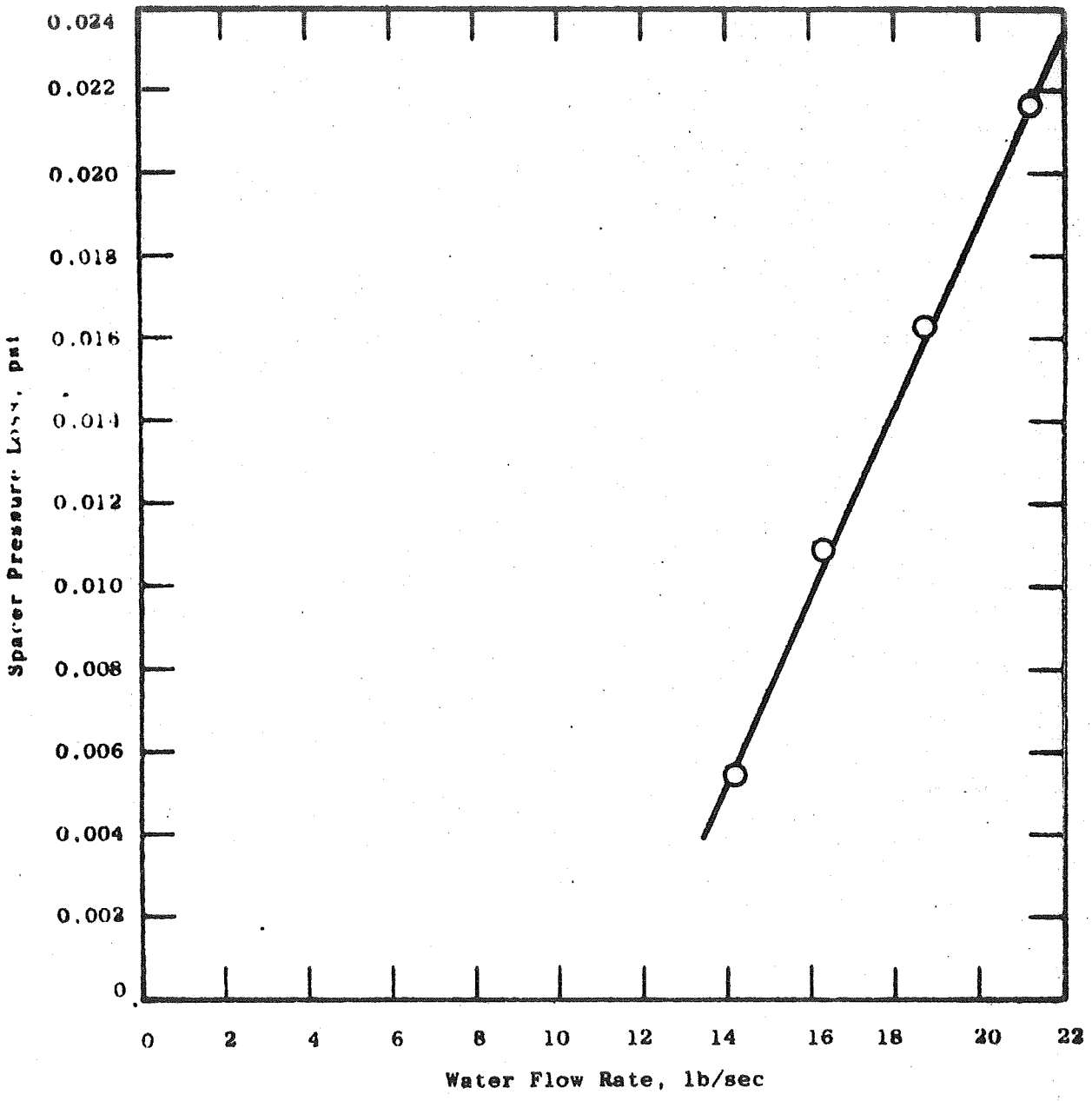

Figure 25. Spacer Pressure Loss Measured for Proposed Auxiliary Heat Exchanger Design.

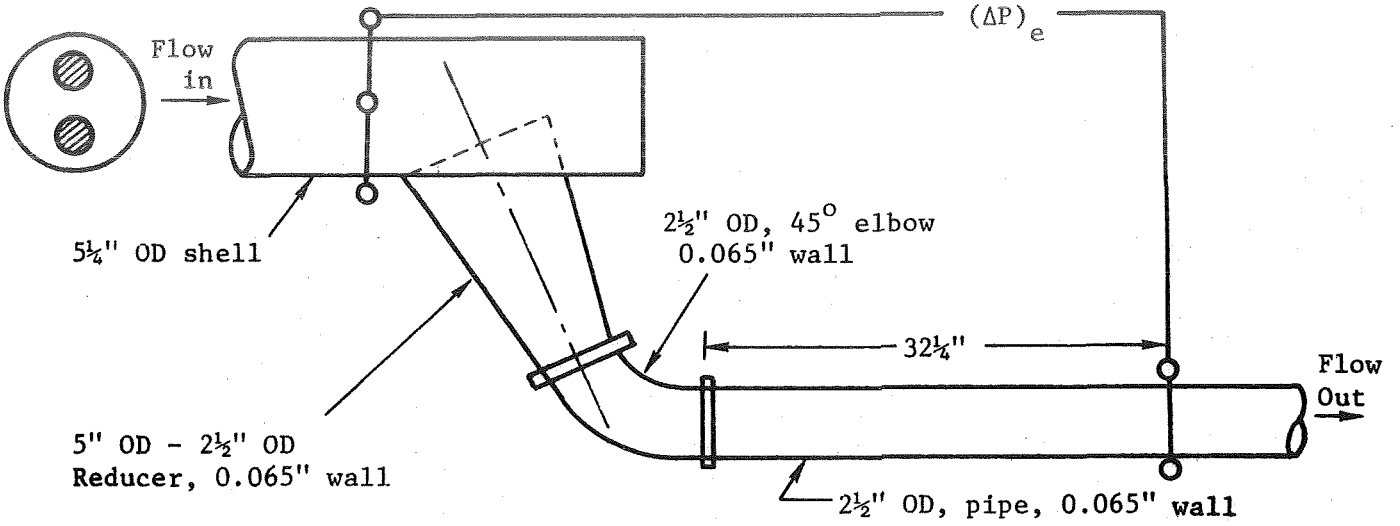

Sketch (c)

The measured pressure drops across this modified exit section, $(\Delta P)_e$, are tabulated in Table 10. The total exit loss consisted of three components, i.e., loss due to the partial reducer, loss due to the 45 degree elbow and loss due to the 2-1/2-inch O.D., 32-1/4-inch long pipe. In an effort to estimate the pressure drop due to the partial reducer alone, reliable sources were used for predicting the pressure losses due to elbow and pipe, which were then subtracted from the total measured exit pressure drop. For the elbow, the pressure drop can be evaluated by the equation following.

$$(\Delta P)_{elbow} = C_{90} C_\theta \left(\frac{\rho V^2}{2g}\right) \tag{27}$$

C_{90} is the loss coefficient for a 90 degree bend and C_θ is the correction factor for bends other than 90 degrees. Curves shown in Figures 16 and 17 cited from Reference 12 were used to evaluate C_{90} and C_θ for the present case. For pipe flow, the pressure loss is generally given by

$$(\Delta P)_{pipe} = f \left(\frac{L}{D}\right)\left(\frac{V^2}{2g}\right) \tag{28}$$

where f, the frictional factor, can be calculated from the Blasius correlation or from the Moody curve in Figure 12 by knowing the pipe flow Reynolds number.

Following this approach, the pressure loss due to the reducer alone was obtained by subtracting $(\Delta P)_{elbow}$ and $(\Delta P)_{pipe}$ from the measured

TABLE 10

WATER TEST RESULTS MODIFIED EXIT SECTION

$Re \times 10^{-4}$	$(\Delta P)_{Meas.}$	$(\Delta P)_{pipe}$ *	$(\Delta P)_{elbow}$ *	$(\Delta P)_{red.}$	$K_{red.}$
4.83	0.929	0.146	0.238	0.545	1.165
5.65	1.195	0.178	0.290	0.726	1.27
5.7	1.225	0.182	0.296	0.747	1.28
6.14	1.323	0.205	0.333	0.785	1.20
6.54	1.499	0.236	0.386	0.877	1.16
6.56	1.555	0.238	0.388	0.929	1.21
6.7	1.633	0.24	0.390	1.003	1.31
7.08	1.802	0.283	0.460	1.059	1.15
7.36	1.837	0.296	0.481	1.020	1.08
7.87	2.104	0.338	0.552	1.214	1.13

* Remarks: $(\Delta P)_{pipe}$ calculated by $(\Delta P)_{pipe} = f \left(\frac{L}{D}\right) H_v$.

$(\Delta P)_{elbow}$ calculated by $(\Delta P)_{elbow} = C_{90}\, C_{\theta}\, H_v = 0.51\, H_v$.

value of $(\Delta P)_e$. Subsequently, the loss coefficient for the reducer was evaluated based upon its smallest area velocity head. Results of these calculations are presented in Table 10 and Figure 26. The loss coefficient of the reducer is slightly larger than the value of K recommended by conventional pressure drop tables for reducers. The reason for the higher value for K_{red} might be due to the added turning loss when entering the reducer.

FLOW VISUALIZATION

Visual and photographic observations of the shell-side flow mixing phenomena were simultaneously made with the static pressure drop measurements. The evaluation of the shell-side flow mixing produced by adding mixing devices such as coiling wire and flow blockages was of particular interest.

As described before two wire coil combinations (wire diameter x pitch) were used as mixing promoters by wrapping the wire coil around the inside of the shell. Upstream dye injections were used for visualization of the shell-side flow mixing phenomena. As illustrated in the following sketch, dye was injected at three upstream locations each from top, bottom and middle. As shown in Figure 27, the shell-side flow had indicated no mixing at all without either the use of wire coil or the flow blockage on the inner wall.

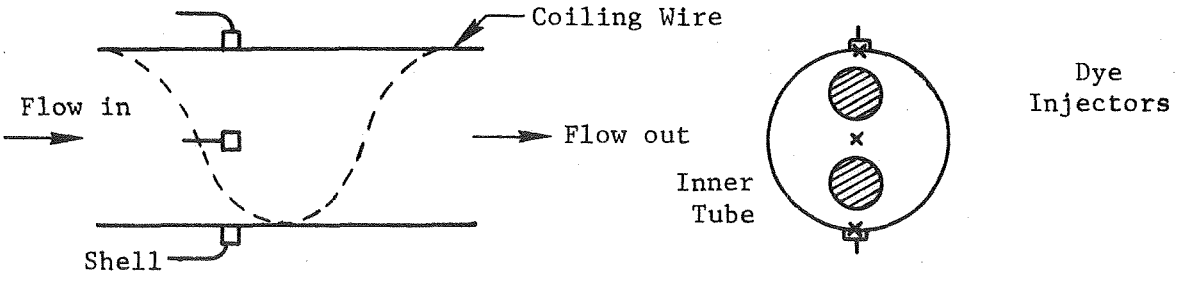

Sketch (d)

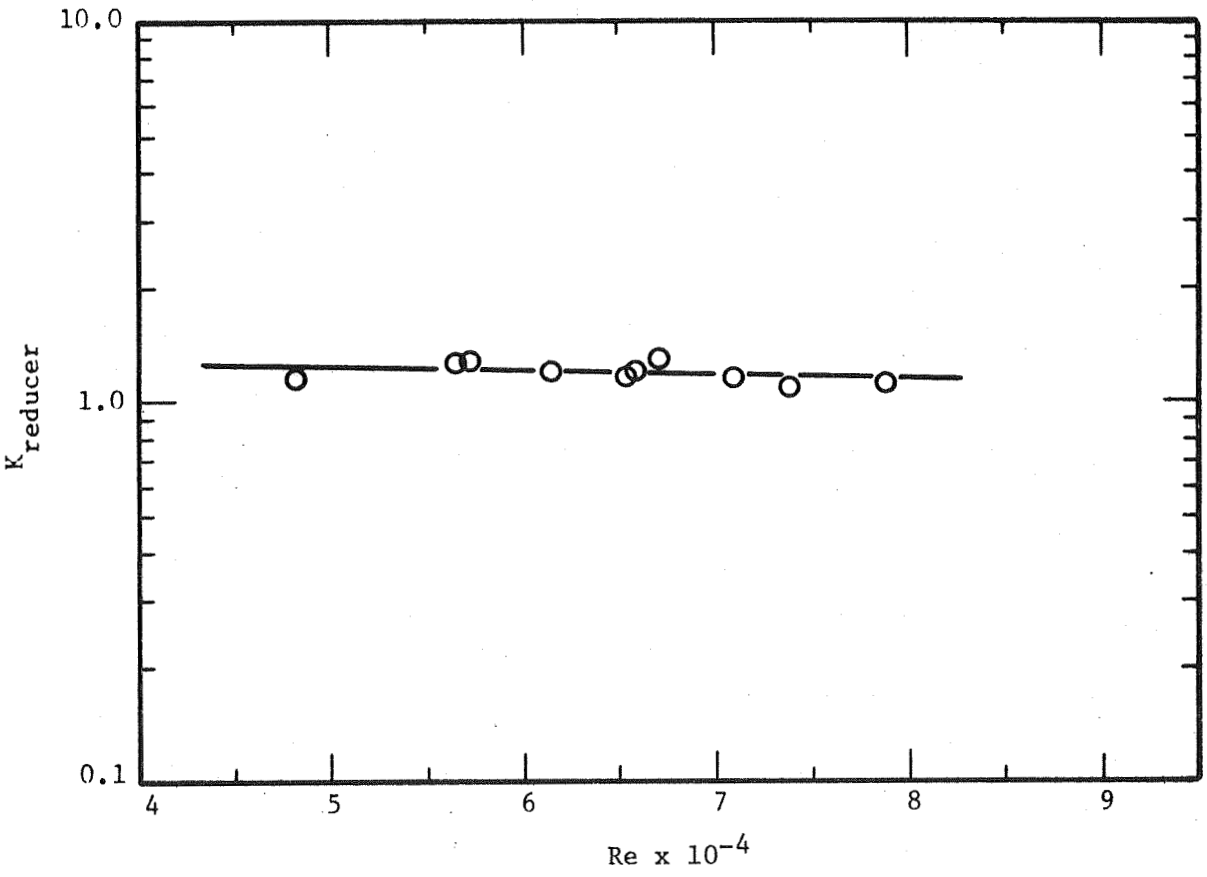

Figure 26. Loss Coefficient for the Partial Reducer.

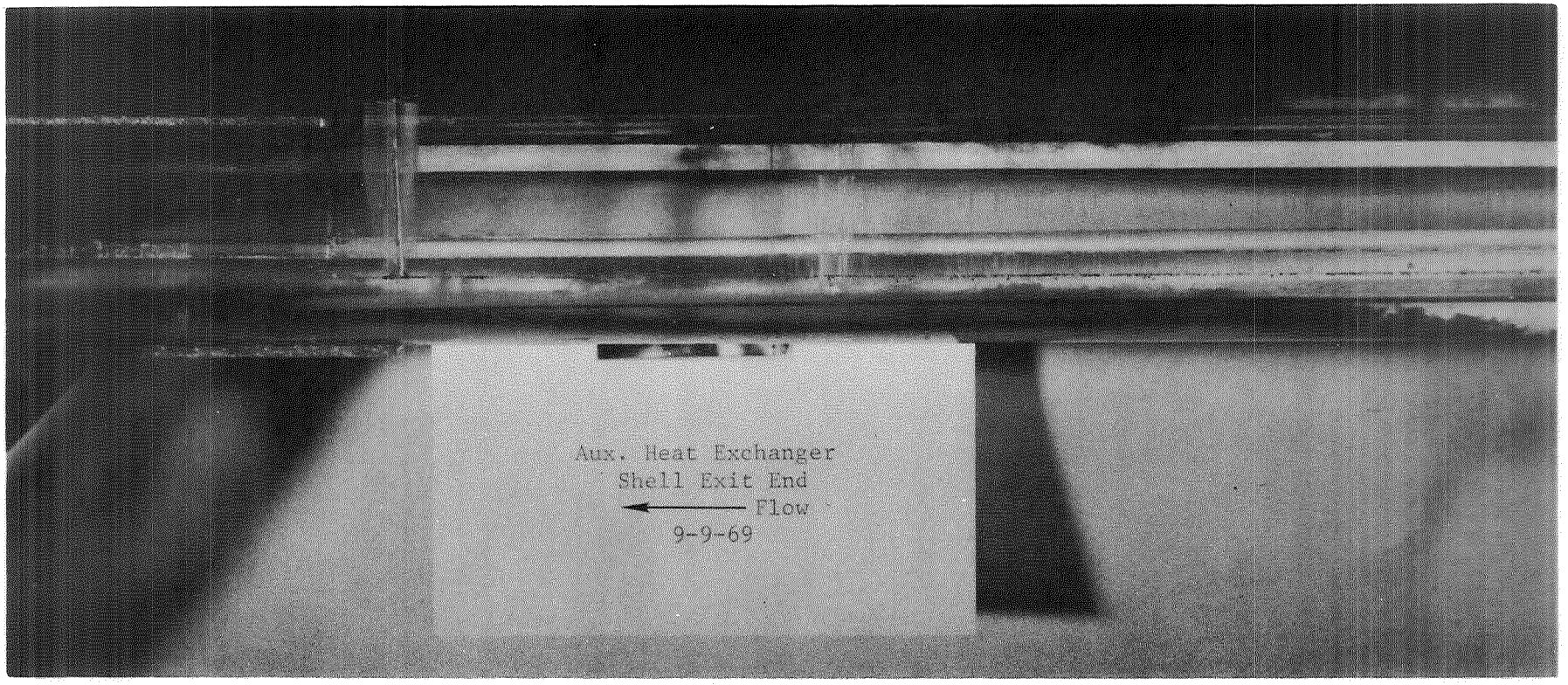

Figure 27. Poor Mixing of Shell-Side Flow Without Any Mixing Promoter. (P69-9-11A)

The mixing effects of wire coil and flow blockage were then evaluated by observing the mixing level of shell-side flow with the aid of dye injections. Furthermore, the distances required for developing a fully mixed region were also visually determined. In general, the wire coil combinations indicated much better mixing of the shell-side flow. As evidenced by visual observation, very little mixing effect was noted when the half-moon shaped flow blockages were added as shown in Figure 28. On the other hand, as shown in Figures 29 and 30, reasonably good mixing did occur with the use of a wire coil insert (3/8" dia x 6" pitch).

When a 3/8" dia x 12" pitch coil was substituted, mixing was not as good, particularly in the center portion of the shell between the two inner tubes. The pressure drop for this geometry, however, was somewhat less than for the 6" pitch geometry. Therefore, it was decided to test a wire coil on the inner tubes in conjunction with the 12" pitch coil on the shell. Flow mixing was greatly enhanced using this approach, but the total pressure drop increased to an unreasonably high value, as shown in Figure 31. Based on the visual observations and the pressure drop data a 3/8" dia x 6" pitch wire coil insert was selected for the final design. It is believed that this geometry is the best compromise between good heat transfer and low pressure drop.

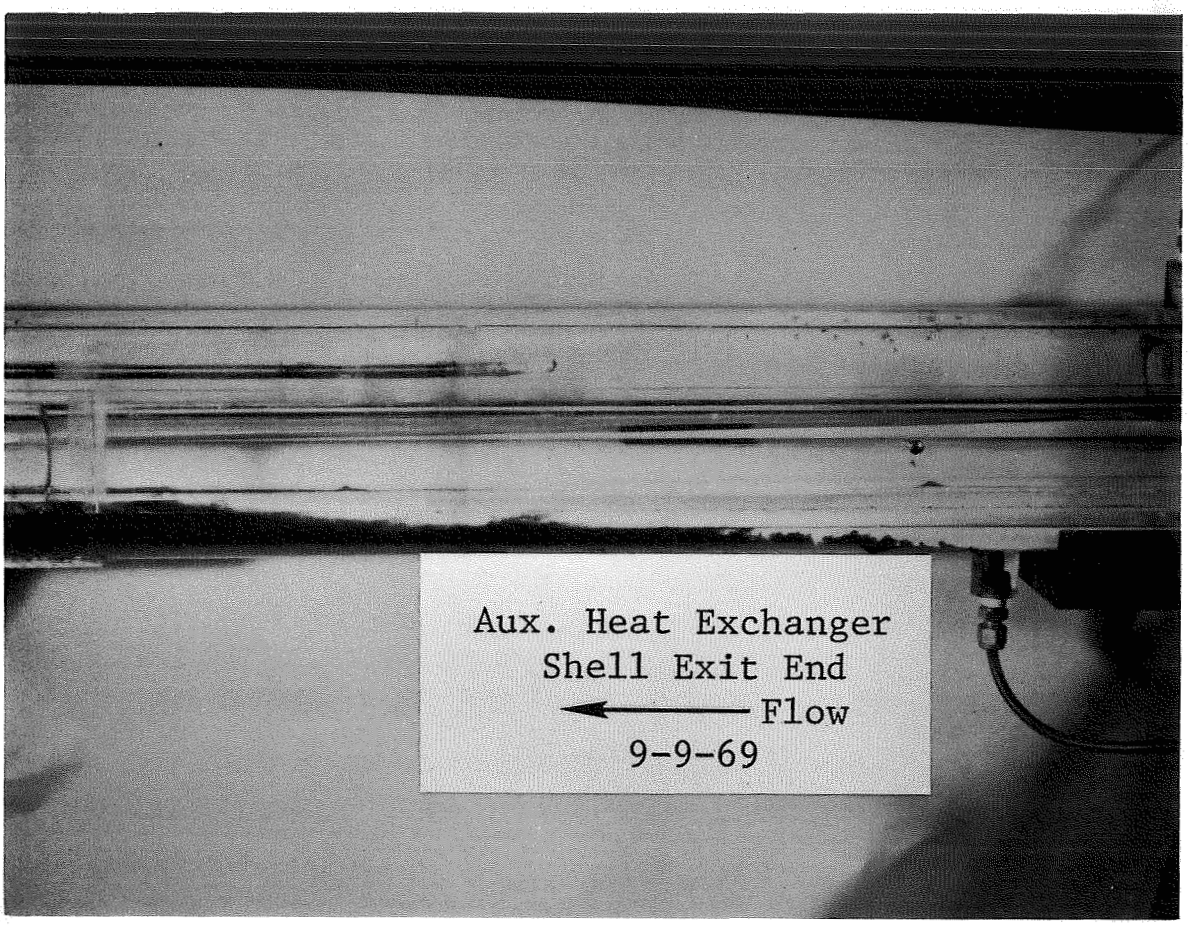

Figure 28. Poor Mixing of Shell-Side Flow With Half-Moon Shaped Flow Blockages.

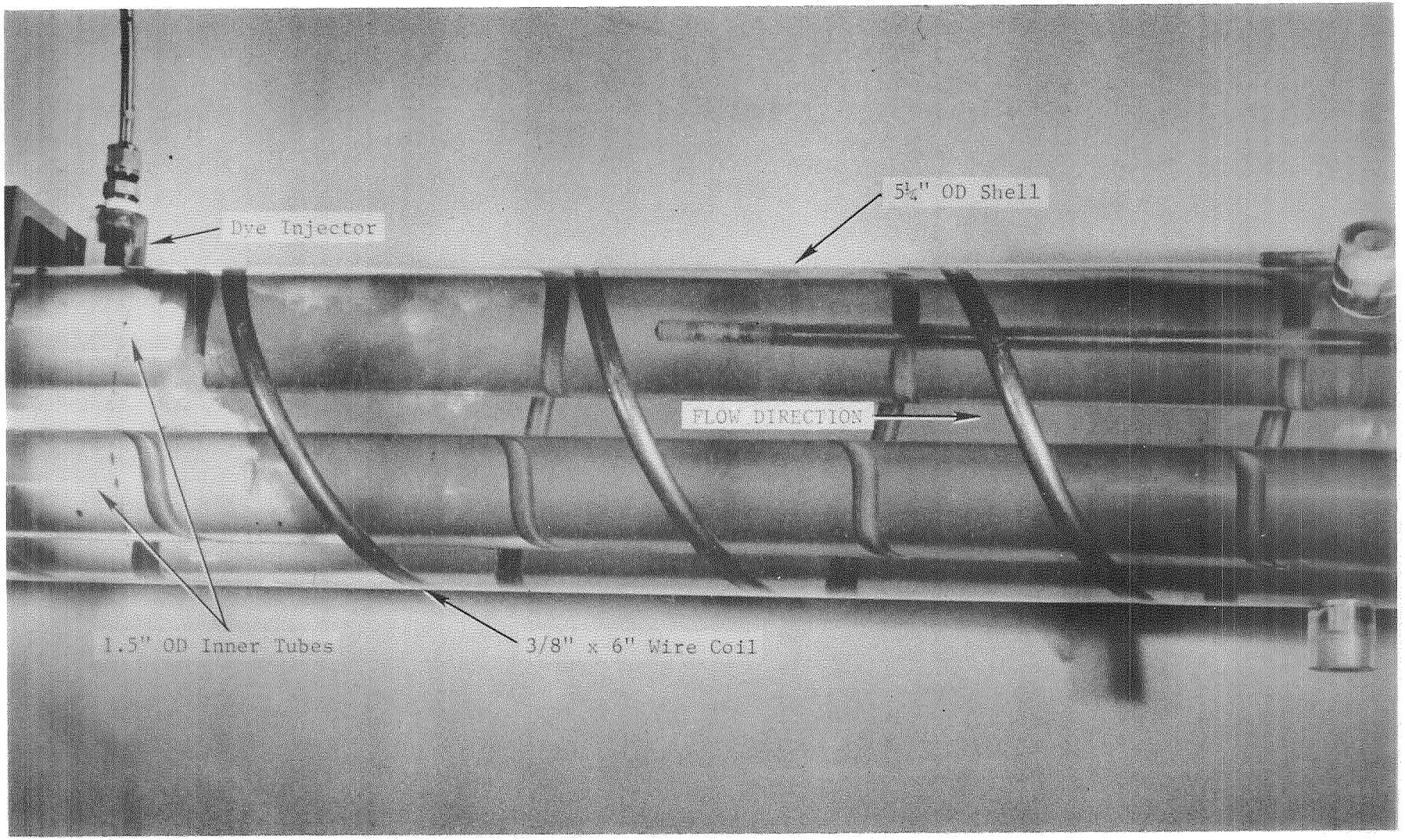

Figure 29. Good Mixing of Shell-Side Flow by Installing 3/8" x 6" Wire Coil Dye Injected From Top. (P69-9-23A)

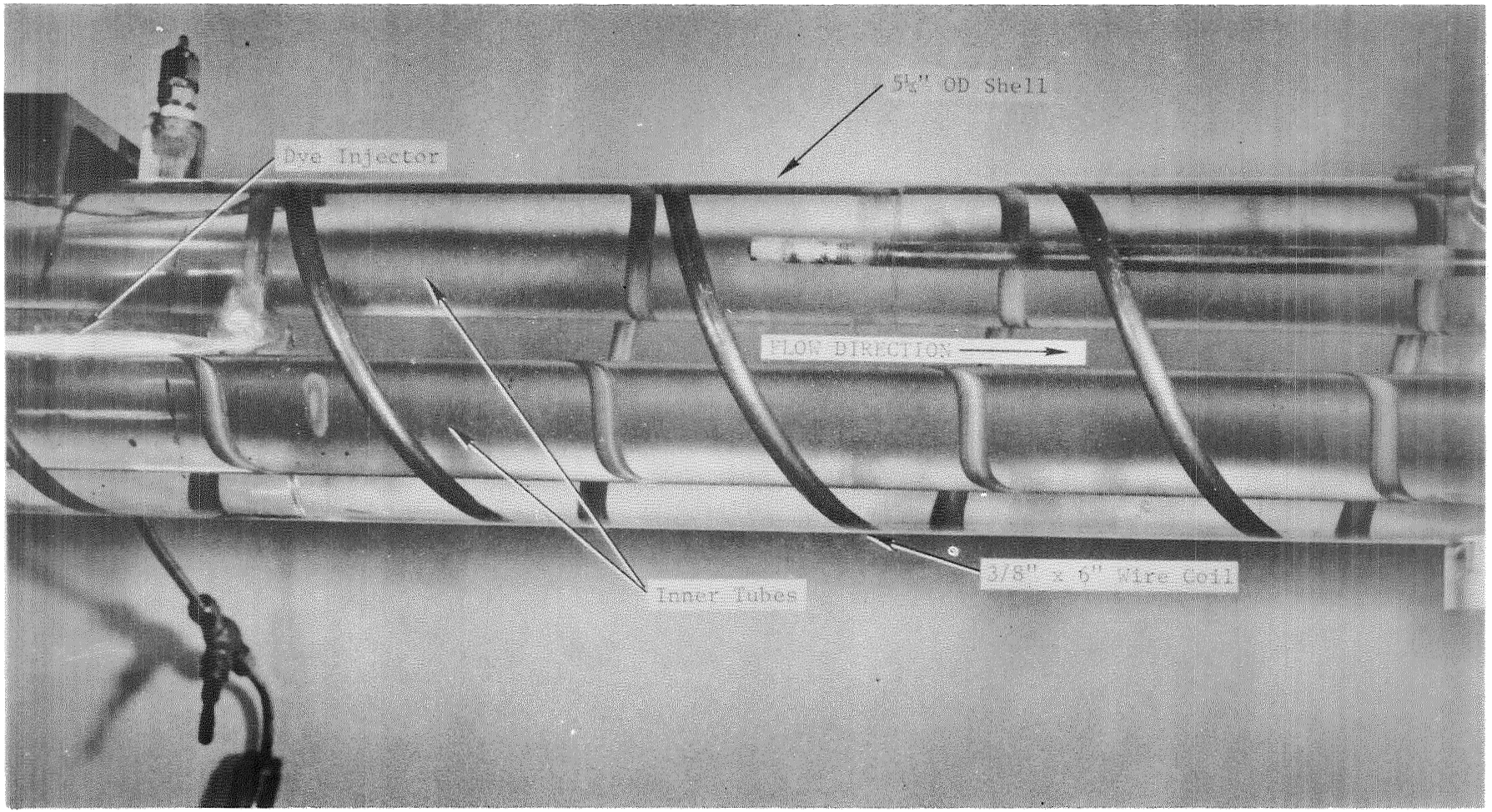

Figure 30. Partial Mixing of Shell-Side Flow in the Center Portion. (Dye Injected Between Two Inner Tubes) (P69-9-23B)

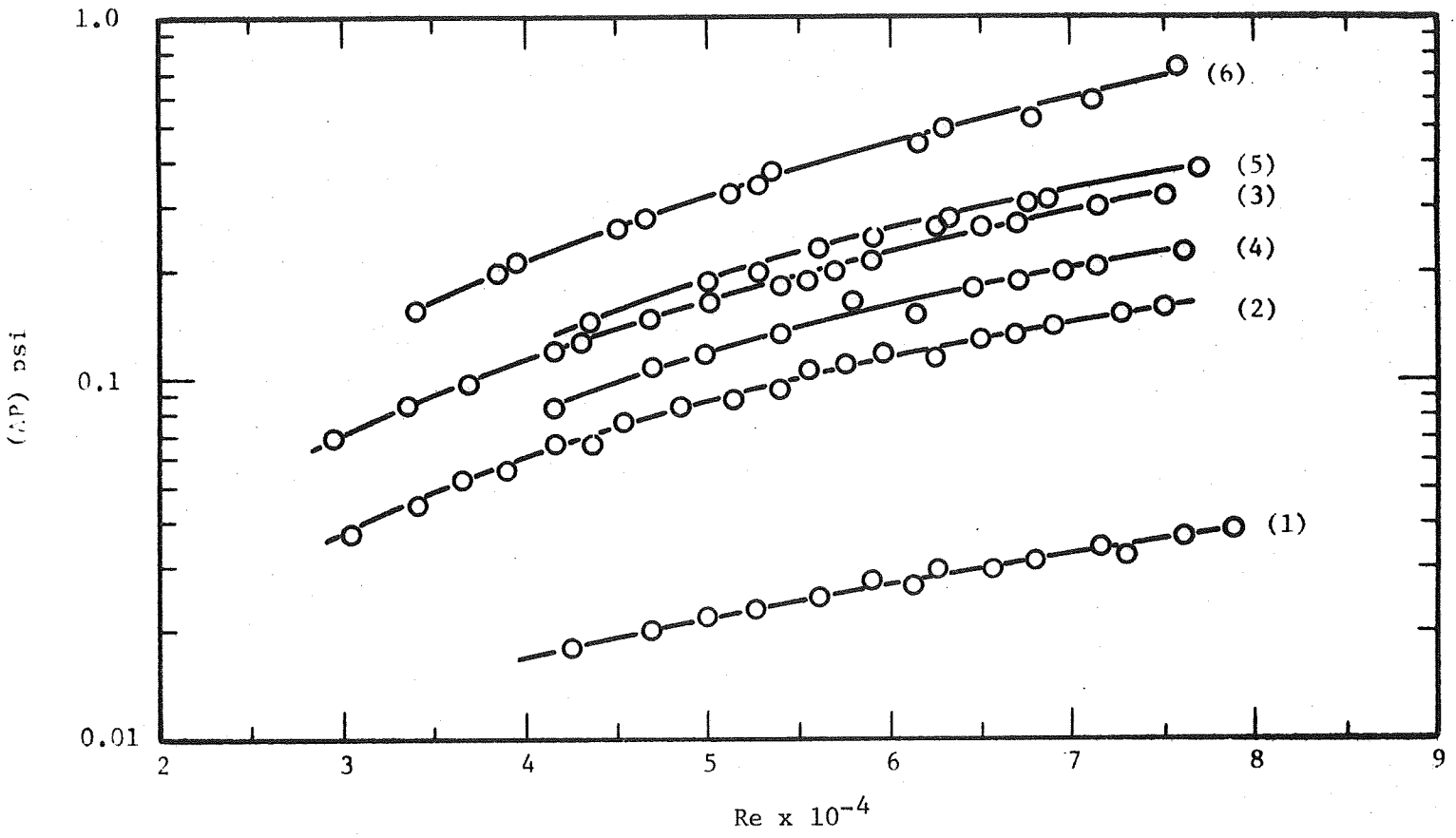

(1) No Turbulence Promoters
(2) (3/8" x 12") on Shell Side
(3) (3/8" x 6") on Shell Side
(4) (1/4" x 4") on Inner Tubes (None on Shell)
(5) (1/4" x 2.2") on Inner Tubes (None on Shell)
(6) (3/8" x 12") on Shell Side plus
(1/4" x 2.2") on Inner Tube

Figure 31. Comparison of Axial Pressure Drop With Various Mixing Promoters.

V. FINAL HEAT EXCHANGER DESIGN CALCULATIONS

The design approach for the NaK-NaK heat exchanger as described before consists generally of determining the tube length for any tentatively selected cross sectional geometry under the prescribed design conditions and then using this configuration to check the pressure drop limitations from hydraulic calculations. Step-by-step design calculations are provided following for the case of the 100 KW NaK-NaK heat exchanger. The design specifications are listed in Table 11 for convenience.

A. THERMAL DESIGN CALCULATIONS

(1) Given Conditions

Primary NaK Flow Rate	7.5 lb/sec
Auxiliary NaK Flow Rate	0.32 lb/sec
Primary NaK Inlet Temperature	1300°F
Auxiliary NaK Inlet Temperature	110°F
Auxiliary NaK Exit Temperature (Minimum)	1100°F
Thermal Power (Maximum)	100 KW

(ii) Selected Geometry

Shell O.D.	5 inches
Shell Wall Thickness	0.120 inch
Shell I.D.	4.75 inches
Annulus O.D.	1.5 inches
Annulus Wall Thickness	0.050-inch
Annulus I.D.	1.4 inches
Tube O.D.	1.25 inches
Tube Wall Thickness	0.065 inch
Tube I.D.	1.12 inches
Material (Shell, Annulus, Tube)	SS 316

TABLE 11

SYSTEM CONDITIONS @ HEAT EXCHANGER INTERFACE

Auxiliary Heat Exchanger Design Conditions

Parameter		Value
Thermal energy transfer capability	(minimum)	70 KW_t
	(maximum)	100 KW_t
Pressure drop, primary loop side	(maximum)	0.15 psi
Pressure drop, auxiliary loop side	(maximum)	1.0 psi
NaK outlet temperature, auxiliary loop side	(minimum)	1100°F

Auxiliary Heat Exchanger Interface Conditions

Parameter	Value
Flow rate, primary loop side	27,000 lb/hr
Flow rate, auxiliary loop side	1150 lb hr
NaK inlet temperature, primary loop side	1300°F
NaK inlet temperature, auxiliary loop side	110°F

Shell-Side Net Flow Area

$$A_F = \frac{\pi}{4}\left[(4.75)^2 - 2\,(1.5)^2 - (3/8)^2\right]$$

$$= 14.1 \text{ in}^2$$

Mass Velocity

$$G_P = \frac{144\ W_p}{A_F} = \frac{144(7.5)}{14.1}$$

$$= 76.6 \text{ lb/ft}^2\text{-sec}$$

$$G_A = \frac{144\ (0.32)}{\frac{\pi}{4}\ (1.12)^2} = 44.3 \text{ lb/ft}^2\text{-sec}$$

Reynolds Number

$$D_e = \frac{4 \times 14.1}{\pi[5 + 2\ (1.5) + 0.375]} = 2.146 \text{ inches}$$

$$N_{ReP} = \frac{300\ (De)\ (G_p)}{\mu} = \frac{300\ (2.146)\ (76.6)}{0.35}$$

$$= 1.41 \times 10^5$$

$$N_{ReA} = \frac{300\ (1.12)\ (44.3)}{0.53} = 2.88 \times 10^4$$

Heat Transfer Coefficient

(The Lubarsky-Kaufman equation is used to predict h due to its lowest prediction of h among other cited equations in Part IV.

$$h_p = \frac{k}{D_e}\left[0.625\ (N_{Pr}\ N_{Re})^{0.4}\right]$$

$$= \frac{14.8 \times 12}{2.146}\left[0.625\ (0.00496 \times 1.41 \times 10^5)^{\ 0.4}\right]$$

$$= 82.6\ (8.55) = 706\ \text{Btu/hr-ft}^2 - {}^{o}\text{F}$$

$$h_A = \frac{15.1 \times 12}{1.15}\left[0.625\ (0.00737 \times 2.88 \times 10^4)^{0.4}\right]$$

$$= 157.5 \times 5.33 = 840\ \text{Btu/hr-ft}^2\text{-}{}^{o}\text{F}$$

Wall Equivalent Heat Transfer Coefficient

SS 316 Tube Wall

$$h_{ss} = \frac{2k_{ss}}{D_i \ell n\left(\frac{D_o}{D_1}\right)} = \frac{2 \times 132}{1.1\ \ell n\left(\frac{1.25}{1.12}\right)} = 2720\ \text{Btu/hr-ft}^2\text{-}{}^{o}\text{F}$$

Static NaK Layer

$$h_{NaK} = \frac{2(14.84 \times 12)}{1.25\ \ell n\left(\frac{1.4}{1.25}\right)} = 2520\ \text{Btu/hr-ft}^2\text{-}{}^{o}\text{F}$$

SS 316 Annulus

$$h_{an} = \frac{2(159)}{1.4\ \ell n\left(\frac{1.5}{1.4}\right)} = 3360\ \text{Btu/hr-ft}^2\text{-}{}^{o}\text{F}$$

Composite Wall Heat Transfer Coefficient
(Referred to Tube Inside Diameter)

$$h_w = \left[\frac{1}{2720} + \frac{1}{2520}\left(\frac{1.25}{1.12}\right) + \frac{1}{3360}\left(\frac{1.4}{1.12}\right)\right]^{-1}$$

$$= (0.368 + 0.431 + 0.362)^{-1} \times 10^3$$

$$= 860\ \text{Btu/hr-ft}^2\text{-}{}^{o}\text{F}$$

Overall Heat Transfer Coefficient (Referred to tube inside diameter)

$$U = \left[\frac{1}{1.15 \times 706} + \frac{1}{860} + \frac{1}{840}\right]^{-1}$$

$$= 292\ \text{Btu/hr-ft}^2\text{-}{}^{o}\text{F}$$

Log-Mean Temperature Difference

Primary NaK Exit Temperature

$$= 1300 - \frac{100}{1.054 \times 7.5 \times 0.21} = 1240^{o}\text{F}$$

$$(\Delta T)_n = \frac{1130 - 200}{\ell n \frac{1130}{200}} = 537^{o}F$$

Required Heat Transfer Tube Length

$$L = \frac{1}{\pi D_1} \left[\frac{Q}{U (\Delta T)_{\ell m}}\right]$$

$$= \frac{1}{\pi(1.15)} \left[\frac{3600 \times 100 \times 144}{1.054 \times 292 \times 537}\right]$$

$$= 84.5 \text{ inches}$$

The actual length of about 90 inches provides some design margin.

B. HYDRAULIC DESIGN CALCULATIONS

(i) Given Conditions (Final Heat Exchanger Design)

(a) Shell-side flow subject to a 90 degree turn from 5-inch OD inlet pipe into the heat transfer section.

(b) Shell-side flow passage in the heat transfer section equipped with two spacers (as shown in Figure 24 and 3/8-inch x 6-inch wire coil).

(c) Exit section consisting of an elbow, a reducer, and a 3-inch extended pipe. The dimensions are as follows:

4-inch x 90° LR elbow
4-inch to 2-1/2-inch OD reducer
3-inch long, 2-1/2-inch OD pipe

All three have 0.083-inch wall thicknesses.

(d) 90-inch active axial length.

(e) A 10-inch long 0.625-inch OD tube with wall thickness of 0.035-inch was used in the auxiliary NaK flow inlet as a thermal protection.

(f) Shell and tube dimensions, flow rates and temperature levels are the same as used in the thermal design calculation.

(ii) Pressure Drop Prediction

Tube-side Pressure Drop

(1) For 10-inch inlet tube, T = 150°F

$\rho = 53$ lb/ft^3, $\mu = 1.4$ lb/ft

$$N_{Re} = \frac{GD_1}{\mu} = \left(\frac{1150}{3600}\right) \frac{144 \times 4}{\pi(0.555)^2} \left(\frac{0.555}{1.4}\right) \times 300 = 2.26 \times 10^4$$

$$f = \frac{0.316}{\left(2.26 \times 10^4\right)^{1/4}} = 0.0258$$

The pressure drop due to 10-inch long, 0.625-inch OD tube will be

$$(\Delta P) = f \left(\frac{L}{D}\right) H_v = 0.0258 \left(\frac{10}{0.555}\right) \frac{(190)^2}{64.4 \times 53 \times 144}$$

$$= 0.0342 \text{ psi}$$

(2) For sudden expansion from 0.555-inch ID tube to 1.12-inch ID tube

Velocity Head at smaller cross sectional area

$$= \frac{(190)^2}{64.4 \times 53 \times 144} = .0735 \text{ psi}$$

For diameter ratio equal to $(\frac{0.555}{1.12}) = 0.483$ loss coefficient for sudden expansion is equal to approximately 0.55 from Figure 15 cited from Reference 11.

Then the pressure drop due to this sudden expansion will be

$$(\Delta P) = 0.55 \times 0.0735 = 0.0403 \text{ psi}$$

(3) For 90-inch long auxiliary NaK tube at T = 700°F, $\rho = 49$ lb/ft^3, $\mu = 0.53$ lb/ft-hr

$$\text{Velocity Head} = \frac{(44.3)^2}{64.4 \times 144 \times 49} = 0.433 \times 10^{-2} \text{ psi}$$

$$f = \frac{0.316}{(N_{Re})^{\frac{1}{4}}} = 0.316 \left[(2.88 \times 10^4)\right]^{-\frac{1}{4}} = 0.0243$$

Then the pressure drop due to 90-inch long auxiliary NaK tube is

$$\Delta P = f \frac{L}{D_i} H_v = 0.0243 \left(\frac{100}{1.15}\right) 0.433 \times 10^{-2}$$

$$= 0.00915 \text{ psi}$$

(4) Total tube-side pressure drop

$$(\Delta P)_t = 0.0342 + 0.0403 + 0.00915$$

$$= 0.0836 \text{ psi}$$

Shell-Side Pressure Drop

(1) Inlet Turn

The pressure drop in the inlet turn is caused by a 90 degree tee bend and a sudden contraction (flow area changes from 17.7 in^2 to 14.1 in^2). From the hydraulic test results, the loss coefficients, K, were determined to be between 1.5 and 1.2 over a Reynolds number range of 3×10^4 to 7.5 to 10^4. The K values slightly decreased as the Reynolds numbers increased.

Thus, the inlet turning loss is estimated as

$$(\Delta P) = KH_v = 1.5 \times \frac{(76.6)^2}{64.4 \times 44.3 \times 144} = 1.5 \times 0.0143$$

$$= -.0214 \text{ psi}$$

(2) Axial Flow Passage

Hydraulic pressure drops for the shell-side flow passage equipped with coiling copper wire over an axial length of 67-inches were accurately measured. Test results are directly used here to predict the pressure drop for axial flow across the 90-inch long shell side flow passage.

For 3/8-inch x 6-inch wire coil

$$(\Delta P) = (3.5 \times 0.0143) \frac{90}{67} = 0.0672 \text{ psi}$$

(3) Tube Supports

The loss coefficients for tube supports correlated from hydraulic test data were in the range of 0.14 to 0.18. Using these values, the pressure drop for shell-side flow across two supports is estimated as

$$(\Delta P) = 2 \times 0.15 \times 0.0142 = 0.00246 \text{ psi}$$

(4) Exit Turn

For the 3-inch long 2-1/2-inch OD, 0.083-inch wall exit pipe

$$\Delta P = f \frac{L}{D} H_v$$

where

$$f = 0.316 \left[(5.04 \times 10^5)\right]^{-\frac{1}{4}} = 0.0116$$

$$H_v = 0.0143 \left[\frac{14.1}{4.27}\right]^2 = 0.156 \text{ psi}$$

$$\Delta P = 0.0116 \left[\frac{3}{2.334}\right] \quad 0.156 = 0.00233 \text{ psi}$$

based upon $N_{Re} = 5.04 \times 10^5$, for smooth steel pipe. Reference 11 gives $f = 0.013$ which is close to the value predicted by the Blasius correlation shown above.

For the 90 degree - 4-inch OD, 0.083-inch wall elbow

$$\Delta P = C_{90} H_v$$

where C_{90} is the loss coefficient for a 90 degree elbow and can be obtained from Reference 12.

$$\Delta P = 0.30 \times 0.0176 = 0.00528 \text{ psi}$$

For the 4-inch - 2-1/2-inch reducer the loss coefficient is estimated from hydraulic test results. Thus, the pressure drop is estimated as,

$$\Delta P = 1.1 \times 0.156 = 0.172 \text{ psi}$$

(5) Total Estimated Shell-Side Pressure Drop

For the final design the total shell-side pressure drop is estimated as follows,

$$\Delta P = 0.0214 + 0.0672 + 0.00246 + 0.00233 + 0.172 + 0.00528 = 0.2707 \text{ psi}$$

The predicted pressure drop of 0.2707 psi is about 80% higher than the specified value of 0.15 psi. The predicted value is somewhat conservative because of the use of hydraulic test results directly and the use of rough surface loss coefficients for the elbow. The model hydraulic test results might be expected to yield a higher pressure drop than the actual heat exchanger due to its rough construction, especially in the high pressure drop end region.

One remark must be made here that the curvature effect is not taken into account in the thermal and hydraulic calculations. The curvature effect upon the prediction of heat transfer coefficients and pressure drop is believed to be negligibly small in the present case based upon estimates made using equations from Reference 13.

C. START-UP AND SHUT-DOWN TEMPERATURE ANALYSIS

The auxiliary NaK-NaK heat exchanger with one auxiliary loop side active shall be capable of operating for a minimum of 100 sequences for both startup and shutdown operations. The startup and shutdown conditions are specified in Tables 12 and 13, respectively. Steady state calculations were made to predict the auxiliary NaK flow exit temperature, T_{NaKAo} and to compare it with the value specified in Tables 12 and 13 for each of the five startup and four shutdown cases. These calculations were performed to determine the auxiliary NaK flow exit temperature for the actual design in order to provide more realistic values for the startup and shutdown conditions. For each calculation the final values of the given quantities (such as flow rates, NaK flow inlet temperature, etc.) listed in Tables 12 and 13 were used. Calculating procedures are as follows: Heat balance equation,

$$Q = W_p (C_p)_p (T_{NaKpi} - T_{NaKpo}) = W_A (C_p)_A (T_{NaKAo} - T_{NaKAi})$$

and heat transfer equation,

$$Q = U (\pi D_i L) \frac{(T_{NaKpo} - T_{NaKAi}) - (T_{NaKpi} - T_{NaKAo})}{\ln \left(\frac{T_{NaKpo} - T_{NaKAi}}{T_{NaKpi} - T_{NaKAo}} \right)}$$

The above two equations are used to calculate T_{NaKpo} and T_{NaKAo} with the remaining quantities known from Tables 12 and 13. An iteration process is involved to solve the required temperatures because the specific C_p has to be evaluated at the average temperature, i.e., $C_p = f\left(\frac{T_{NaKi} + T_{Nako}}{2}\right)_p$ for either primary NaK flow or auxiliary NaK flow.

The computer outputs are presented in Table 14 for all the startup and shutdown operations. The final design dimensions used for these calculations are:

5-inch OD shell with 0.120-inch wall

90-inch active length

1.5-inch OD annulus with 0.049-inch wall

1.25-inch OD tube with 0.065 wall

TABLE 12

AUXILIARY HEAT EXCHANGER CONDITIONS DURING STARTUP

		Phase[1]	I	II	III	IV	V	VI	VII
		Duration of Phase	5 Hrs.	2 Min.	5-10 Min	50-100 Sec.	50 Sec(min)	7-10 Min	Long Term Steady-State
NaK Flow, Primary Loop Side									
Initial		Lb/Hr	0	11,600	27,000	27,000	49,000	49,000	
Final		Lb/Hr	11,600	27,000	27,000	49,000	49,000	49,000	49,000
Max. Rate of Change		Lb/Hr/Sec	11,600	180	0	2,455			
NaK Inlet Temp. Primary Loop Side									
Initial		°F	50-1100	1330	1330	1330	1140(min)	1200-1250	
Final		°F	1330	1330	1330	1130(min)	1200-1250	1110-1160	1110-1160
Max. Rate of Change		°F/Sec	0.1[2][3]	2	Negl.	5	~5	1	
NaK Press., Primary Loop Side									
Initial		Psia	5-35	35	35	35	30	30	30
Final		Psia	35	35	35	30	30	30	
Max. Rate of Change		Psia/Sec	.004	Negl.	Negl.	0.18	-	-	
NaK Flow, Auxiliary Loop Side									
Initial		Lb/Hr	0	500	1150	1150	2100		
Final		Lb/Hr	500	1150	1150	2100	2100	0	0
Max. Rate of Change		Lb/Hr/Sec	500	7.5	-	~ 100	-		
NaK Inlet Temp, Auxiliary Loop Side									
Initial		°F	50	50	110	110	125	N/A	N/A
Final		°F	50	110	110	125	125		
Max. Rate of Change		°F/Sec	-	1	-	0.5	-		
NaK Outlet Temp, Auxiliary Loop Side									
Initial		°F	50	1250	1100	1100	760	N/A	N/A
Final		°F	1250	1100	1100	760	760		
Max. Rate of Change		°F/Sec	.3[3]	3	-	8	-		
NaK Press., Auxiliary Loop Side									
Initial		Psia	18-25	18-25	33-50	33-50	50.75	60-85	60-85
Final		Psia	18-25	33-50	33-50	50-75	60-85	60-85	60-85
Max. Rate of Change		Psia/Sec	-	.25	-	5		-	-

[1] Phase Description

I 0-95 Hz inverter output, reactor outer temp. increased to 1330°F.
II NPMA's accelerated from 95 to 220 Hz operation.
III NPMA's at 220 Hz operation, system transient stabilization period.
IV Mercury Injection, TAA & PMA acceleration to rated speed.
V Mercury flow at ~ 50%, TAA & PMA's rated speed.
VI Mercury flow increased to rated.
VII System at rated conditions.

(2) During Phase I rate of change of primary loop temp ~°F/Sec for ~ 6 min. period.

(3) Transients occur after flows reach final values.

TABLE 13

AUXILIARY HEAT EXCHANGER CONDITIONS DURING SHUTDOWN

	PHASE[1]	I	II	III	IV
	Duration of Phase	30 Sec.	~200 Sec.	~200 Sec.	~ 5 Hr.
NaK Flow, Primary Loop Side					
Initial	Lb/Hr	49,000	49,000	27,000	27,000
Final	Lb/Hr	49,000	27,000	27,000	16,000
Max. Rate of Change	Lb/Hr/Sec	-			
NaK Inlet Temp, Primary Loop Side					
Initial	°F	1200-1250	1200-1250	1180-1220	1130-1170
Final	°F	1200-1250	1180-1220	1130-1170	1100-1150
Max. Rate of Change	°F/Sec	-	4	0.5	
NaK Flow, Auxiliary Loop Side					
Initial	Lb/Hr	0	~2100	1150	1150
Final	Lb/Hr	~2100	1150	1150	500
Max. Rate of Change	Lb/Hr/Sec	2000	50	-	7.5
NaK Inlet Temp, Auxiliary Loop Side					
Initial	°F	300	325	250	500
Final	°F	325	250	200	50 (Min)
Ma . Rate of Change	°F/Sec	1	1	0.3	0.2
NaK Outlet Temp, Auxiliary Loop Side					
Initial	°F	-	840	1020	970
Final	°F	840	1020	970	1080
Max. Rate of Change	°F/Sec	~8	~3	0.3	0.5

[1] Phase Description

I. Mercury flow at ~50% rated, TAA & PMA's at rated speed. (Time period to permit stabilization of AHE conditions).

II. Mercury flow reduced to Zero, TAA decel. PMA's switched to inverter at 220 Hz, reactor power reduced by fast setback.

III. NPMA's at 220 Hz operation. Time period for system stabilization.

IV. Decay heat removal period. NPMA's decel. to remain at 95 Hz operation.

TABLE 14

PREDICTED VALUES OF T_{NaKAo} DURING TRANSIENT PERIOD

		STARTUP OPERATIONS					SHUTDOWN OPERATIONS			
		1	2	3	4	5	6	7	8	9
W_{NaKp}	$\frac{lb}{hr}$	11600	27000	27000	49000	49000	49000	27000	27000	16000
C_p NaKp	$\frac{Btu}{lb-°F}$	0.2114	0.2114	0.2114	0.2094	0.2103	0.2103	0.2100	0.2096	0.2093
T_{NaKpi}	°F	1330°	1330°	1330°	1130°	1225°	1225°	1200°	1150°	1125°
* T_{NaKpo} (predicted)	°F	1275.25	1281.73	1281.74	1096.18	1188.23	1195.03	1162.18	1111.99	1091.01
W_{NaKA}	$\frac{lb}{hr}$	500	1150	1150	2100	2100	2100	1150	1150	500
C_p NaKA	$\frac{Btu}{lb-°F}$	0.2102	0.2098	0.2098	0.2114	0.2105	0.2091	0.2097	0.2105	0.2122
T_{NaKAi}	°F	50°	110°	110°	125°	125°	325°	250°	200°	50°
* T_{NaKAo} (Predicted)	°F	1327.53	1251.80	1251.80	906.62	982.10	1028.31	1139.15	1088.47	1122.93
T_{NaKAo} (Specified value)	°F	1250	1100	1100	760	760	840	1030	970	1080

* Predicted Values for the case:
5" O.D. shell with 120 mil wall
90" heated length
125" O.D. tube with 65 mil wall
1.5" O.D. Annulus with 49 mil wall

VI. MANUFACTURING AND QUALITY ASSURANCE

The intended use of the Auxiliary Loop Heat Exchangers was in a combined system test of the SNAP-8 power conversion system. As a result the materials, manufacturing and quality conformance requirements were quite stringent.

All stainless steel tubing, sheet, and bar stock were procured to applicable ASTM specifications and then subjected to ultrasonic inspection, dye penetrant inspection, and grain size determinations.

The 5-inch diameter tubing was roll formed to the proper curvature after being filled with resin to reduce ovality and prevent local buckling. After the resin was removed the tubing was capped and pressurized internally to about 3000 psi to further reduce ovality. The 1-1/4" dia. tubing was inserted in the 1-1/2 dia. tubing and these were formed to the required curvature as a subassembly. This subassembly, as well as all other parts for the heat exchanger, are shown in an exploded view in Figure 32.

The wire coil inserts were fabricated from 3/8" dia. rod by winding on a mandrel and stretching the coil to the proper pitch. The straight coil sections were then pulled through the curved 5" dia. tubing and were fillet welded to the ID of the tubing. A partial view of the coil insert is shown in Figure 33.

Final assembly was performed in the fixture shown in Figure 34 using gas tungsten arc welding for all joining of parts. All welds were helium leak checked, dye penetrant inspected, and X-rayed to insure that the welds met all of the quality requirements of the contract.

The quality assurance provisions of this program also required a proof pressure test, flow test, center of gravity determination, and a final cleaning of all internal surfaces to a cleanliness level 5 as defined in AGC-STD-1191B. The HRL tubes were pressurized with argon to 355 psia with

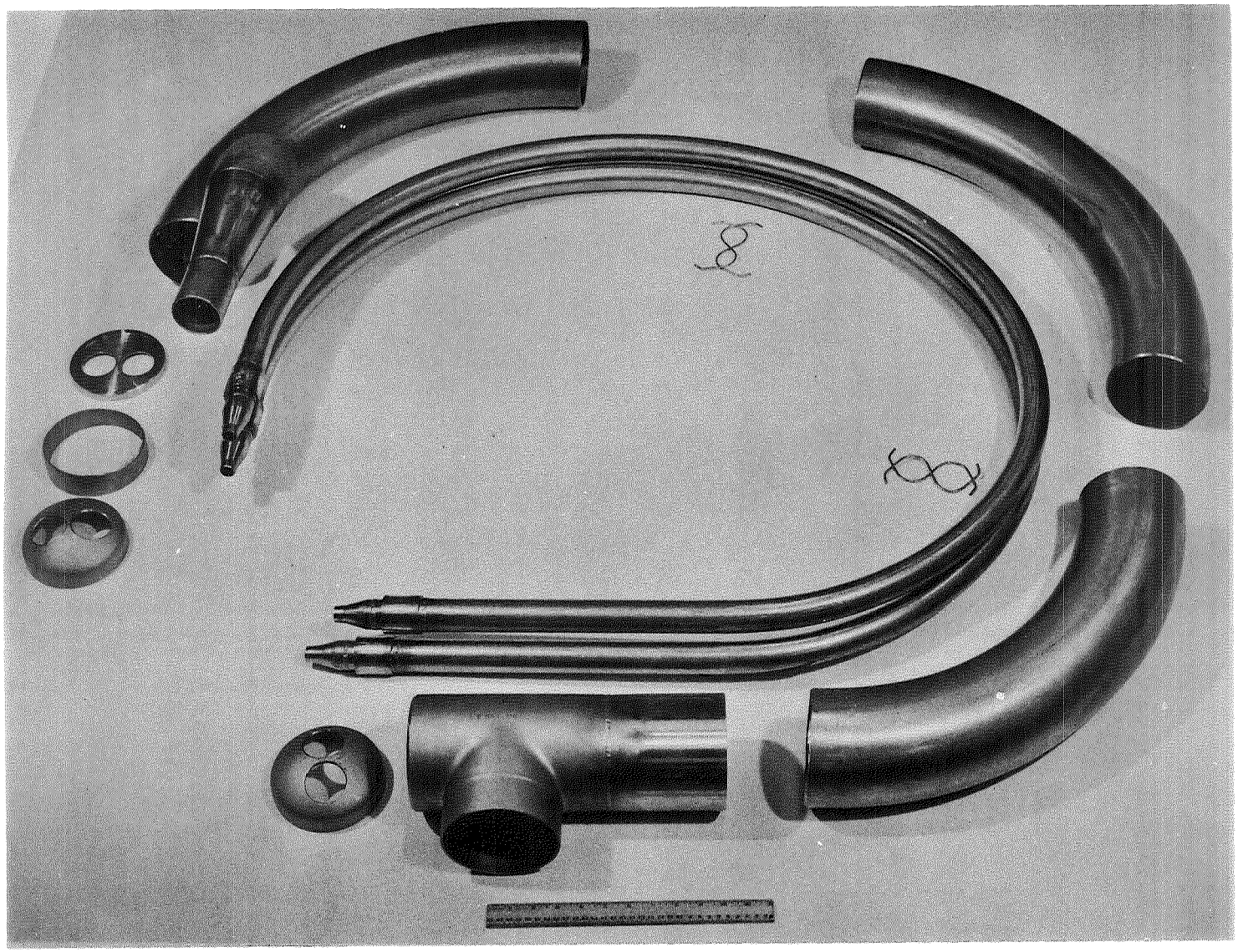

Figure 32. SNAP-8 ALHE Component Parts. (P70-4-7C)

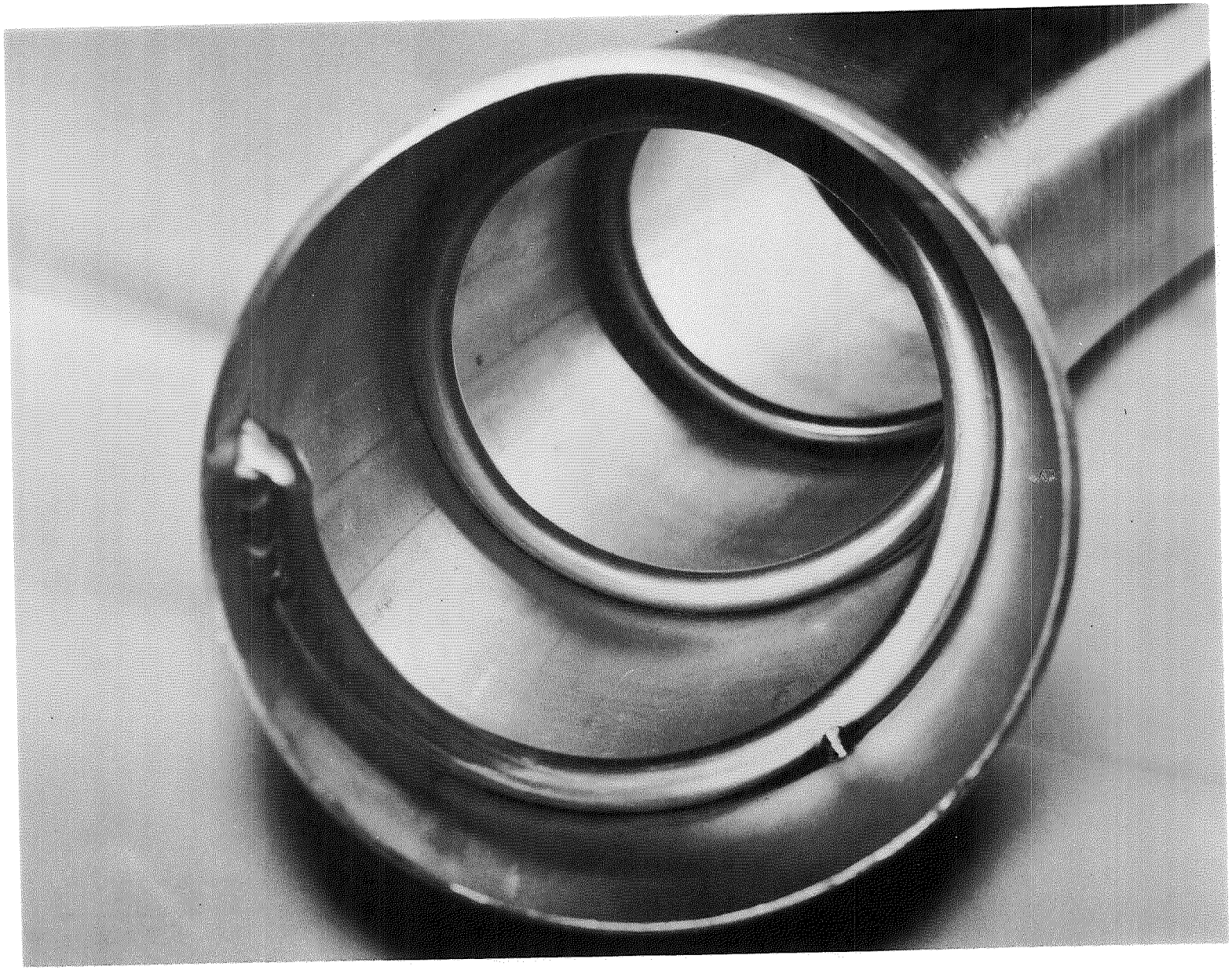

Figure 33. Partial View of Wire Coil Insert. (P70-4-7A)

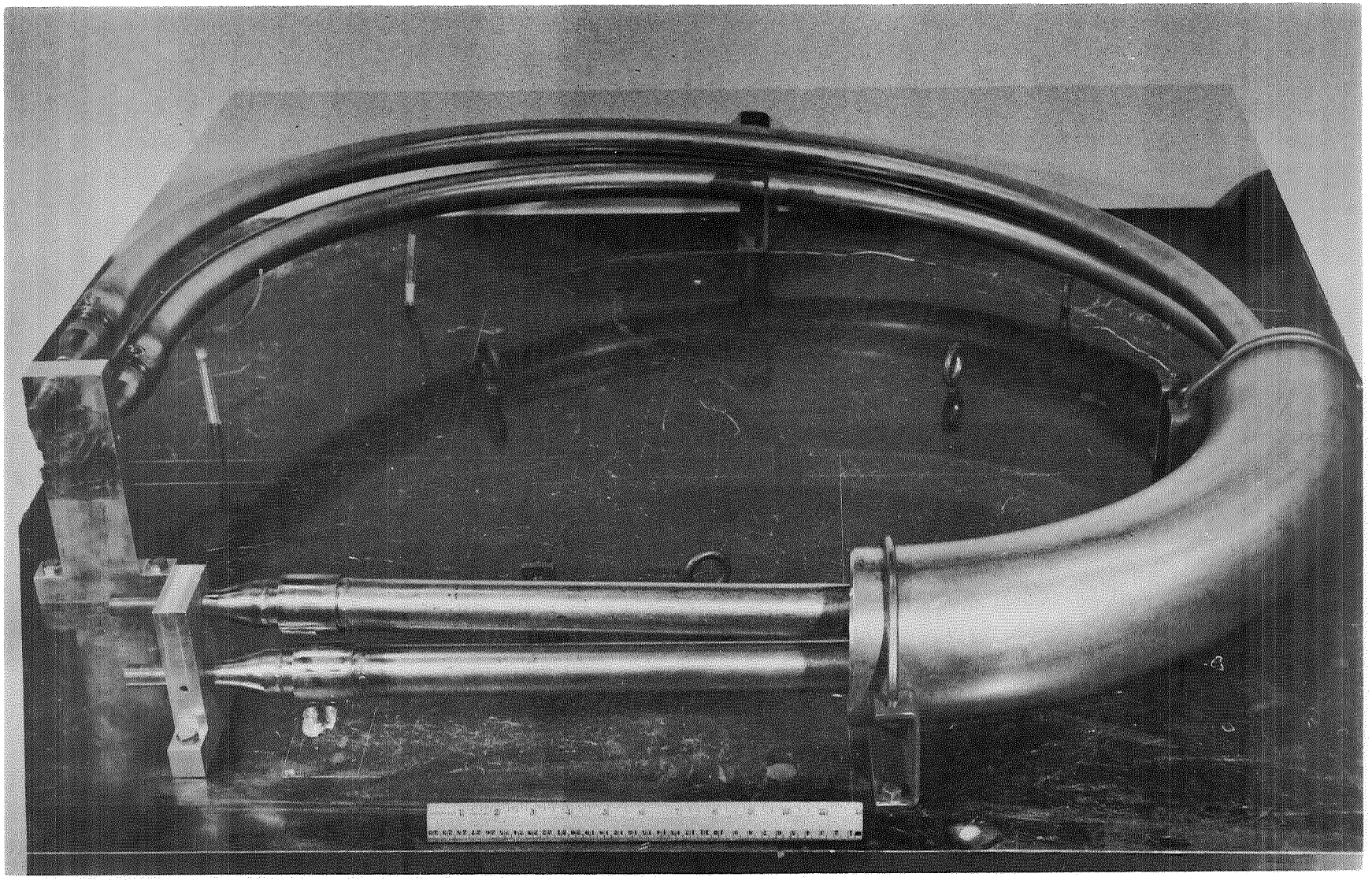

Figure 34. SNAP-8 ALHE Final Assembly Weld Fixture. (P70-4-7B)

the static NaK annuli and the shell at atmospheric pressure. Next the shell was pressurized to 315 psia while the tube side and static NaK annuli remained at atmospheric pressure. In both cases the proof pressure level was maintained for 10 minutes. Shell side flow test was conducted over a range of Reynolds numbers from 29,000 to 75,000 using essentially the same test setup as described in the Shell Side Model Tests. Results are summarized in Table 15. A comparison between the predicted and measured pressure drops is presented in Table 16. The predicted values are based on model flow tests and the tendency is to underpredict the actual ΔP by 15 to 20%. This result is not surprising because the curvature effect was not considered in the model test and there were some discontinuities in the wire coil insert which did not occur in the model test. Instrument errors could account for the remainder of the discrepancy. Similar flow tests were conducted on one of the HRL tubes and the results are summarized in Table 17.

Following the flow test, all passages of the heat exchanger were flushed with filtered demineralized water. Samples were drawn from the final rinse water and a particle count was made in accordance with ARP-598[18]. Additional flushing was done and samples were taken until the particle count was within that specified for cleanliness level 5 in AGC-STD-1191B. The unit was then drained, evacuated and baked out, back-filled with argon, and sealed in preparation for shipment.

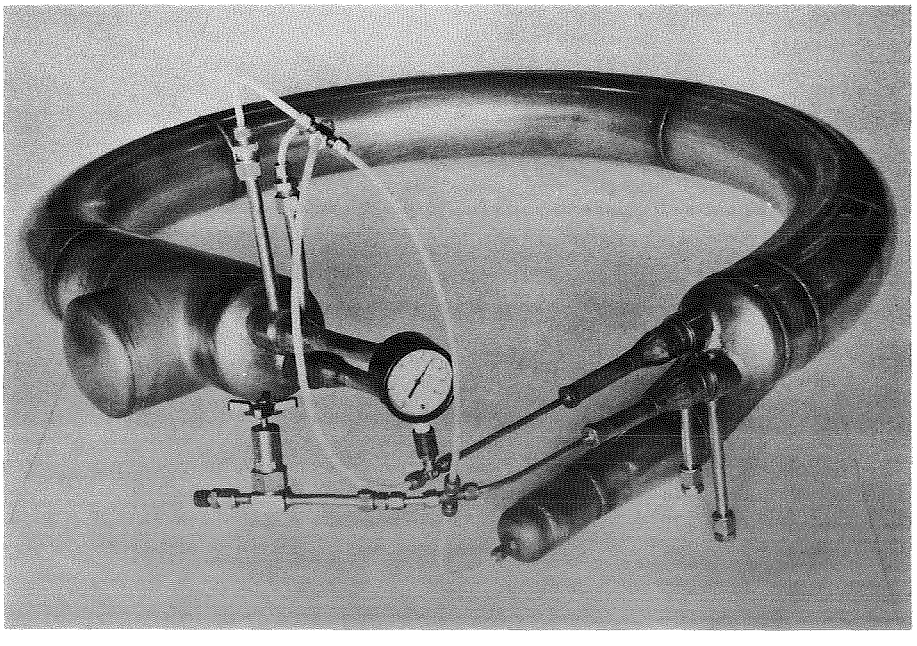

Figure 35. SNAP-8 ALHE Ready For Shipment.

TABLE 15

PROTOTYPE SNAP-8 ALHE SHELL SIDE HYDRAULIC TEST RESULT

RUN NO.	$(\Delta P)_{ori}$ in-Hg	W_{H_2O} lb/sec	G lb/ft^2-sec	R_e x 10^{-4}	Δh_{i-o} (Meriam Fluid) in.	Δh_{i-o} (Hg) in.	P_{i-o}* psi
1	1.2	10.5	108	2.94	10		1.04
2	1.5	11.6	119	3.25	10.9		1.10
3	2.4	14.3	146	4.05	17.2		1.55
4	2.8	15.6	160	4.35	19.1		1.69
5	3.0	16.2	165	4.5		3.2	1.79
6	3.6	17.6	179	4.9	24.2		2.04
7	4.0	18.7	191	5.25	26.8		2.22
8	5.2	20.9	214	5.8		5.2	2.69
9	5.4	21.4	218	5.98		5.4	2.80
10	6.1	22.4	228	6.25		6.1	3.11
11	7.0	24.2	248	6.75		7.0	3.52
12	7.9	25.7	263	7.2		7.6	3.80
13	8.8	26.9	275	7.5		8.4	4.16

* Corrected with elevation head only, possible experimental errors in obtaining ΔP_{i-o} are not considered.

TABLE 16

COMPARISON BETWEEN MEASURED AND PREDICTED PRESSURE DROP

SHELL SIDE FLOW

RUN NO.	R_e x 10^{-4}	$(\Delta P)_m$ psi	$(H_v)_p$ psi	$(\Delta P)_p$ psi	$\frac{(\Delta P)_m}{(\Delta P)_p}$	Percent of Underestimation
1	2.94	1.04	0.020	0.893	1.17	17%
2	3.25	1.10	0.024	1.003	1.10	10%
3	4.05	1.55	0.037	1.326	1.17	17%
4	4.35	1.69	0.043	1.473	1.15	15%
5	4.5	1.79	0.047	1.573	1.14	14%
6	4.9	2.04	0.056	1.773	1.15	15%
7	5.25	2.22	0.063	1.923	1.15	15%
8	5.8	2.69	0.079	2.313	1.16	16%
9	5.98	2.80	0.082	2.403	1.16	16%
10	6.25	3.11	0.091	2.583	1.20	20%
11	6.75	3.52	0.106	2.853	1.23	23%
12	7.2	3.80	0.119	3.213	1.18	18%
13	7.5	4.16	0.13	3.47	1.19	19%

TABLE 17

COMPARISON OF PREDICTED AND MEASURED PRESSURE DROP FOR ALHE TUBE-SIDE FLOW

W_{H_2O} (lb/sec)	0.372	0.509	0.732
$(\Delta P)_{exp.\ 0.5" \rightarrow 0.62"}$ (psi)	0.0154	0.0288	0.0595
$2(\Delta P)_{0.62" \times 6"}$ (psi)	0.0274	0.0494	0.0974
$(\Delta P)_{c'0.62" \rightarrow 0.55"}$ (psi)	0.00348	0.00653	0.0134
$(\Delta P)_{0.55" \times 10"}$ (psi)	0.0448	0.0773	0.145
$(\Delta P)_{exp.\ 0.55" \rightarrow 1.15"}$ (psi)	0.0521	0.0976	0.2
$(\Delta P)_{1.15" \times 90"}$ (psi)	0.0121	0.0218	0.04
$(\Delta P)_{c\ 1.15" \rightarrow 0.62"}$ (psi)	0.0163	0.0306	0.063
$(\Delta P)_{c,\ 0.62" \rightarrow 0.5"}$ (psi)	0.0154	0.0288	0.0595
$(\Delta P)_{TOTAL,\ predicted}$ (psi)	0.187	0.341	0.678
$(\Delta P)_{TOTAL,\ measured}$ (psi)	0.212	0.338	0.62
$\frac{(\Delta P)_{measured}}{(\Delta P)_{predicted}}$	1.135	0.99	0.916

VII. CONCLUDING REMARKS

General thermal and hydraulic design approaches for liquid metal heat exchangers have been discussed and outlined. Efforts have been made to clarify design difficulties in regard to various assumptions and uncertainties involved in the thermal and hydraulic areas. Pressure losses and flow mixing for shell-side flow passing complicated geometries have been measured and correlated by water flow tests. Some of these measured results were used for design calculations. A 100 KW NaK shell and tube heat exchanger has been worked out step-by-step as an illustrated design example. Some general conclusions and remarks resulting from this effort are in order.

The calculated thermal performance of the heat exchanger is generally higher than the levels specified in AGC-10622. Complex problems such as nonuniform axial heat flux distribution and nonuniform shell-side velocity distribution and their effects upon prediction of shell-side heat transfer coefficient were not considered. Heat transfer through the static NaK layer between the tube and the annulus was considered as conduction only. Hence, the effect from natural convection of this confined layer was neglected. Temperature distribution in the region following the thermal baffle cannot be analyzed by a simple method due to the complex geometry in this end region.

The predicted pressure drop for the shell side flow in NaK is about 80% higher than the value specified in AGC-10622. This compromise was necessary to insure good heat transfer characteristics. The wire coil has been identified as a good shell-side flow mixing device through visual study with dye injection. For better results of shell-side flow mixing, additional wire coils could be wrapped around the two inner tubes. However, this approach was not incorporated in the final design because of the added pressure drop penalty. The predicted tube side pressure drop is considerably below the specified allowable pressure drop.

The thermostructural analysis of the SNAP-8 ALHE assembly indicates that the stresses generated during steady state operation will not exceed design stress allowables. The largest thermal stresses generated during this operation will occur in the 1.5-inch OD tube at joint 8 in Figure 3. The values of stress obtained will be conservative since the support between the 1.5-inch OD tube and the 5-inch OD shell was assumed rigid. Experiments performed at GE-NSP to determine the force and deflection relationship of the wire spring supports indicated that a 180 lb. load will displace the 1.5-inch OD tube, relative to the 5-inch OD shell, to a new equilibrium position determined by the thermal mismatch. This means that the tube is merely displaced transversely to relieve the thermal load, thereby reducing the thermal stresses generated during steady state operation.

VIII. REFERENCES

1. Beitch, L, "MASS System - The Computer Program for General Redundant Structures with Vibratory and General Static Loading", General Electric Company, Flight Propulsion Division, Evendale, Ohio, TIS R 66FPD172, September 1966.

2. Timoshenko, S.V. and Woinowsky-Krieger, S, "Theory of Plates and Shells". McGraw-Hill Book Company, 1959.

3. ASME Boiler and Pressure Vessel Code, Sections 1 and 3.

4. SNAP-8 Auxiliary Heat Exchanger Dwg. No. 47R199403, August 22, 1969.

5. Structural Design Criteria, SNAP-8 Specification AGC-10650A, Aerojet-General Corporation, February 12, 1969.

6. Lyon, R.N., "Liquid Metal Heat Transfer Coefficient", Trans. AiCHE, 47, pp 75-79 (1955).

7. Lubarsky, B. and Kaufmann, S.J., "Review of Experimental Investigation of Liquid Metal Heat Transfer", NASA Report 1270 (1956).

8. Dwyer, O.E., "Heat Transfer to Fluids Flowing Through Pipes, Annuli and Parallel Plates", USAEC Report No. BNL-6692 (1963).

9. McAdams, W.H., Heat Transmission, McGraw-Hill Co., New York (1954).

10. Hsia, E.S. and Fuller, R.A., "Shell-Side Hydraulic Characteristics of a Full-Scale SNAP-8 Multiple-Tube Model Boiler", Report for the Contract NAS 3-10610, General Electric Co. (1969).

11. Design Data - Heat Transfer and Fluid Flow Section G403.3, General Electric Company (1959).

12. Flow of Fluids, Technical Paper No. 410, Crane Co. (1957).

13. Kays, W.M., Convective Heat and Mass Transfer, McGraw-Hill Book Co., New York (1966).

14. Specification AGC-10622, Part I, Heat Exchanger NaK/NaK, Auxiliary Prototype.

15. ASME, Section I, Power Boilers, A-24, Table PG-23.1.

VIII. REFERENCES (Cont'd)

16. ASME, Section III, Nuclear Vessels, Class A, Table N-421.

17. United States Steel Corporation, National Tube Division, Pipes and Tubes for Elevated Temperature Service, Bulletin #26.

18. SAE-ARP-598, Procedure for the Determination of Particulate Contamination of Hydraulic Fluids by the Particle Count Method.

APPENDIX A

Page intentionally left blank

APPENDIX A

THERMAL STRESS DISCONTINUITY

The thermal stresses generated at the inlet connector are principally due to the thermal mismatch between the tube and connector, which are at different average temperatures. Compatibility requires that the deflection and slope of the tubing connected to the fitting be equal.

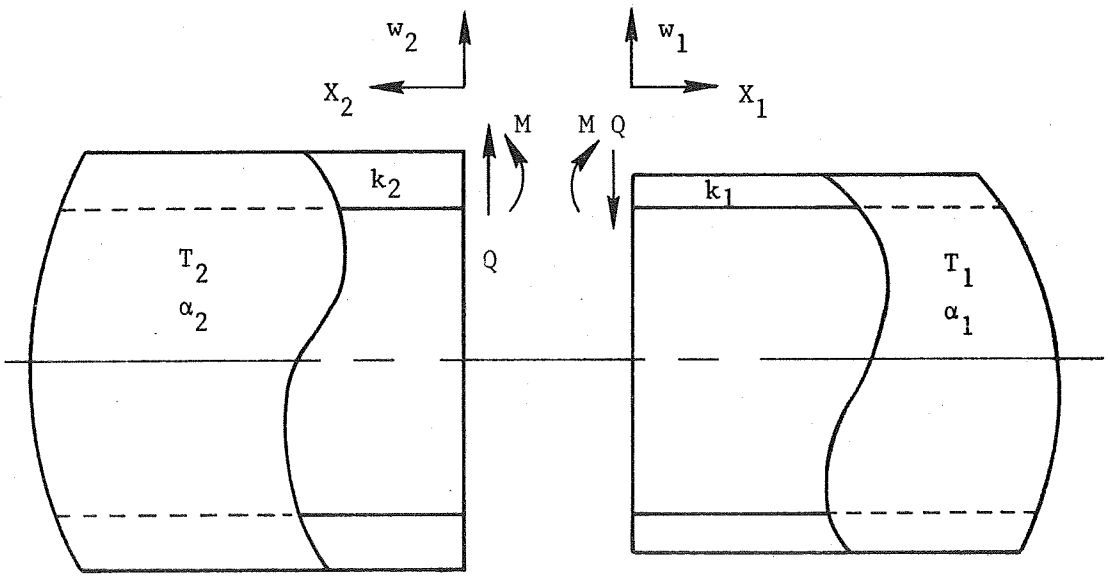

From Reference 2, Timoshenko has derived the deflection and slope of a cylinder subjected to edge loads.

$$W = \frac{1}{2\beta^3 D} (\beta M + Q) \qquad (1)$$

$$W'_{x=0} \quad \frac{1}{2\beta^2 D} (2\beta M + Q) \qquad (2)$$

Once the shear Q and moment M have been obtained by solving (5), the meridional and hoop stresses, respectively, can be determined by equations (6) and (7).

$$\sigma_\theta = \pm \frac{6M}{h^2} \tag{6}$$

$$\sigma_\phi = \frac{E}{(R + 1/2)} \pm 6 \gamma \frac{M}{h^2} \tag{7}$$

When the appropriate material properties and geometry are substituted in the foregoing equations, the results shown in Figures 4 and 5 are obtained.

DETERMINATION OF MAXIMUM POSSIBLE STRESS f_{ms}

$f_{ms} = K_{mA} f_c$

f_c = maximum calculated stress level

K_{5A} = 1.1 dimensional variation

K_{6A} = 1.1 manufacturing/dimensional deviation

K_{7A} = stress concentration factor

K_{8A} = 1.25 uncertainty factor

FACTOR OF SAFETY FS

$$FS = \frac{2F}{f_{ms}} = 1.60 \frac{F_y}{f_c} \geqq 1.25$$

NORMALIZED FACTOR OF SAFETY

$$FS = 1.28 \frac{F_y}{f_c} \geqq 1.0$$

ACCORDING TO ASME CODE:

FACTOR OF SAFETY

$$FS = \frac{3S_m}{f_c} \geqq 1.0$$

where S_m = design stress intensity

f_c = maximum calculated stress

where

E = Young's modulus

h = cylinder thickness

ν = Poisson's ratio

R = mean radius

$$D = \frac{E\,h^3}{12\,(1-\nu^3)} \qquad \text{modulus of rigidity}$$

$$\beta^4 = \frac{3\,(1-\nu^2)}{R^2\,h^2} \qquad \text{parameter}$$

The compatibility requirement at the jointure of the two cylinders becomes:

$$W_1 + W_2 = \Delta W \tag{3}$$

$$W_1' + W_2' = 0 \tag{4}$$

where

$$\Delta W = R_1\,\alpha_1\,T_1 = R_2\,\alpha_2\,T_2$$

When equations (1) and (2) are substituted into the equations (3) and (4), the result is a set of two simultaneous equations which are conveniently written in matrix notation.

$$\begin{bmatrix} F_{11} & F_{12} \\ F_{21} & F_{22} \end{bmatrix} \begin{Bmatrix} M \\ Q \end{Bmatrix} = \begin{Bmatrix} \Delta W \\ 0 \end{Bmatrix} \tag{5}$$

The elements of the IF matrix are given by:

$$F_{11} = 1/2 \left[\frac{1}{\beta_1^{\,2} D_1} + \frac{1}{\beta_2^{\,2} D_2} \right]$$

$$F_{12} = \left[\frac{1}{\beta_1^{\,3} D_1} \quad \frac{1}{\beta_2^{\,3} D_2} \right]$$

$$F_{21} = \left[\frac{1}{\beta_1 D_1} \quad \frac{1}{\beta_2 D_2} \right]$$

$$F_{22} = 1/2 \left[\frac{1}{\beta_1^{\,2} D_1} \quad \frac{1}{\beta_2^{\,2} D_2} \right]$$

BASED ON YIELD STRESS, ASME CODE BECOMES:

$$FS = \frac{2F_y}{f_c} = 1.0$$

STRUCTURAL INTEGRITY RELATION USED IN ANALYSIS OF SNAP-8 ALHE

ACCORDING TO SPEC. AGC-10650:

Allowable Stress F

$$F = .8\ F_y$$

where $K_{im} = 1$

$K_{2m} = .8$

$K_{3m} = 1$

$K_{4m} = 1$

Maximum Possible Stress f_{ms}

$$f_{ms} = f_c$$

where $K_{5A} = 1$

$K_{6A} = 1$

$K_{7A} = 1$

$K_{8A} = 1$

CRITERION

MINIMUM FACTOR OF SAFETY FOR SNAP-8 HEAT EXCHANGER

FS = 1.25 Against Yield

FS = 1.50 Against Ultimate

STEADY STATE STRESS

$$FS = \text{FACTOR OF SAFETY} = \frac{F}{f_{ms}}$$

where

f_{ms} = maximum possible steady stress

F = allowable stress

DETERMINATION OF ALLOWABLE STRESS F

$$F = K_{nm} F_c$$

where

F_c = curve stress

K_{im} = .8 material factor if no yielding is allowed

K_{2m} = { .8 material deviation factor when ultimate is used
.85 when y ld is used

K_{3m} = material decay

K_{4m} = .9 weld confidence factor

Page intentionally left blank

APPENDIX B

Page intentionally left blank

APPENDIX B - DSCS PROGRAM "CURVED"

A DSCS program called "CURVED" has been developed to calculate elemental free-free stiffness matrices for curved beams of rectangular or circular cross-section with either in-plane or out-of-plane loadings.

The equations of Reference 1 were used to calculate the influence coefficient matrix of a beam element. This was then inverted to obtain the restrained stiffness matrix Phi (ϕ). A transformation matrix, Beta (β), was developed to go from the restrained condition to a free-free beam element. The elemental free-free stiffness matrix, STIFF, is given by:

$$\text{STIFF} = \beta^T \phi \beta \qquad (1)$$

The general beam element has 12 DOF as shown below; 6 on each end consisting of 3 force and 3 moment DOF:

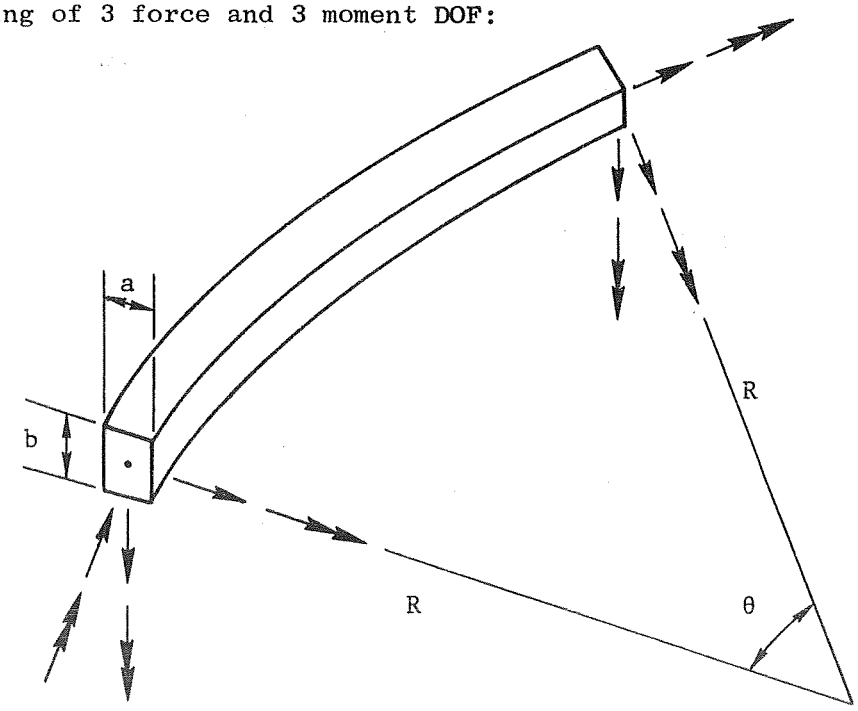

The in-plane and out-of-plane deformations are uncoupled; therefore, the 12 x 12 stiffness matrix can be separated into two 6 x 6 stiffness matrices, i.e.,

IN-PLANE

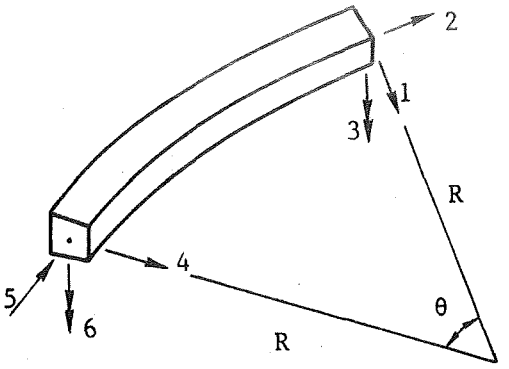

OUT-OF-PLANE

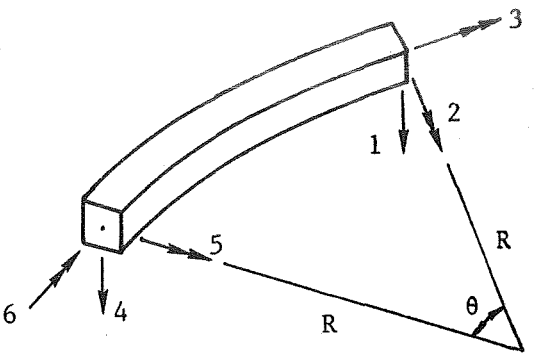

Each of these cases yields a different 6 x 6 free-free stiffness matrix.

PROGRAM INPUT:

Input to the computer is in the following order:

1. Type of cross-section
   a. Rectangular
   b. Circular
2. Type of Loading
   a. In-Plane
   b. Out-of-Plane
3. Properties and element geometry
   a. Elastic Modulus, psi
   b. Shear modulus, psi
   c. } Von Karman coefficients related
   d. } to cross-section distortion, KI,KO (1)
   e. Radius of element, R (inches)
   f. Angle of element, θ (degrees)

NOTE 1: KI is the in-plane Von Karman coefficient and KO is the out-of-plane coefficient. These relate the effects of cross-section distortion. If these values are not known, set KI = KO = 1 which, would not consider any cross-sectional deformation.

4. Cross-section dimensions
   a. Radii - outer and inner for circular cross-section
   b. Width (in-plane dimension) and height (out-of-plane dimension) for rectangular cross section

PROGRAM OUTPUT:

The program calculates the resulting free-free stiffness matrix and prints it out.

SIGN CONVENTIONS:

All sign conventions are shown in their positive directions in the previous figures and obey the right hand rule.

SAMPLE PROBLEM:

Let us consider a sample problem for a hollow circular beam with the following properties:

a. Out-of-plane loading
b. $E = 30. \times 10^6$ psi
c. $G = 10.6 \times 10^6$ psi
d. KO = KI = 1.
e. R = 15.0 IN.
f. $\Theta = 30.$ Degrees
g. R (Outer) = .75 IN.
h. R (Inner) = .70 IN.

Output for the sample case and a listing of the program are shown on the succeeding pages.

Influence coefficients for in-plane loading:

$$\phi'_{11} = \left[6\Theta - 8 \sin(\Theta) + \sin(2\Theta)\right] \frac{R^3 Ki}{4EI}$$

$$\phi'_{12} = \left[3 - 4\cos(\Theta) + \cos(2\Theta)\right] \frac{R^3 Ki}{4EI}$$

$$\phi'_{13} = \left[\Theta - \sin(2\Theta)\right] \frac{R^3 Ki}{4EI}$$

$$\phi'_{22} = \left[2\Theta - \sin(2\Theta)\right] \frac{R^3 Ki}{4EI}$$

$$\phi'_{23} = \left[1 - \cos(\Theta)\right] \frac{R^2 Ki}{EI}$$

$$\phi'_{33} = \frac{\Theta R Ki}{EI}$$

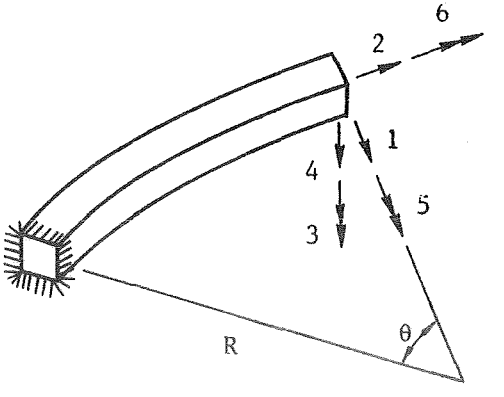

SAMPLE CASE OUTPUT

```
$FORT CURVED


CURVED BEAM INFORMATION: X-SECTION & TYPE
 FOR RECTANGULAR X-SECTION, S=1.
 FOR CIRCULAR X-SECTION,    S=2.
 FOR IN-PLANE LOADS,        P=1.
 FOR OUT-OF-PLANE LOADS,    P=2.


 READ IN VALUES OF S,P=2.,2.

 READ IN VALUES OF E,G,KO,KI,R,THETA(DEGREES)
 LET KO=KI=1 IF NOT SURE OF ACTUAL VALUE.
 =3Ø.E6,1Ø.6E6,1.,1.,15.,3Ø.


 FOR A SOLID CIRCULAR BEAM,R(INNER)=Ø.
 READ IN VALUES OF R(OUTER),R(INNER)
 =.75,.7Ø

                    STIFFNESS MATRIX (BY ROWS)

 Ø.4456Ø3E+Ø5  Ø.258779E+Ø5  Ø.172164E+Ø6  -Ø.4456Ø3E+Ø5  -Ø.258779E+Ø5
 Ø.172164E+Ø6

 Ø.258779E+Ø5  Ø.182158E+Ø6  Ø.115971E+Ø6  -Ø.258779E+Ø5  -Ø.151773E+Ø6
 Ø.257190E+Ø4

 Ø.172164E+Ø6  Ø.115971E+Ø6  Ø.887693E+Ø6  -Ø.172164E+Ø6  -Ø.257192E+Ø4
 Ø.464483E+Ø6

-Ø.4456Ø3E+Ø5 -Ø.258779E+Ø5 -Ø.172164E+Ø6   Ø.4456Ø3E+Ø5   Ø.258779E+Ø5
-Ø.172164E+Ø6

-Ø.258779E+Ø5 -Ø.151773E+Ø6 -Ø.257193E+Ø4   Ø.258779E+Ø5   Ø.182158E+Ø6
-Ø.115971E+Ø6

 Ø.172164E+Ø6  Ø.257191E+Ø4  Ø.464483E+Ø6  -Ø.172164E+Ø6  -Ø.115971E+Ø6
 Ø.887693E+Ø6




PROGRAM STOP AT 116Ø

READY
```

PROGRAM LISTING

```
$LIST CURVED

10/21/69  13.454

ØØØ1Ø       COMMON B(6,6),PHI(6,6),PP(6),WORK(3,3),C(6,6),F(6,6),STIFF(6,6)
ØØØ2Ø       PRINT 5
ØØØ3Ø     5 FORMAT(//" CURVED BEAM INFORMATION: X-SECTION & TYPE"/
ØØØ4Ø &      "  FOR RECTANGULAR X-SECTION, S=1."/
ØØØ5Ø &      "  FOR CIRCULAR X-SECTION,    S=2."/
ØØØ6Ø &      "  FOR IN-PLANE LOADS,        P=1."/
ØØØ7Ø &      "  FOR OUT-OF-PLANE LOADS,    P=2."///)
ØØØ8Ø       PRINT:" READ IN VALUES OF S,P"
ØØØ9Ø       READ:S,P
ØØ1ØØ       PRINT:" READ IN VALUES OF E,G,KO,KI,R,THETA(DEGREES)"
ØØ1Ø5       PRINT:" LET KO=KI=1 IF NOT SURE OF ACTUAL VALUE."
ØØ11Ø       PRINT:" "
ØØ12Ø       READ:E,G,AKO,AKI,R,THETA
ØØ13Ø       TH=THETA*3.14159265/18Ø.
ØØ14Ø       STH=SIN(TH)
ØØ15Ø       S2TH=SIN(2.*TH)
ØØ16Ø       CTH=COS(TH)
ØØ17Ø       C2TH=COS(2.*TH)
ØØ18Ø       IF (S.EQ.2.) GO TO 1Ø
ØØ19Ø       PRINT:" "
ØØ2ØØ       PRINT:" FOR A SOLID RECTANGULAR BEAM,A(INNER)=B(INNER)=Ø."
ØØ21Ø       PRINT:" READ IN VALUES OF A(OUTER),B(OUTER),A(INNER),B(INNER)"
ØØ215       PRINT:" A(IN-PLANE DIMENSION),B(OUT-OF-PLANE DIMENSION)"
ØØ22Ø       PRINT:" "
ØØ23Ø       READ:AAO,BBO,AAI,BBI
ØØ24Ø       AIIN=1./12.*(BBO*AAO**3.-BBI*AAI**3.)
ØØ25Ø       AIOUT=1./12.*(BBO**3.*AAO-BBI**3.*AAI)
ØØ251       GO TO 2Ø
ØØ252    1Ø PRINT:" "
ØØ253       PRINT:" FOR A SOLID CIRCULAR BEAM,R(INNER)=Ø."
ØØ254       PRINT:" READ IN VALUES OF R(OUTER),R(INNER)"
ØØ26Ø       PRINT:" "
ØØ27Ø       READ:RO,RI
ØØ28Ø       AIIN=3.14159265/4.*(RO**4.-RI**4.)
ØØ29Ø       AIOUT=AIIN
ØØ3ØØ    2Ø AJ=AIIN+AIOUT
ØØ31Ø       GAMMA=E*AIOUT/(G*AJ)
ØØ32Ø       EII=E*AIIN
ØØ33Ø       EIO=E*AIOUT
ØØ34Ø       GJ=G*AJ
ØØ35Ø *
ØØ36Ø *     BUILD UP ELEMENTAL STIFFNESS MATRIX PHI
ØØ37Ø *
ØØ38Ø       DO 3Ø I=1,6
ØØ39Ø       DO 3Ø J=1,6
ØØ4ØØ    3Ø PHI(I,J)=Ø.Ø
```

```
ØØ41Ø       PHI(1,1)=(6.*TH-8.*STH+S2TH)*R**3.*AKI/(4.*EII)
ØØ43Ø       PHI(1,2)=(3.-4.*CTH+C2TH)*R**3.*AKI/(4.*EII)
ØØ44Ø       PHI(2,1)=PHI(1,2)
ØØ45Ø       PHI(1,3)=(TH-STH)*R**2.*AKI/EII
ØØ46Ø       PHI(3,1)=PHI(1,3)
ØØ47Ø       PHI(2,2)=(2.*TH-S2TH)*R**3.*AKI/(4.*EII)
ØØ48Ø       PHI(2,3)=(1.-CTH)*R**2.*AKI/EII
ØØ49Ø       PHI(3,2)=PHI(2,3)
ØØ5ØØ       PHI(3,3)=TH*R*AKI/EII
ØØ51Ø       PHI(4,4)=(TH/2.-S2TH/4.)*R**3.*AKO/EIO
ØØ52Ø &      +(3.*TH+S2TH/2.-4.*STH)*GAMMA*R**3./(2.*EIO)
ØØ53Ø       PHI(4,5)=(S2TH-2.*TH)*R**2.*AKO/(4.*EIO)
ØØ54Ø &      -(TH-2.*STH+S2TH/2.)*GAMMA*R**2./(2.*EIO)
ØØ55Ø       PHI(5,4)=PHI(4,5)
ØØ56Ø       PHI(4,6)=(C2TH-1.)*R**2.*AKO/(4.*EIO)
ØØ57Ø &      -(1.-2.*CTH+CTH**2.)*GAMMA*R**2./(2.*EIO)
ØØ58Ø       PHI(6,4)=PHI(4,6)
ØØ59Ø       PHI(5,5)=(TH-S2TH/2.)*R*AKO/(2.*EIO)
ØØ6ØØ &      +(TH+S2TH/2.)*R*GAMMA/(2.*EIO)
ØØ61Ø       PHI(5,6)=(STH**2.)*R*AKO/(2.*EIO)
ØØ62Ø &      -(STH**2.)*GAMMA*R/(2.*EIO)
ØØ63Ø       PHI(6,5)=PHI(5,6)
ØØ64Ø       PHI(6,6)=(TH+S2TH/2.)*R*AKO/(2.*EIO)
ØØ65Ø &      +(TH-S2TH/2.)*R*GAMMA/(2.*EIO)
ØØ66Ø       CALL MTINV (PHI,6,6,6,PP)
ØØ67Ø *
ØØ68Ø *     BUILD UP FREE TRANSFORMATION MATRIX BETA
ØØ69Ø *
ØØ7ØØ       DO 4Ø I=1,6
ØØ71Ø       DO 4Ø J=1,6
ØØ72Ø       B(I,J)=Ø.Ø
ØØ73Ø    4Ø IF (I.EQ.J) B(I,J)=1.
ØØ74Ø       B(1,4)=-CTH
ØØ75Ø       B(1,5)=-STH
ØØ76Ø       B(1,6)=-R*(1.-CTH)
ØØ77Ø       B(2,4)=STH
ØØ75Ø       B(2,5)=-CTH
ØØ79Ø       B(2,6)=-R*STH
ØØ8ØØ       B(3,6)=-1.
ØØ81Ø       B(4,1)=1.
ØØ82Ø       B(4,4)=-1.
ØØ83Ø       B(4,5)=-R*(1.-CTH)
ØØ84Ø       B(4,6)=R*STH
ØØ85Ø       B(5,2)=1.
ØØ86Ø       B(5,5)=-CTH
ØØ87Ø       B(5,6)=-STH
ØØ88Ø       B(6,3)=1.
ØØ89Ø       B(6,5)=STH
ØØ9ØØ       B(6,6)=-CTH
ØØ91Ø       DO 5Ø I=1,3
ØØ92Ø       DO 5Ø J=1,6
ØØ93Ø       II=I
ØØ94Ø       IF (P.EQ.2.) II=II+3
ØØ95Ø    5Ø F(I,J)=B(II,J)
```

```
ØØ96Ø       DO 6Ø I=1,3
ØØ97Ø       DO 6Ø J=1,3
ØØ98Ø       II=I
ØØ99Ø       JJ=J
Ø1ØØØ       IF (P.EQ.2.) II=II+3
Ø1Ø1Ø       IF (P.EQ.2.) JJ=JJ+3
Ø1Ø2Ø    6Ø WORK(I,J)=PHI(II,JJ)
Ø1Ø3Ø *
Ø1Ø4Ø *     CALCULATE STIFF=BETA(TRANSPOSE)*PHI*BETA
Ø1Ø5Ø *
Ø1Ø6Ø       CALL MTMPY (Ø,F,WORK,C,-6,3,3,6,3)
Ø1Ø7Ø       CALL MTMPY (Ø,G,F,STIFF,6,3,6,6,6)
Ø1Ø8Ø       PRINT:"                          STIFFNESS MATRIX (BY ROWS)"
Ø1Ø9Ø       PRINT:" "
Ø11ØØ       DO 8Ø I=1,6
Ø111Ø       PRINT 7Ø,(STIFF(I,J),J=1,6)
Ø112Ø    7Ø FORMAT (5E14.6/)
Ø113Ø    8Ø PRINT:"
Ø114Ø       PRINT 9Ø
Ø115Ø    9Ø FORMAT (////)
Ø116Ø       STOP
Ø117Ø       END
```

Influence coefficients for in-plane loading:

$$\phi'_{11} = [6\theta - 8 \sin(\theta) + \sin(2\theta)] \frac{R^3 K_i}{4EI}$$

$$\phi'_{12} = [3 - 4 \cos(\theta) + \cos(2\theta)] \frac{R^3 K_i}{4EI}$$

$$\phi'_{13} = [\theta - \sin(\theta)] \frac{R^2 K_i}{EI}$$

$$\phi'_{22} = [2\theta - \sin(2\theta)] \frac{R^3 K_i}{4EI}$$

$$\phi'_{23} = [1 - \cos(\theta)] \frac{R^2 K_i}{EI}$$

$$\phi'_{33} = \frac{\theta R K_i}{EI}$$

Influence coefficients for out-of-plane loading:

$$\phi'_{44} = \left[\frac{\theta}{2} - \frac{1}{4} \sin(2\theta)\right] \frac{R^3 K_o}{EI} + \left[3\theta + \frac{1}{2} \sin(2\theta) - 4 \sin(\theta)\right] \frac{\gamma R^3}{2EI}$$

$$\phi'_{45} = [\sin(2\theta) - 2\theta] \frac{R^2 K_o}{4EI} - \left[\theta - 2 \sin(\theta) + \frac{1}{2} \sin(2\theta)\right] \frac{\gamma R^2}{2EI}$$

$$\phi'_{46} = [\cos(2\theta) - 1] \frac{R^2 K_o}{4EI} - [1 - 2 \cos(\theta) + \cos^2(\theta)] \frac{\gamma R^2}{2EI}$$

$$\phi'_{55} = \left[\theta - \frac{1}{2} \sin(2\theta)\right] \frac{R K_o}{2EI} + \left[\theta + \frac{1}{2} \sin(2\theta)\right] \frac{\gamma R}{2EI}$$

$$\phi'_{56} = [\sin^2(\theta)] \frac{R K_o}{2EI} - [\sin^2(\theta)] \frac{\gamma R}{2EI}$$

$$\phi'_{66} = \left[\theta + \frac{1}{2} \sin(2\theta)\right] \frac{R K_o}{2EI} + \left[\theta - \frac{1}{2} \sin(2\theta)\right] \frac{\gamma R}{2EI}$$

Where ϕ of Eq. 1 is equal to $[\phi']^{-1}$ and $\gamma = EI/GJ$.

DISTRIBUTION LIST
FINAL REPORT
CONTRACT NAS 3-13445

NASA
Washington, D.C. 20546
Attn: P. R. Miller (RNP)

NASA
Washington, D.C. 20546
Attn: James J. Lynch (RNP)

NASA
Washington, D.C. 20546
Attn: George C. Deutsch (RR)

NASA
Washington, D.C. 20546
Attn: Dr. Fred Schulman (RNP)

NASA
Washington, D.C. 20546
Attn: H. Rochen (RNP)

NASA
Scientific & Tech. Info. Facility
P.O. Box 33
College Park, Maryland 20740
Attn: Acquisitions Branch
(SQT-34054) 2 Copies

NASA
Ames Research Center
Moffett Field, California 94035
Attn: Librarian

NASA
Goddard Space Flight Center
Greenbelt, Maryland 20771
Attn: Librarian

NASA
Langley Research Center
Hampton, Virginia 23365
Attn: Librarian

NASA
Manned Spacecraft Center
Houston, Texas 77001
Attn: Librarian

NASA
George C. Marshall Space Flight Center
Huntsville, Alabama 35812
Attn: Librarian

NASA
Jet Propulsion Laboratory
4800 Oak Grove Drive
Pasadena, California 91103
Attn: Librarian

NASA
Lewis Research Center
21000 Brookpark Road
Cleveland, Ohio 44135
Attn: Librarian

NASA
Lewis Research Center
21000 Brookpark Road
Cleveland, Ohio 44135
Attn: H. O. Slone, MS 500-201

NASA
Lewis Research Center
21000 Brookpark Road
Cleveland, Ohio 44135
Attn: G. M. Ault, MS 3-13

NASA
Lewis Research Center
21000 Brookpark Road
Cleveland, Ohio 44135
Attn: P. L. Stone, MS 106-1

NASA
Lewis Research Center
21000 Brookpark Road
Cleveland, Ohio 44135
Attn: G. M. Thur, MS 500-202

NASA
Lewis Research Center
21000 Brookpark Road
Cleveland, Ohio 44135
Attn: J. E. Dilley, MS 500-309

Report Distribution List - NAS 3-13445 - Final (Continued)

NASA
Lewis Research Center
21000 Brookpark Road
Cleveland, Ohio 44135
Attn: Maxine Sabala, MS 3-19

NASA
Lewis Research Center
21000 Brookpark Road
Cleveland, Ohio 44135
Attn: E. R. Furman, MS 500-202

NASA
Lewis Research Center
21000 Brookpark Road
Cleveland, Ohio 44135
Attn: M. J. Saari, MS 500-202

NASA
Lewis Research Center
21000 Brookpark Road
Cleveland, Ohio 44135
Attn: Report Control Office,
MS 5-5

NASA
Lewis Research Center
21000 Brookpark Road
Cleveland, Ohio 44135
Attn: V. F. Hlavin, MS 3-14
(Final Only)

NASA
Lewis Research Center
21000 Brookpark Road
Cleveland, Ohio 44135
Attn: R. E. English, MS 500-201

NASA
Lewis Research Center
21000 Brookpark Road
Cleveland, Ohio 44135
Attn: M. Gutstein, MS 500-201

National Bureau of Standards
Washington, D.C. 20546
Attn: Librarian

AFSC
Aeronautical Systems Division
Wright-Patterson AFB, Ohio 45433
Attn: Charles Armbruster (ASRPP-10)

AFSC
Aeronautical Systems Division
Wright-Patterson AFB, Ohio 45433
Attn: Librarian

AFML
Wright-Patterson AFB, Ohio 45433
Attn: O. O. Srp (MAMP)

Army Ordnance Frankford Arsenal
Bridesburg Station
Philadelphia, Pennsylvania 19137
Attn: Librarian

U.S. Atomic Energy Commission
Washington, D.C. 20545
Attn: M. J. Whitman

U.S. Atomic Energy Commission
Washington, D.C. 20545
Attn: J. M. Simmons

Argonne National Laboratory
9700 South Cass Avenue
Argonne, Illinois 60440
Attn: Librarian

Brookhaven National Laboratory
Upton, Long Island, New York 11973
Attn: Librarian

Brookhaven National Laboratory
Upton, Long Island, New York 11973
Attn: Dr. D. H. Gurinsky

Brookhaven National Laboratory
Upton, Long Island, New York 11973
Attn: Dr. J. R. Weeks

Oak Ridge National Laboratory
Oak Ridge, Tennessee 37831
Attn: J. Devan

Oak Ridge National Laboratory
Oak Ridge, Tennessee 37831
Attn: R. MacPherson

Oak Ridge National Laboratory
Oak Ridge, Tennessee 37831
Attn: Librarian

Report Distribution List - NAS 3-13445 - Final (Continued)

Office of Naval Research
Power Division
Washington, D.C. 20360
Attn: Librarian

Bureau of Weapons
Research and Engineering
Materials Division
Washington, D.C. 20546
Attn: Librarian

U.S. Naval Research Laboratory
Washington, D.C. 20390
Attn: Librarian

Aerojet Nuclear Systems Company
Power Systems Operations
Azusa, California 91703
Attn: A. Sellers

Aerojet Nuclear Systems Company
Power Systems Operations
Azusa, California 91703
Attn: Librarian

AiResearch Manufacturing Company
Division of the Garrett Corporation
Sky Harbor Airport
402 South 36th Street
Phoenix, Arizona 85034
Attn: Librarian

AiResearch Manufacturing Company
Division of the Garrett Corporation
9851-9951 Sepulveda Boulevard
Los Angeles, California 90009
Attn: Librarian

IIT Research Institute
10 West 35th Street
Chicago, Illinois 60616
Attn: Librarian

Babcock & Wilcox Company
Research Center
Alliance, Ohio 44601
Attn: Librarian

North American Aviation, Inc.
Atomics International Division
8900 DeSoto Avenue
Canoga Park, California 91304
Attn: Librarian

AVCO
Research & Advanced Development Dept.
201 Lowell Street
Wilmington, Massachusetts 01887
Attn: Librarian

Electro-Optical Systems, Inc.
Advanced Power Systems Division
Pasadena, California 91107
Attn: Librarian

Fansteel Metallurgical Corporation
North Chicago, Illinois 18201
Attn: Librarian

Philco Corporation
Aeronutronics
Newport Beach, California 92663
Attn: Librarian

General Dynamics Corporation
General Atomic Division
John Jay Hopkins Lab
P.O. Box 608
San Diego, California 92112
Attn: Librarian

General Electric Company
Nuclear Systems Programs
Space Division
Cincinnati, Ohio 45215
Attn: R. D. Brooks

General Electric Company
Space Division
3198 Chestnut Street
Philadelphia, Pennsylvania 19104
Attn: Librarian

General Dynamics/Fort Worth
P.O. Box 748
Fort Worth, Texas 76101
Attn: Librarian

General Motors Corporation
Allison Division
Indianapolis, Indiana 46206
Attn: Librarian

Hamilton Standard
Division of United Aircraft Corp.
Windsor Locks, Connecticut 06096
Attn: Librarian

Hughes Aircraft Company
Engineering Division
Culver City, California 90230
Attn: Librarian

Lawrence Radiation Laboratory
Livermore, California 94550
Attn: Librarian

Lockheed Missiles and Space Div.
Lockheed Aircraft Corporation
Sunnyvale, California 90221
Attn: Librarian

Teledyne Isotopes
Nuclear Systems Division
110 West Temonium Road
Temonium, Maryland 21093

Martin Marietta Corporation
Metals Technology Laboratory
Wheeling, Illinois 60090

Materials Research Corporation
Orangeburg, New York 10962
Attn: Librarian

McDonnel Aircraft
St. Louis, Missouri 63166
Attn: Librarian

MSA Research Corporation
Callery, Pennsylvania 16024
Attn: Librarian

National Research Corporation
70 Memorial Drive
Cambridge, Massachusetts 02142
Attn: Librarian

North American Aviation
Los Angeles Division
Los Angeles, California 90009
Attn: Librarian

United Aircraft Corporation
Pratt & Whitney Aircraft Division
400 Main Street
East Hartford, Connecticut 06108
Attn: Librarian

Republic Aviation Corporation
Farmingdale, Long Island, New York 11735
Attn: Librarian

Sandia Corporation
P.O. Box 5800
Albuquerque, New Mexico 87116
Attn: Librarian

Solar
2200 Pacific Highway
San Diego, California 92112
Attn: Librarian

Southwest Research Institute
8500 Culebra Road
San Antonio, Texas 78228
Attn: Librarian

Superior Tube Company
Norristown, Pennsylvania 19404
Attn: Librarian

TRW Inc.
23555 Euclid Avenue
Cleveland, Ohio 44117
Attn: Librarian

Union Carbide Corporation
1020 West Park Avenue
Kokomo, Indiana 46901
Attn: Librarian

Union Carbide Corporation
1020 West Park Avenue
Kokomo, Indiana 46901
Attn: Technology Department

Westinghouse Electric Corporation
Astronuclear Laboratory
P.O. Box 10864
Pittsburgh, Pennsylvania 15236
Attn: Librarian

Wah Chang Corporation
Albany, Oregon 97321
Attn: Librarian

Whittaker Corporation
Nuclear Metals Division
West Concord, Massachusetts 01781
Attn: Librarian

Wright-Patterson Air Force Base
Research and Technology Division
Dayton, Ohio 45404
Attn: M. P. Wannemacher, APIP-1

Defense Metals Information Center
Battelle Memorial Institute
Columbus Laboratories
505 King Avenue
Columbus, Ohio 43201
Attn: R. T. Niehoff

Defense Metals Information Center
Battelle Memorial Institute
Columbus Laboratories
505 King Avenue
Columbus, Ohio 43201
Attn: Librarian